USE OF GEOSYNTHETICS ON SUBGRADE AND ON LOW AND VARIABLE FILL FOUNDATION

by

Eirini Christoforidou

A Thesis

Submitted to the Faculty of Purdue University

In Partial Fulfillment of the Requirements for the degree of

Master of Science in Civil Engineering

Lyles School of Civil Engineering

West Lafayette, Indiana

December 2021

THE PURDUE UNIVERSITY GRADUATE SCHOOL
STATEMENT OF COMMITTEE APPROVAL

Dr. Antonio Bobet, Chair
Lyles School of Civil Engineering

Dr. Maria Caterina Santagata
Lyles School of Civil Engineering

Dr. Philippe L. Bourdeau
Lyles School of Civil Engineering

Approved by:
Dr. Dulcy M. Abraham

Dedicated to my parents: Anastasia and Avraam

and my brother: Chris

ACKNOWLEDGEMENTS

First of all, I would like to express my gratitude to my advisor, Prof. Antonio Bobet, for his patience, guidance, and support that made this work possible. His guidance and motivation helped me throughout the research and writing of this thesis.

Besides my advisor, I would like to thank my graduate committee members Prof. Maria Caterina Santagata and Prof. Philippe L. Bourdeau, for their advice, support and for serving on my committee. The completion of this thesis would not have been possible without the help and advice from Prof. Philippe L. Bourdeau.

Last but not the least, I am grateful to my parents, brother, and friends for their endless love and support.

The work presented in this thesis was supported by the Indiana Department of Transportation.

TABLE OF CONTENTS

LIST OF TABLES

LIST OF FIGURES

ABSTRACT

There are significant problems during construction to establish an adequate foundation for fills and/or subgrade for pavements when the natural ground has low-bearing soils. Geosynthetics such as geogrids, geotextiles and/or geocells could provide an alternative, less costly in time and money, to establish an adequate foundation for the fill and/or subgrade. There is extensive evidence in the literature and on DOTs practices about the suitability of using geotextiles in pavements as separators. Previous studies have also shown that the use of geogrids in flexible pavements as a reinforcing mechanism could decrease the thickness of the base layer and/or increase the life of the pavement. In this study, analyses of selected pavement designs using Pavement ME, while considering geogrid-enhanced base or subgrade resilient modulus values, showed that geogrid-reinforcement, when placed at the interface between subgrade and base, did not produce significant benefits, as only a modest increase in pavement life was predicted. In addition, parametric finite element analyses were carried out to investigate the potential benefits of placing a geogrid at the base of a fill over a localized weak foundation zone. The analyses showed that the use of geogrids is beneficial only when: (a) the stiffness of the weak foundation soil is about an order of magnitude smaller than the rest of the foundation soil; and (b) the horizontal extent of the weak foundation soil is at least 30% of the base of the embankment foundation. The largest decrease in differential settlements at the surface of the fill, resulting from geogrid-reinforcement, was less than 20% and, therefore, it is unlikely that the sole use of geogrids would be sufficient to mitigate differential settlements. Based on previous studies, a geocell mattress, which is a three-dimensional geosynthetic filled with different types of materials, could act as a stiff platform at the base of an embankment and bridge over weak zones in the foundation. However, given the limited experience on the use of geocells, further research is required to demonstrate that geocells can be effectively used instead of other reinforcement methods.

1. INTRODUCTION

1.1 Problem statement

ASTM defines geosynthetics as "a planar product manufactured from a polymeric material used with soil, rock, earth, or other geotechnical-related material as an integral part of a civil engineering project, structure, or system." They can be classified as Geotextiles, Geogrids, Geocomposites, Fibrillated Geofibers and Geofilaments (Pinto, 2003). Geosynthetics are used for the following applications (Pinto, 2003): as a barrier, for drainage, for filtration, separation, protection, to provide protection for surface erosion and for reinforcement. They have been used in roads and railways, foundations, embankments and slopes and retaining walls. Geosynthetics have been utilized as reinforcement below fills on weak soils since the late 60s (John, 1987). In fact, in 1970, only 5 to 6 geosynthetics were available, in contrast to the early 2000s, when there were available more than 600 different geosynthetic products (Holtz, 2001). This shows an explosion-like of applications for these materials in construction.

Geosynthetics work as soil reinforcement due to the following mechanisms (Koerner, 1998 and Jewell, 1996): (a) shear strength enhancement, due to the soil-geosynthetic interface resistance; (b) anchorage or pullout, when the geosynthetic resists being pulled from the soil; (c) tensile membrane and lateral deformation restraint effects, when the geosynthetic supports normal load. These mechanisms result in a shear stress reduction effect on the underlying soil, reduced permanent deformation and improved bearing capacity (Bourdeau et al., 1982; Bourdeau and Ashmawy, 2012; Espinoza and Bray, 1995; Shukla, 2004). For instance, the weight of the embankment is transferred to the underlying soil as a normal stress but also as a shear stress, as the fill tries to deform. The shear stress reduces the bearing capacity of the foundation (Jewell, 1987; Rowe et al., 2015) and thus decreases the stability of the embankment. Placement of a geosynthetic reinforcement between the fill and the soil reduces the shear stress at the soil foundation, by imposing tension in the geosynthetic and restraining the fill lateral deformation, thus increasing the stability of the embankment. The geosynthetic also redistributes the normal load, due to its membrane effect, by providing a vertical support to the fill, which results in a reduction of the applied normal stress to the foundation (Bourdeau et al., 1982; Hausmann, 1990). It is important to mention that, although geosynthetics can improve the short-term performance,

i.e. bearing capacity, immediate settlements, resilience under repeated loading and constructability, they will not reduce the long-term settlements of tall embankments due to consolidation or creep of the soil underneath.

Geosynthetics are very attractive, not only because of the separation (they prevent particle movement across layers) and reinforcement (as previously discussed) properties, but also because they facilitate construction over poor-quality soils and make activities less dependent on weather. They are easy to place and may be used to mitigate poor local soil conditions. Thus, they are attractive for their potential cost savings, when used properly (Pinto, 2003).

The literature is very rich on the description of these materials, their properties and usage. Work has been done in the characterization of these materials in the laboratory (e.g. Pinto, 2003), in the field (e.g. Rowe et al., 2015) and numerically (e.g. Bourdeau, 1989; Espinoza, 1994; Espinoza and Bray, 1995; Rowe et al. 2015). Of particular interest are studies done by DOTs on their long-term usage, especially because their potential for creep and possible degradation over time, such as the work on monitoring geosynthetics in local roadways done by the Minnesota DOT (Clyne, 2011). It was found that geogrids had a much more consistent performance than geotextiles, but it was also stated that the conclusions should be taken as tentative and that more research was needed.

1.2 Research objectives and scope of the work

There are significant problems during construction to establish an adequate foundation for fills when the natural ground has low-bearing soils, generally wet clays, or in areas that are water-logged. There are also difficulties in establishing an acceptable foundation over the subgrade for similar reasons. A particular problem exists with the subgrade in underpasses, when excavation is needed, and the water table is close to the ground surface.

The improvement of the foundation for the fill and subgrade is usually a costly and time-consuming process that may require the replacement of the natural soil and/or the placement of clean granular materials to create a working platform.

Geosynthetics such as geogrids, geotextiles and/or geocells along with granular soils or light-weight materials can provide an alternative, less costly in time and money, to establish an adequate foundation for the fill and/or subgrade. They can also help create a stable working platform to achieve adequate compaction, by enhancing lateral confinement of the aggregate

during compaction and acting as a separator layer between the subgrade and the aggregate layer. In addition, geosynthetics would help distribute the vertical load and provide lateral restraint, thus reducing settlements; they would separate the natural ground from the fill and subgrade, thus reducing fine migration; and would help with drainage.

The objective of this study is to advance the knowledge on the use of geosynthetics as reinforcement elements and provide recommendations for their use in embankment foundations and in pavements.

The scope of the study is as follows:

1. Improve understanding of the load- and displacement-transfer mechanisms between geosynthetics and soil. There is vast literature on the performance of geosynthetics under different working conditions, and yet there are still fundamental questions that need to be addressed to better understand not only the interaction that exists between soil and geotextile, but also what properties of the geosynthetic are critical for each particular application.

2. Determine geosynthetic performance for different applications. The focus of this study is on the use of geosynthetics in the subgrade for improving pavement performance, and in the foundation of roadways or embankment for decreasing settlements, and for facilitating construction on poor (wet) soils.

1.3 Organization of the Thesis

This thesis contains five chapters. Chapter 1 introduces the topic of the research. Chapter 2 presents a comprehensive literature review which highlights the benefits of using geogrid-reinforcement in the base course of flexible pavements, geocell-reinforced base layers in unpaved and paved roads, and geosynthetic-reinforcement at the base of embankments constructed over weak foundations. It also summarizes the best practices of INDOT and other DOTs regarding the use of geosynthetics in roadway applications. In Chapter 3, the potential for structural benefits of placing a geogrid at the interface between subgrade and base course of a flexible pavement is provided for select design examples, using methods and software readily available to DOT engineers and practitioners. Chapter 4 discusses the results of a numerical model of a geosynthetic-

reinforced embankment over a localized weak foundation zone. It describes the parametric study performed to investigate the effects of factors such as the modulus of the weak zone, its width, the type of geogrid-reinforcement, and the location of the weak zone, as well as the potential benefits of using geogrid-reinforcement placed at the base of the embankment. Chapter 5 includes a summary of the work and conclusions.

2. LITERATURE REVIEW

2.1 Introduction

ASTM defines geosynthetics as “a planar product manufactured from polymeric material used with soil, or other geotechnical engineering material as an integral part of a human-made project, structure or system”. According to Koerner (2005), there are eight types of geosynthetics: geotextiles, geogrids, geonets, geomembranes, geosynthetic clay liners, geopipes and geocomposites. These geosynthetics can perform the following functions: (1) separation, (2) reinforcement, (3) filtration, (4) drainage, and (5) containment (barrier). In transportation infrastructure, geosynthetics have been used in roads and railways, foundations, embankments, and slopes and retaining walls. They have also been used in other fields of Civil Engineering such as, dams’ construction, landfill liners and covers, and coastal protection. The first attempt to use fabrics for road reinforcement was done by the South Carolina Highway Department in 1926, where they used a heavy cotton fabric above a subgrade soil. Geotextiles have been used as reinforcement in unpaved roads, beneath railroad ballast, within embankments, and earth dams since the late 60s (Koerner, 2005).

Geotextiles are one of the largest groups of geosynthetics used in construction. They are made of synthetic fibers, which are transformed into flexible, porous fabrics using woven or nonwoven textile manufacturing techniques. The polymeric materials that are mainly used in the manufacture of geotextiles are polypropylene or polyester. Some of the types of geotextiles that are available, depending on the way they are manufactured, are the woven monofilament, woven slit-film, woven multifilament, nonwoven needle-punched, and nonwoven heat-bonded.

Geotextiles can serve in four functions (separation, reinforcement, filtration, drainage). They can be used to separate dissimilar materials so that the functioning of both materials is preserved. Also, they can contribute with their tensile capacity to improve the overall strength of soil, which, by itself, can resist to compression but not to tension. Specifically, geotextiles can reinforce the soil via the following mechanisms: (1) membrane effect, when a normal load is applied and produces deflection of underlaying layers, tension is generated in the deflecting geotextile, it redistributes pressure on the lower layer and, as a result, overall deflections are reduced (Bourdeau, 1989) ; (2) resistance to shearing, when a geosynthetic contributes to shear strength across the soil-

geosynthetic interface; (3) enhanced confinement of the overlaying layer, through interface friction and tension resistance, which reduces the deformability of the soil layer (Bourdeau et al., 1990); and (4) anchorage effect, when a tensile force tends to pull the geosynthetic out of the soil (Koerner, 2005). These mechanisms lead to a reduction in the shear stress that is applied in the underlying soil, reduction of the peak normal stress, reduction in permanent deformation and increased bearing capacity (Bourdeau et al., 1982; Bourdeau and Ashmawy, 2012; Espinoza and Bray, 1995; Shukla, 2004). A geotextile can also serve as filter, allowing the movement of liquid across its cross section while retaining soil particles. Geotextiles can also act as drainage layers, collecting and transporting underground water.

Another type of geosynthetic widely used is geogrids, which serve only as reinforcement. Geogrids were introduced to the U.S. market in the early 80s and consist of parallel sets of ribs (longitudinal and transverse) forming a grid with large apertures, which allow for interlocking of the surrounding soil or aggregates particles. The polymer materials used in the manufacturing of geogrids are mostly high-density polyethylene or polypropylene. There are two types of geogrids: uniaxial geogrids, which possess higher tensile strength and modulus in the machine-longitudinal direction than in the machine-transversal direction, and biaxial geogrids, which possess the same tensile properties in both transversal and longitudinal directions. Uniaxial geogrids are used in MSE walls and slope stabilization where the main tension orientation is known, while biaxial geogrids are mainly used in pavements and foundations, where there is no preferential direction of tensile stress. Geogrids, as compared to geotextiles, have higher tensile modulus and stronger interface interaction with soil (through interlocking as opposed to simple friction) and thus most of their strength is mobilized by relatively small deformations (Ashmawy, 1995) whereas geotextiles are more extensible and large deformation is required for mobilizing their tension. Geogrid reinforcement mechanisms are similar to those of geotextiles. Typical geotextiles and geogrids are depicted in Figure 2.1.

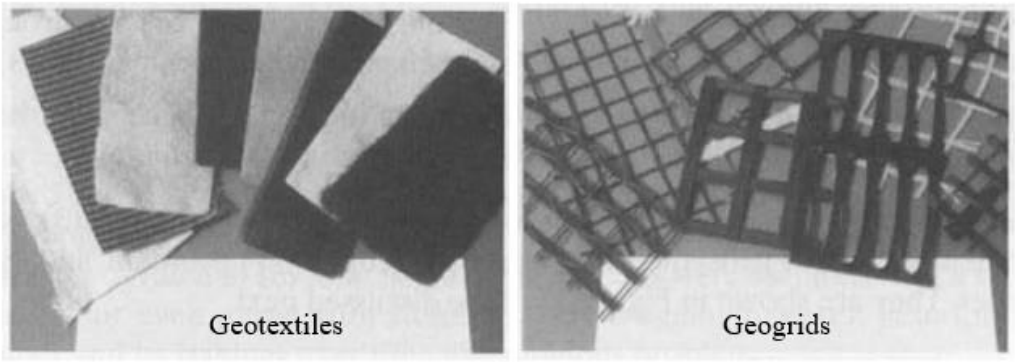

Figure 2.1 Geotextiles and geogrids (adapted from Koerner, 2005).

A special type of geosynthetic is the geocell. Geocells are three-dimensional honeycombed interconnected cells that completely encase the filling soil to form a composite mattress. They have been made of high-density polyethylene (HDPE) or geotextile, but recently novel polymeric alloys have been gradually replacing HDPE. They are mostly used for slope stabilization, erosion protection, but also as reinforcement and confinement layers, and for base course reinforcement in roadway systems. Geocell mattresses can be used also as base course reinforcement over weak subgrades in unpaved and paved roads and as basal reinforcement for embankments constructed over weak foundation soils. The most important mechanisms for geocell-reinforcement are lateral and vertical confinement and tensioned-membrane effects.

There is rich literature on the use of geosynthetics for a wide range of applications. The focus of this chapter is to summarize the experience that already exists on the use of geosynthetics in the subgrade for improving pavement performance, and in the foundation of roadways or embankment for decreasing settlements, and for facilitating construction on poor (wet) soils.

According to Holtz et al. (2008), two types of roadways should be considered: permanent and temporary. Permanent roads include both paved and unpaved roads that remain in service for 10 years or more. Temporary roads, that are unpaved, remain in service for only a short period of time. In temporary, unpaved roads, geosynthetics reinforcement can allow to save on the amount of gravel needed to support traffic or/and reduce permanent deformation (or rutting) of the aggregate surface. Furthermore, geosynthetics combined with aggregate over very soft, wet subgrade soils can provide a stable working platform to facilitate construction. In unpaved low-volume roads, when geotextiles are placed above soft subgrades (CBR $\leq$ 3), they act primary as

separators and filters and, as secondary function, as reinforcements. In contrast, geogrids, when used in the same conditions, act primarily as reinforcements (Holtz et al., 2008).

The application of geosynthetics to paved road construction, together with a comprehensive bibliography, has been summarized by Perkins et al. (2012). In permanent paved roads, geotextiles can be used as separators (as an alternative to granular separator layers) and as a form of subgrade stabilization. The need for separators (granular or geotextiles) and the selection of geotextiles for this function were addressed in a recent JTRP research study (Getchell et al., 2020). Detailed discussion of this topic will not be repeated herein. In summary, geotextile separators must be selected with index mechanical properties that will allow them to survive installation and construction efforts without damage (survivability criterion) and with pore size index properties that meet filter criteria against the subgrade fine particles migration. It should be noted that a geogrid may through interlocking and lateral restraint, if the particle size to aperture size ratio is optimal, prevent penetration and loss of overlaying aggregates into the underlaying subgrade. It would then function as separator, in addition to reinforcement, but geogrids cannot meet filter requirements for separators and must be substituted with geotextiles for this function (Perkins et al., 2012). The subgrade stabilization process involves the placement of a geosynthetic and a subsequent aggregate lift to provide an adequate roadbed when poor subgrade conditions exist. Geosynthetics used for subgrade stabilization perform multiple functions of separation, filtration, and reinforcement. However, if there is no free draining (i.e. open graded) base course, geotextiles with lateral drainage capabilities can also be used for this purpose. Finally, geosynthetics such as geogrids can provide base reinforcement when they are placed within or at the bottom of unbound aggregate layers in a flexible pavement. Geogrids are also used for subgrade stabilization to facilitate construction over weak subgrades (CBR $\leq$ 3) (Holtz et al., 2008).

Based on several case histories, Holtz et al. (2008) proposed the use of geosynthetics in roadway construction in the presence of the following subgrade conditions: weak soils (AASHTO: A-5, A-6, A-7-5, and A-7-6) with low-undrained shear strength (c_u < 90 kPa (2000 psf), CBR < 3, $M_R \approx <$ 30 MPa (4500 psi)), high water table situations, and subgrades with high sensitivity.

Geosynthetics have been also used at the base of embankments to resist the horizontal shear stresses caused by the embankment fill when the foundation soil does not have enough shear strength. Geosynthetics, such as geogrids and geotextiles, improve the bearing capacity of the foundation soil and reduce differential settlements. According to Bonaparte et al. (1987),

reinforced embankments over weak foundations are divided into two categories: embankments over uniform weak soils, and embankments over locally weak foundation zones. The first category is the most common and refers to embankments constructed on overall very soft, saturated silt, clay, or peat layers. The second category refers to foundations that contain local anomalies and reinforcement is used to bridge over the weak zones.

The objective of this chapter is to summarize research on the benefits of using: geogrid-reinforcement in the base course of flexible pavements, geocell-reinforced bases in unpaved and paved roads, and geosynthetic-reinforcement at the base of embankments constructed over weak foundations. Finally, the best practices of INDOT and other DOTs regarding the use of geosynthetics in roadway applications are summarized.

2.2 Base course reinforcement in flexible pavements

One of the most common applications for geosynthetics in flexible pavements is the use of geogrids as a base or subbase course reinforcement. Their benefits have been studied through experimental and numerical methods by many authors. Limited field investigation has also shown the potential contribution of the geogrid to the performance of the pavement. By definition, flexible pavements consist of multiple material layers with decreasing stiffness from the top to the bottom. This type of pavement usually includes asphalt concrete layer, base course, subbase (not always required) and subgrade. The geosynthetic is usually placed within the base material or at the interface between the subgrade and base course. Among all the geosynthetics, biaxial geogrids are the most used for this application, due to their higher tensile modulus compared to geotextiles.

Geosynthetics, when placed at the interface between subgrade and base, can provide reinforcement through the following three mechanisms: (1) lateral restraint of the base and subgrade through friction (geotextiles) and interlock (geogrids) between the aggregate, subgrade soil and geosynthetic; (2) increase in the bearing capacity by forcing the shear failure surface to move upwards in the soil; and (3) tension-membrane support of the wheel load (wheel path rutting more than 100 mm {4 in.} is required to develop membrane type support) (Holtz et al., 2008).

In 1986 and 1990, Georgia Department of Transportation (GDOT) constructed two pavement test sites, which included control sections and sections with biaxial geogrid as a reinforcement in the base course. The purpose of this study was to evaluate the condition of the pavements in a long-term period. The pavement performance evaluations consisted of deflection

measurements, rut measurements, and crack surveys. After the final field evaluation, that was conducted in 2005, they came up with the following conclusions: (1) There is no significant reinforcement benefit when geogrid is used in pavements with a firm subgrade of CBR value higher than 8; (2) The placement of a geogrid in a thin base layer shows comparable performance with a thicker base layer without geogrid; and (3) The geogrid placed in the base layer can effectively replace the lime-stabilized subgrade (Aran, 2006).

The improvement that the geogrid can contribute to the pavement performance depends on the following factors: (1) the properties of the geogrid (tensile modulus, aperture size, internal connection strength, polymer resilience); (2) the strength of the subgrade; (3) the location of the geogrid inside the pavement and (4) the thickness of the base layer. Al-Qadi et al (2008) suggested that placement of the geogrid at the interface between subgrade and base gives better performance when the pavement consists of a thin base course layer (i.e. 203 mm) and that for a thick base (i.e. 457 mm) it is preferred to be placed in the top one-third of the base given that thin hot-mix asphalt (HMA) layer (i.e. 75 mm) is used. However, Haas et al (1988) suggested that the optimum location of geogrid in thick base layers is in the middle portion. In addition, they proved that the geogrid should not be placed in a zone of compression, such as near the top of the base layer or within the higher half of a thick base over a very soft subgrade. This discrepancy between the two studies shows how variables like subgrade strength, shape, size and magnitude of load, and type and location of reinforcement affect the benefit of geogrid base reinforcement. Furthermore, most of the studies suggest the use of geogrids when there is a poor-quality subgrade because only in this case the geogrid can be mobilized, and rutting minimized.

In their study, Abu-Farsakh and Chen (2011) investigated, through laboratory cyclic plate loading tests on reinforced pavement test sections, the effect of the tensile modulus and the location of the geogrid on the performance of the pavement. The achieved thickness of the pavement layers was the following: 51 mm for HMA, and 305 mm for base course layer. The estimated CBR of the subgrade was 0.5. Figure 2.2 shows the development of pavement surface permanent deformation with increasing number of cycles for an unreinforced section and for sections reinforced with a geogrid. In the figure, GG3 and GG4 denote triaxial geogrids with tensile modulus of 430 kN/m and 475 kN/m, respectively. Triaxial geogrid is a unique type of geogrid with triangular structure. It is manufactured from a punched polypropylene sheet oriented in multiple, equilateral directions to form its triangular apertures. Geogrid GG4 is placed at the interface of the base course with the

subgrade, in the middle of the base or in the upper one-third of the base, while geogrid GG3 is placed at the interface or in the middle of the base. The results in figure show that the pavement section with the geogrid placed in the upper one-third of the base layer leads to the largest decrease in the permanent deformation of the pavement and it is followed by the section with the geogrid placed at the interface between subgrade and base layer. It must be noted, though, that in the section where the geogrid was placed in the upper one-third a new compaction method was used, that facilitated the interlocking between the geogrid and the base material. Thus, the comparison is questionable between this section and all the others. Moreover, it can be noticed that the geogrid GG4, with higher tensile modulus, shows better performance than the geogrid GG3.

Abu-Farsakh et al. (2014), through finite element modeling, reached the same conclusions as Abu-Farsakh and Chen (2011) from physical experiments, and showed that the magnitude of reduction in permanent deformation of a pavement depends on the geogrid tensile modulus, the subgrade strength and the thickness of the base course layer. Table 2.1 summarizes the characteristics of the pavement sections that were studied numerically and Figures 2.3 and 2.4 show plots of permanent deformation with number of cycles for unreinforced and reinforced cases of the four sections. For each section, a geogrid (GG1 or GG3) was simulated at the interface between the subgrade and the base course, with the geogrid GG3 having higher tensile modulus than geogrid GG1. As we observe in the figures, a greater reduction was obtained for weaker subgrades, thinner base course layers or for higher tensile modulus geogrids. These results are, also, summarized in Table 2.2, where the percentage decrease in permanent deformation for each section is shown.

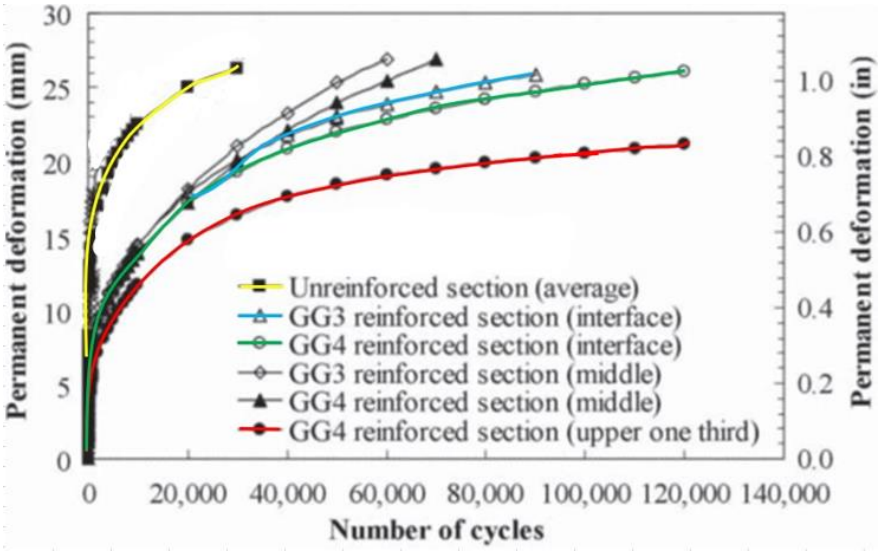

Figure 2.2 Surface permanent deformation of the pavement for different types and locations of geogrids (adapted from Abu-Farsakh and Chen, 2011).

Table 2.1 Pavement sections (adapted from Abu-Farsakh et al., 2014).

Section	Base Course Thickness (mm)	Subgrade Quality
1a	150	Weak
1b	150	Moderate
4a	300	Weak
4b	300	Moderate

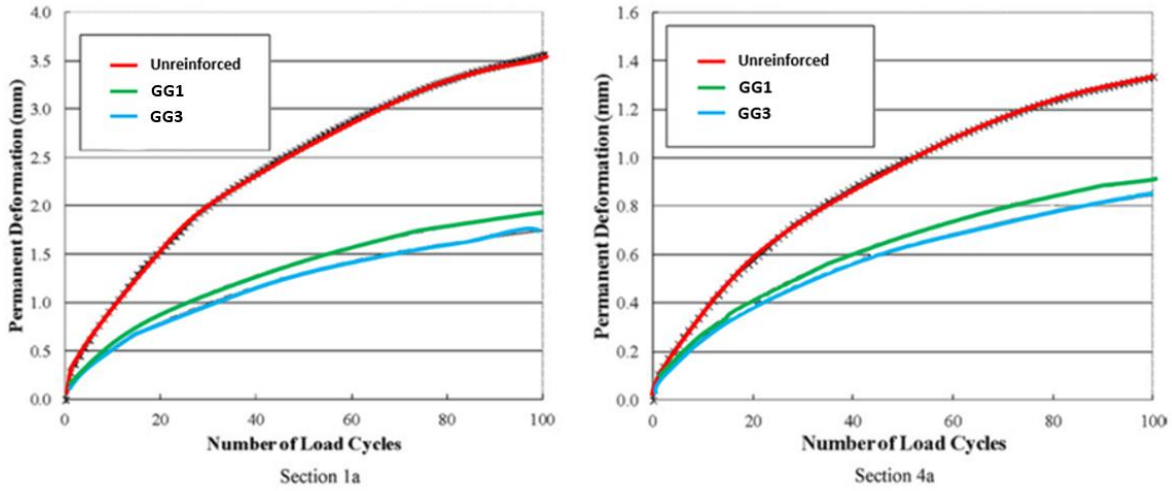

Figure 2.3 Development of permanent deformation for different pavement sections (geogrid placed at the interface between subgrade and base course)-Sections 1a, 4a (adapted from Abu-Farsakh et al., 2014).

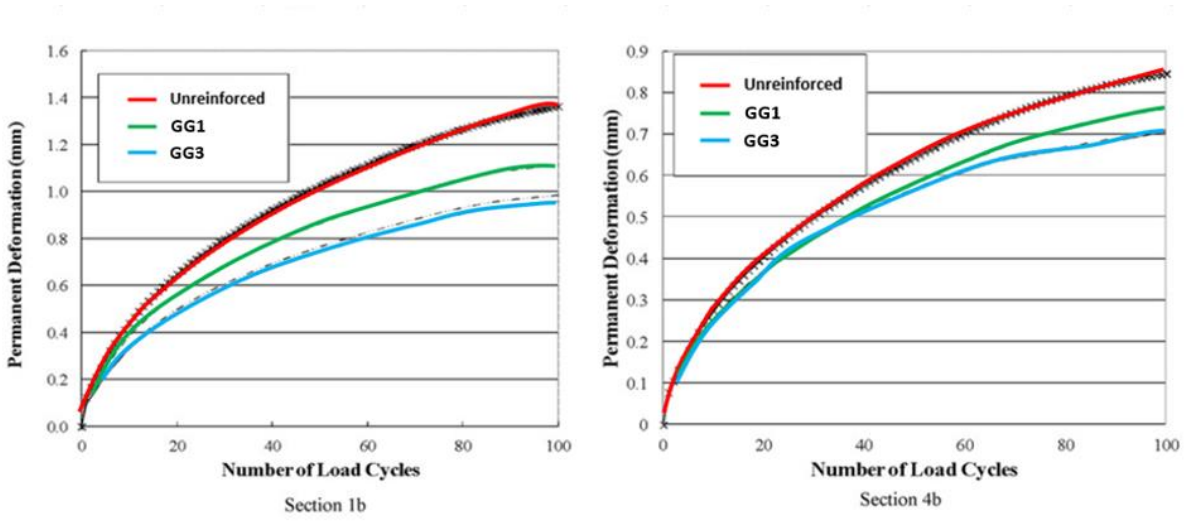

Figure 2.4 Development of permanent deformation for different pavement sections (geogrid placed at the interface between subgrade and base course)-Sections 1b, 4b (adapted from Abu-Farsakh et al., 2014).

Table 2.2 Percentage decrease in permanent deformation for each section.

Section	Percentage Decrease in Permanent Deformation (%)		Subgrade Quality	Base Layer Thickness
	Geogrid G1	Geogrid G3		
1a	43	51	Weak subgrade	Thin base layer
1b	19	26	Moderate subgrade	
4a	31	35	Weak subgrade	Thick base layer
4b	12	18	Moderate subgrade	

2.2.1 Quantifying the structural contribution of geogrid to base reinforcement

Studies have tried to quantify the contribution of the geogrid base reinforcement to the pavement performance. The most widely used ways of quantifying the benefit of the geogrid base reinforcement are by evaluating the amount of reduction in the thickness of aggregate layer (Montanelli et al., 1997) or by estimating the increase in the service life of the pavement structure (Al-Qadi et al., 1997). Recently, the benefit of the reinforcement has been quantified by estimating the equivalent resilient modulus of the geogrid-reinforced base course and comparing it with the resilient modulus of the non-reinforced base course. This method was followed by Sun et al.

(2017), Chen and Abu-Farsakh (2012) and Kim et al. (2005). The results presented by these authors are discussed below.

Sun et al. (2017), using the measured surface permanent deformations and stresses on the top of the subgrade obtained from cyclic plate loading tests on pavement sections, presented a method for the back-calculation of the equivalent resilient modulus of the geogrid-reinforced base. The Modulus Improvement Factor (MIF) was used in this study to capture the benefits of a geogrid placed at the interface between the subgrade and the base course and it is defined as:

$$MIF = \frac{M_{R\ (reinforced\ base)}}{M_{R\ (nonreinforced\ base)}} \tag{2.1}$$

Table 2.3 shows the back-calculated modulus and the percentage increase in modulus for non-reinforced and geogrid-reinforced pavement sections with different base course thicknesses. Geogrids T1 and T2 were triaxial geogrids with a radial stiffness of 270 kN/m and 365 kN/m, respectively. From the results presented in the table, it can be noticed that the values of MIF range from 1.4 to 2 (40% to 100% increase in modulus) for the reinforced bases with the geogrids T1 and T2. Furthermore, higher values of MIF are obtained for the section with the stiffer geogrid T2 and with the thinner base layer (i.e. 150 mm).

Table 2.3 Back-calculated resilient modulus of geogrid-reinforced bases and Modulus Improvement Factors (MIFs) (adapted from Sun et al., 2017).

Base Thickness (m)	**Reinforcement**	**Back Calculated Modulus**		**Percentage Increase in Modulus (%)**
		Modulus (MPa)	**MIF**	
0.15	Non-reinforced	59	-	-
	T1 reinforced	108	1.83	83
	T2 reinforced	122	2.07	107
0.23	Non-reinforced	77	-	-
	T1 reinforced	117	1.53	52
	T2 reinforced	152	1.99	97
0.30	Non-reinforced	106	-	-
	T1 reinforced	144	1.36	36
	T2 reinforced	174	1.64	64

Similar results are also shown in the study of Chen and Abu-Farsakh (2012). The authors, using previous cyclic plate loading test results from their study in 2011, quantified the increase in the resilient modulus of the base course when geogrid was placed at different locations throughout the base layer. Table 2.4 shows the percentage increase in resilient modulus of the base course for each pavement section that had different base course thickness and geogrid was added in different locations throughout the layer. Four types of geogrids, two biaxial (GG1, GG2) and two triaxial (GG3, GG4),were used, from which geogrid GG4 had the highest stiffness and geogrid GG1 the lowest stiffness. As we observed in Table 2.3, the pavement section with a geogrid placed at the interface between the subgrade and base course, and with a base course thickness of 300 mm, resulted in a percentage increase in modulus that ranged from 36% to 64%. In the study of Chen and Abu-Farsakh (2012), a similar increase in modulus (43%-49%) is observed for the section in which the geogrid is placed at the interface. Both pavement sections in these two studies had a base course thickness close to 300 mm and consisted of a weak subgrade. Finally, one can observe in Table 2.4 that the section with the geogrid placed at the upper one third of the base layer results in a higher percentage improvement in modulus, which is due to the improved compaction method that was used in the cyclic plate loading test for this section.

Table 2.4 Percentage improvement of the base resilient modulus for each pavement section (from geogrid GG1 to GG4 increasing stiffness) (adapted from Chen and Abu-Farsakh, 2012).

Sections	**Base Thickness mm (in)**	**Base Resilient Modulus MPa (psi)**	**Geogrid-Reinforced Base Resilient Modulus MPa (psi)**	**Percentage Improvement (%)**
GG1 (interface)	319 (12.6)	137 (19,852)	150 (21,740)	10
GG2 (interface)	317.5 (12.5)	128 (18,554)	183 (26,580)	43
GG3 (interface)	325 (12.8)	136 (19,697)	195 (28,300)	44
GG4 (interface)	311 (12.2)	128 (18,554)	191 (27,650)	49
GG4 (upper one third)	310 (12.2)	138 (20,009)	262 (38,050)	90

Another approach to capture the benefit of using geosynthetic reinforcement in flexible pavements by calculating the improved resilient modulus of the base layer, was presented by Kim et al. (2005). The authors conducted two types of tests, a Large Scale Model Experiment (LSME) and a Field Test, where they tried to represent flexible pavement sections with a geosynthetic reinforcement in the base layer. Table 2.5 shows the calculated resilient modulus of a 300-mm-

thick unreinforced and geosynthetic-reinforced base layer and the percentage increase in modulus due to the addition of the geosynthetic. Both tests were conducted with the use of geogrid, woven geotextile, nonwoven geotextile or drainage geocomposite. The results in the table show that in both tests the base layer reinforced with geogrid had the best performance. The increase in modulus for this case ranged from 75% to 95%, values that are significantly higher than those reported in the other two studies.

Table 2.5 Percentage increase in resilient modulus of a 300-mm-thick base reinforced with geosynthetic in LSME and Field (adapted from Kim et al., 2005).

Type of Test	Resilient Modulus (MPa)					Percentage Increase in Modulus (%)			
	Unreinforced	Geogrid	Woven Geotextile	Nonwoven Geotextile	Drainage Geocomposite	Geogrid	Woven Geotextile	Nonwoven Geotextile	Drainage Geocomposite
LSME	40	78	76	70	67	95	90	75	67.5
Field Test	93	163	133	135	110	75	43	45	18

A different method to evaluate the structural contribution of geogrids was presented by Sun et al. (2018). In their study, they estimated the equivalent CBR of a geogrid-reinforced working platform, where geogrids were used to reinforce aggregates above a weak subgrade, resulting in a new subgrade with higher CBR value. The equivalent CBR value of the working platform was determined as the CBR value of a subgrade-only section that had the same permanent deformation under the same loading magnitude and number of loading cycles (Sun et al., 2018). To achieve this, they based on cyclic plate loading tests with increasing load magnitude, that were performed on three types of pavement sections. These pavement sections include one section with non-reinforced aggregates over weak subgrade, one with geogrid-reinforced aggregates over weak subgrade and one subgrade-only section. The geogrids used in this study were triaxial geogrids, T1 and T2, with radial stiffness at 0.5% strain of 270 kN/m and 365 kN/m, respectively. Figure 2.5 shows the geogrid-reinforced aggregates over the weak subgrade, which form the new equivalent subgrade.

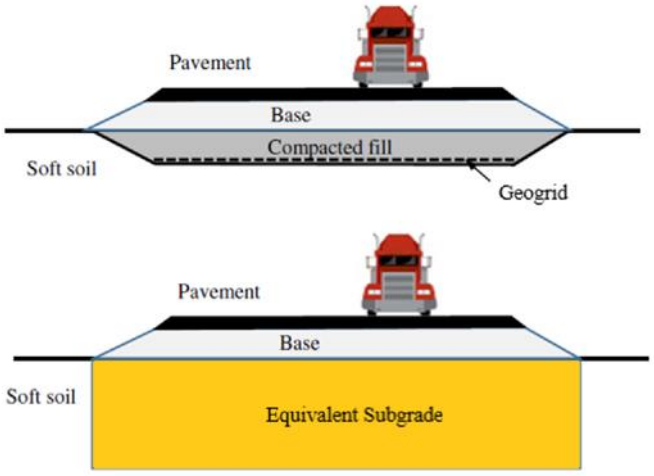

Figure 2.5 Geogrid-reinforced aggregate over weak subgrade as an equivalent subgrade (adapted from Sun et al., 2018).

Figure 2.6 presents plots of the percent of CBR increase, due to the addition of aggregate layer, with the applied pressure for different base thicknesses. It can be noticed that the increase of the CBR of the equivalent subgrade, due to the inclusion of the non-reinforced aggregate layer, tends to be higher for thicker aggregate layers and for lower applied pressures. Figure 2.7 shows plots of the percent of equivalent subgrade CBR increase, due to the addition of a geogrid (T1 or T2), with the applied pressure for different aggregate thicknesses. When geogrid was included, the percent of equivalent subgrade CBR increase, due to the geogrid, tends to be higher for thinner aggregate layers, higher stiffness geogrid and higher applied pressure. Finally, the percent of subgrade CBR increase due to the inclusion of a geogrid was estimated in the range of 30%–85%.

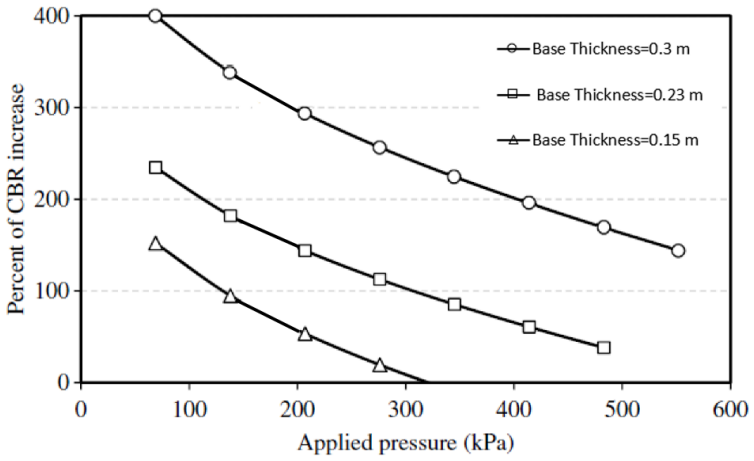

Figure 2.6 Percent of equivalent subgrade CBR increase due to the addition of aggregate layer for different aggregate thicknesses (adapted from Sun et al., 2018).

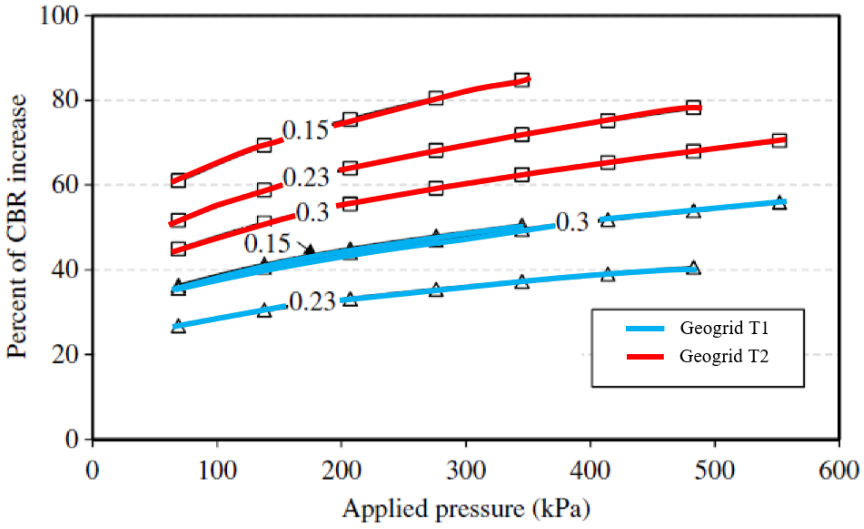

Figure 2.7 Percent of equivalent subgrade CBR increase due to the addition of a geogrid for different aggregate thicknesses (adapted from Sun et al., 2018).

2.3 Geocell-reinforced roads over weak subgrades

Geogrids and geotextiles are commonly used as planar reinforcements at the subgrade-base interface or within the base course to improve the performance of the pavement. However, a special type of geosynthetic, geocell, which is mainly used for slope stabilization, erosion protection, but also for soil reinforcement and confinement, has been studied for base course reinforcement in roadway systems since 1970s. Cellular confinement systems (geocells) are three-dimensional honeycombed polymer matrices formed by interconnected strips and infilled with aggregate or soil. Figure 2.8 shows a typical geometry of a geocell. First, geocells were made of paper, cardboard, aluminum and high-density polyethylene (HDPE), which rapidly dominated and became the most used material (Kief et al., 2015). Recently, novel polymeric alloy geocell or NPA geocell was introduced into the market. NPA geocell, which was developed by PRS Geo-Technologies Ltd., is constructed from a polymeric alloy composed of polyolefin and thermoplastic engineering polymer. Novel polymeric alloy gradually replaced HDPE, due to its high stiffness, resistance to creep, tensile strength and durability under elevated temperatures. The use of geocells constitutes a sustainable solution for road construction or rehabilitation, since a geocell infilled with locally available or recycled material reduces the quantity of virgin aggregate needed for the base course, at the same time increases the life of the pavement, and decreases the maintenance costs (Pokharel et al., 2011).

The geocell concept was initiated by the U.S. Army Corps of Engineers in the late 1970s, when they proposed the idea of using sand-grids as base layers to improve the soft subgrades of unpaved roads used by heavy military vehicles (Webster, 1979; Webster, 1981). These studies showed that sand-confinement systems could effectively replace crushed stone base layers and increase the bearing capacity of the unreinforced soil. In the late 1980s, Bathurst and Jarrett (1988) conducted large scale static load tests and showed that a geocell-reinforced gravel base was equivalent to an unreinforced gravel base with twice the thickness of the geocell. Also, they demonstrated that a stiffer geocell improved further the load-bearing capacity of the base compared to a less stiff geocell. In the 1990s, large triaxial compression tests, to study the influence of the geocell confinement on the stiffness and strength behavior of granular soils, were conducted by Bathurst and Karpurapu (1993) and Rajagopal et al (1998). They showed that the additional confinement that the geocell provided to the soil led to an increase in apparent cohesive strength,

while the friction strength of the granular soil was not affected. This additional cohesive strength is proportional to the tensile strength of the geosynthetic used to form the geocell.

In the 2000s, field tests using HDPE geocells to reinforce the base of asphalt pavements were conducted by Emersleben and Meyer (2008). The results of these tests, which were validated by large scale static load tests in the laboratory, showed that the geocell-reinforced base reduced the vertical stresses on the subgrade by about 30% compared to the unreinforced base, decreased the deflection on the surface, improved the bearing capacity of the infill material between 1.1 and 1.7 times compared to the unreinforced base and increased the stiffness of the base layer. They demonstrated that the load bearing capacity increased with increasing cell height and decreasing cell diameter. A series of static plate load tests was also conducted by Pokharel et al. (2010) and showed that the shape of the geocell, the stiffness and the type of the geocell material, and the infill material played significant roles in the performance of geocell-reinforced bases under static loading. Specifically, they concluded that geocells with a circular shape had better performance than the ones with elliptical shape and that geocells made of novel polymeric alloy had higher stiffness than geocells made of HDPE. Finally, they showed that the geocell-reinforced base could improve bearing capacity by up to a factor of 2.5 and could increase the stiffness by up to 2 times, compared to the unreinforced base.

Rajagopal et al. (2012) conducted field studies and laboratory plate loading tests to investigate the improvement in stiffness of a NPA reinforced sub-base layer of a flexible pavement. They showed that a modulus improvement factor (MIF) of 2.84 could be achieved when the geocell reinforced sub-base had the same thickness as the unreinforced sub-base. They concluded that such improvement could lead to a 50% reduction of the granular layer thickness. Most studies until 2010 focused on the performance of geocell-reinforced bases under static loading. However, geocells used in pavement applications are subjected to repeated loading. After 2010, full-scale moving wheel tests were conducted on NPA geocell-reinforced unpaved and paved road sections above weak subgrades using the accelerated pavement testing (APT) facility at Kansas State University. The findings of some of these studies (Pokharel et al., 2011; Yang et al., 2012; Bortz et al., 2012) are presented in Sections 2.3.2 and 2.3.3.

Figure 2.8 Typical geometry of geocell (https://www.agtec.com/agtec-geocell-ground-grid-paver-4-inch-8-4ft-x-27-4ft.html).

2.3.1 Reinforcement mechanisms

The most important mechanisms for geocell reinforcement are lateral and vertical confinement and tensioned-membrane effects. However, the tensioned-membrane effect is mobilized only when there is significant rutting, which is permitted in unpaved roads. Although the need for rutting could limit the use of geocells in paved roads, the base reinforcement provided by the confinement effect would still be beneficial. As Figure 2.9 shows, the geocell provides vertical confinement in two ways: (1) by friction between the infill material and the geocell wall; and (2) by restraining the soil from moving upwards outside the loading area, as the geocell-reinforced base acts as a mattress (Pokharel, 2010). In addition to the vertical confinement, the lateral confinement of the soil reinforced with a geocell results in a distribution of the load into a wider area, which reduces the vertical stresses on the top of the subgrade and increases the bearing capacity of the base. This is shown in Figure 2.10, where the pressure on the top of the subgrade (p_r) is given by the following equation:

$$p_r = \frac{b}{b + 2htan\theta_c} p_s \qquad (2.2)$$

where p_r is the pressure on the subgrade due to the vertical stress dispersion effect;

p_s is the pressure on the top of the geocell;

b is the width of the pressure p_s on top of the geocell layer;

h is the height of geocell layer; and

θ_c is the dispersion angle of geocell layer

According to Zhang et al. (2010), the bearing capacity increase (Δp_1) due to the vertical stress dispersion effect, is given by the following equation:

$$\Delta p_1 = p_s - p_r = \frac{2htan\theta_c}{b + 2htan\theta_c} p_s \qquad (2.3)$$

When there is significant rutting, a further tension force is provided by the geocell reinforcement due to the membrane effect. The vertical component of this tension force reduces the vertical deformation of the soft subgrade and increases the bearing capacity. According to Zhang et al. (2010), the bearing capacity increase (Δp_2) due to the membrane effect is given by the following equation:

$$\Delta p_2 = \frac{2Tsin\varphi}{b} \qquad (2.4)$$

where T is the tensile force of the geocell;

φ is the angle depicted in Figure 2.11; and

b is the width of the load per unit area on top of the geocell

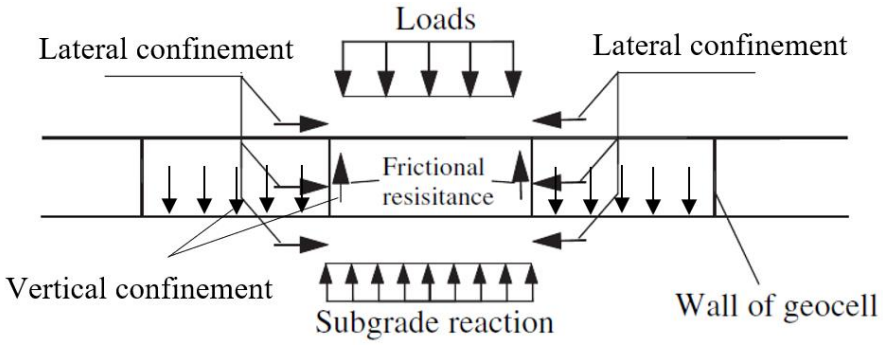

Figure 2.9 Lateral and vertical confinement of the geocell reinforcement (adapted from Zhang et al., 2010).

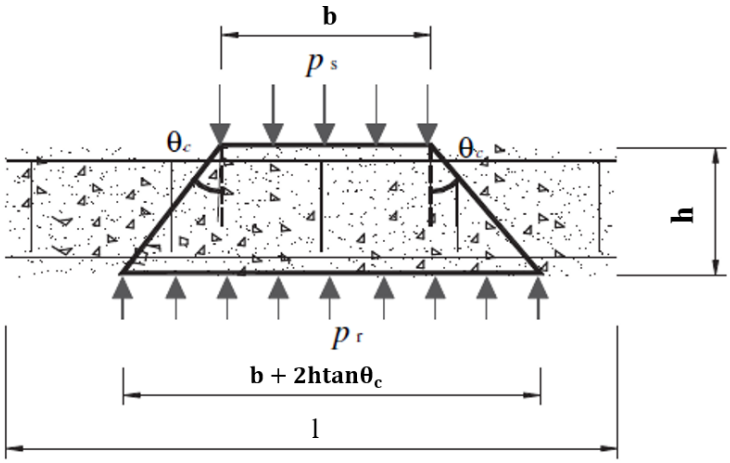

Figure 2.10 Vertical stress dispersion effect of geocell layer (adapted from Zhang et al., 2010).

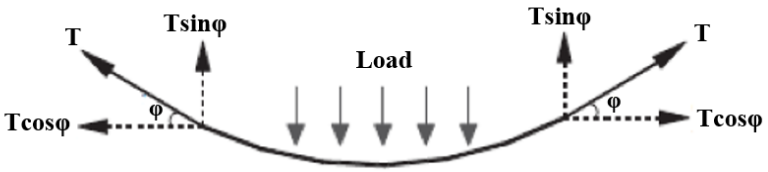

Figure 2.11 Vertical tensioned-membrane effect of the geocell (adapted from Zhang et al., 2010).

On the other hand, Koerner (2005) presented a bearing capacity calculation based on the conventional plastic limit equilibrium mechanism as used in statically loaded shallow foundation bearing capacity. The shear strength between geocell wall and infill soil was considered as the increase in bearing capacity (Δp) of the soil. He suggested that the bearing capacity increase is given by the following equation:

$$\Delta p = 2\tau \qquad (2.5)$$

where τ is the shear strength between geocell wall and soil contained within it:

$$\tau = p tan^2(45 - \varphi/2) tan\theta \qquad (2.6)$$

p is the applied vertical pressure acting on the geocell reinforcement;

φ is the friction angle of soil used to fill the geocell pockets; and

θ is the angle of shearing resistance between soil and the cell wall material (15–20° between sand and HDPE, 25–35° between sand and the nonwoven geotextile)

2.3.2 Rut depth reduction

As it was noted before, geocells are three-dimensional geosynthetics that can be filled with different types of materials and, thus, they can enhance the strength of a soils, which might be locally available. The performance of a geocell infilled with poorly graded, waste or recycled material in terms of rut depth can be similar or even better than that of an unreinforced high-quality aggregate material. The investigation of the performance of different infill materials inside the geocell was the objective of Pokharel et al. (2011) who conducted moving-wheel tests at the Accelerated Pavement Testing (APT) facility at Kansas State University. Specifically, they constructed three geocell-reinforced sections with well-graded aggregate (AB-3), quarry waste (QW), and recycled asphalt pavement (RAP), and one unreinforced section with aggregate AB-3 as a base course. Figure 2.12 shows the cross sections of the test sections with the thickness of each layer. The reinforced sections included 15 cm geocell-reinforced base with 2 cm fill material as a cover and a nonwoven geotextile that was placed as a separator between the subgrade and the reinforced base. Sections 2, 3 and 4 consisted of quarry waste, RAP and aggregate AB-3 as infill material, respectively. The unreinforced section consisted of 30 cm of unreinforced aggregate AB-3. Finally, the geocell used in this study was made from NPA material and the subgrade was classified as A-7-6 clay with CBR = 3.

Figure 2.13 shows the development of the measured rut depths for each test section with increasing number of wheel passes. It can be observed that section 2, with the geocell-reinforced quarry waste, showed the worst performance with a rapidly increasing rut depth, which surpasses the allowable rut depth for unpaved roads (7.5 to 10 cm) after the first 100-wheel passes. On the other hand, sections 3 and 4, with geocell-reinforced RAP and geocell-reinforced AB-3, showed a significant decrease in the rut depth compared to the unreinforced section, with section 3 having the smallest rut depth of all. Although section 4 had a thinner base course layer than section 1, 15 cm geocell-reinforced aggregate with 2 cm cover fill performed better than the 30 cm unreinforced aggregate base course. Finally, RAP as an infill material led to smaller rut depth than the AB-3 aggregate, as the number of passes increased, but both the geocell-reinforced sections failed after 305 wheel passes. A total of 305 passes is considered small for a low-volume local road but it

might be acceptable for temporary roads or construction platforms (Pokharel et al., 2011). Low-volume roads are defined as rural roads with fewer than 1000 vehicles per day for most times of the year (Gross et al., 2011).

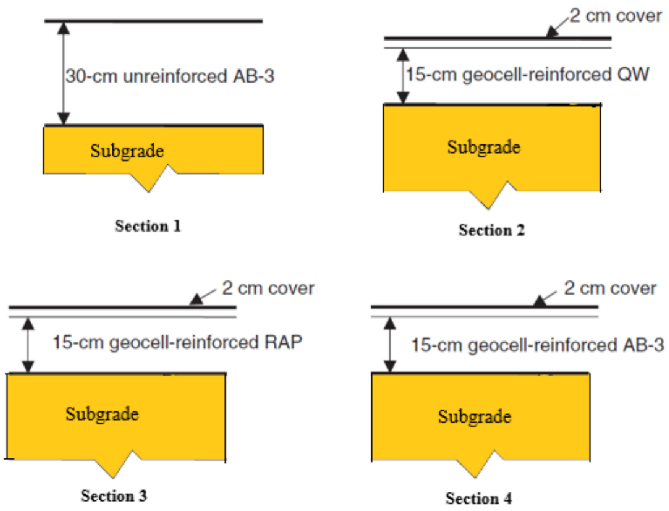

Figure 2.12 Layer profiles of the test sections (adapted from Pokharel et al., 2011).

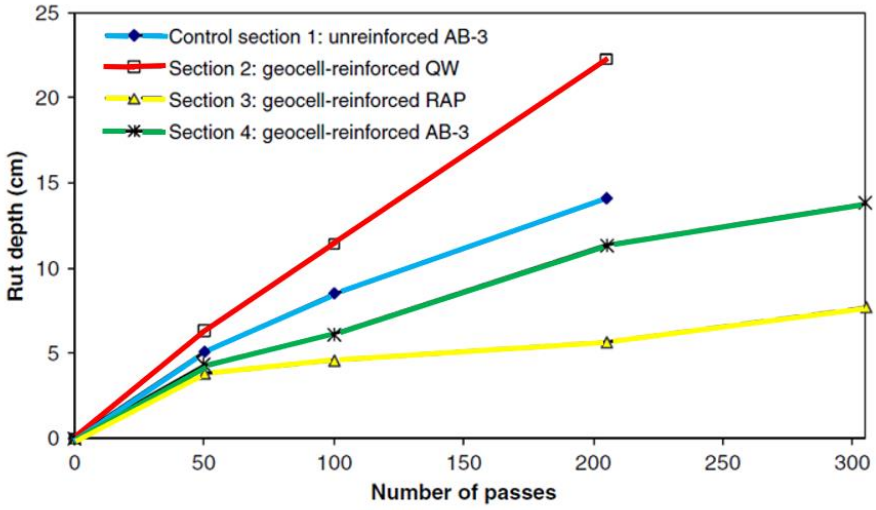

Figure 2.13 Development of rut depth with increasing number of wheel passes (adapted from Pokharel et al., 2011).

A following study was conducted by Yang et al. (2012), who tested geocell-reinforced sand bases, and unreinforced sand (Kansas river sand) and aggregate bases using the Accelerated

Pavement Testing (APT) facility at Kansas State University. Four unpaved road sections were initially constructed in a test pit; two had reinforced sand bases with geocell and the other two had unreinforced sand bases. The cross sections of the pavements are presented in Figure 2.14. The unreinforced sections 0-a and 0-b consisted of 15 cm and 10 cm of sand, respectively, while the reinforced sections 2 and 3 consisted of geocells infilled with sand with the same thickness as sections 0-a and 0-b. On top of the reinforced and unreinforced bases, 7 cm of aggregate was placed. Figure 2.14 also depicts two more sections, sections 1 and 4, which were constructed right after the early failure of the two unreinforced sand bases. Sections 1 and 4 consisted of 22 cm and 17 cm of unreinforced aggregate, respectively.

The geocell used in this study was made of NPA material and the dimensions of the pockets were 25 cm long by 21 cm wide. In the sections where geocell was used, a non-woven geotextile was placed on the subgrade as a separator between the base course and the subgrade. The subgrade was classified as A-7-6 and a CBR of 5 was achieved. Figure 2.15 shows the development of rut depth with increasing number of wheel passes for all the test sections. The unreinforced sections 0-a and 0-b failed after the first wheel pass and later they were replaced by sections 1 and 4, which had much better performance than the previously constructed sections. Also, the unreinforced section 1 and the reinforced section 2, with the same base course thickness, achieved the same rut depth, which implies that 15 cm reinforced sand with 7 cm aggregate cover has a similar performance than a 22 cm unreinforced higher-quality aggregate, both on the same subgrade. Finally, section 3 exhibited extremely high rut depths after 1000-wheel passes compared to the unreinforced section 4, which had the same thickness. The geocell-reinforced sand failed due to tensile failure of some geocell joints in the thin base course, which was unable to carry the traffic load.

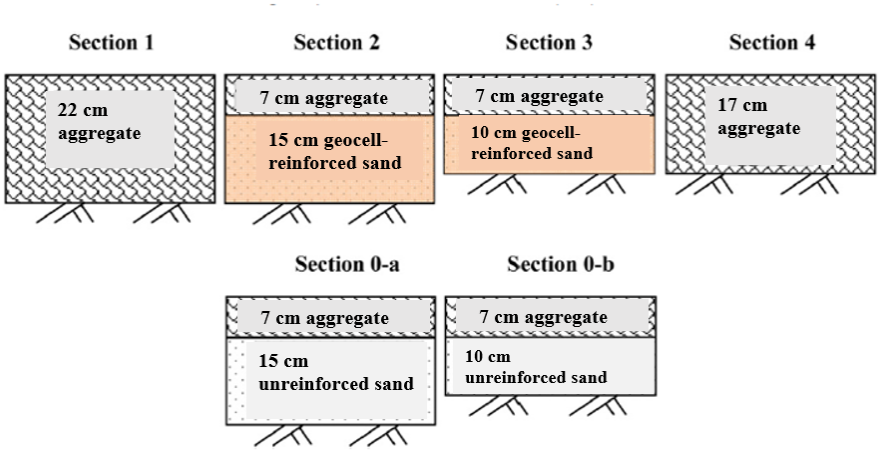

Figure 2.14 Pavement test section profiles (adapted from Yang et al., 2012).

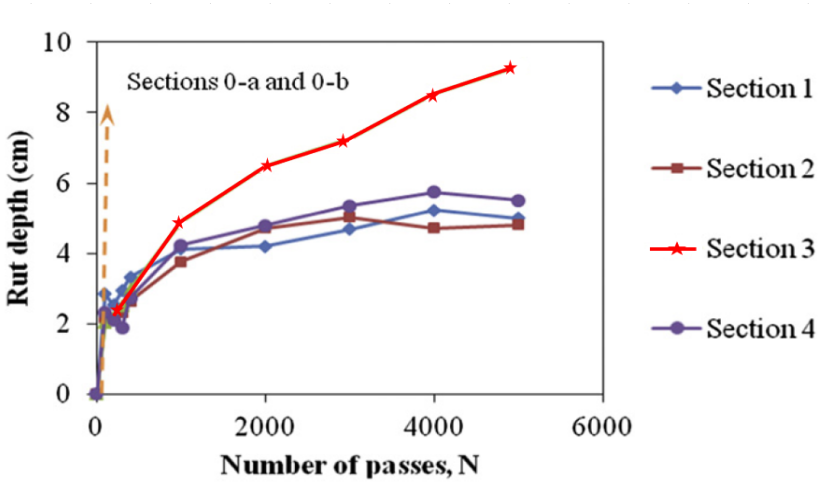

Figure 2.15 Development of rut depth with increasing number of wheel passes (adapted from Yang et al.,2012).

Comparing the results of these two studies, one can see that the section with the geocell-reinforced sand (7 cm aggregate + 15 cm geocell-reinforced sand) failed after 5000 wheel passes, while the sections with geocell-reinforced aggregate and RAP (2 cm fill cover + 15 cm geocell-reinforced base) failed after 300 passes. This indicates that the cover layer thickness and material as well as the strength of the subgrade play an important role in the performance of geocell-reinforced pavements. The section with the geocell-reinforced sand exhibited the largest improvement, increasing the life of the pavement and reducing the quantity of aggregate needed.

The previously mentioned studies referred to cases of unpaved roads and how a geocell could contribute to the reduction of rut depth. Bortz et al. (2012) tested geocells with different infill

materials and a thin HMA overlay on a subgrade classified as A-7-6 clay (CBR = 6), under accelerated pavement testing (APT), to observe how geocells perform in a low-volume paved road system. Similar to what Pokharel et al. (2011) did, they compared the performance of the following infill materials: crushed limestone (AB-3), quarry waste, and RAP. They constructed four lanes of pavement test sections at the Civil Infrastructure System Laboratory (CISL) of Kansas State University (KSU). In their first test, they placed thinner layers of all the materials. The test failed in less than 80,000 repetitions of an 80-kN single axle load. Pavement cross sections from the first test are depicted in Figure 2.16. Lane 1 was made of 300 mm aggregate AB-3 while lanes 2, 3 and 4 consisted of 75 mm geocell with infill material (quarry waste, RAP, and aggregate AB-3) and 25 mm cover. All the lanes, finally, were overlaid with 50 mm HMA. In the second test, they increased the thickness of the layers and achieved 1,200,000 load repetitions without failure. Pavement cross sections for the second test are depicted in Figure 2.17. Lane 1 had 200 mm aggregate AB-3, while lanes 2, 3 and 4 consisted of 100 mm geocell with infill material (quarry waste, RAP, and aggregate AB-3) and 50 mm cover. All the lanes were overlaid with 100 mm HMA.

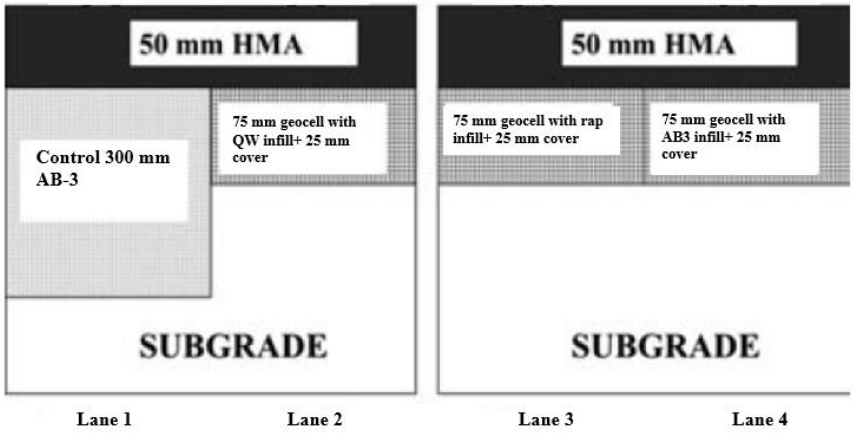

Figure 2.16 Pavement cross sections for the first test (adapted from Bortz et al., 2012).

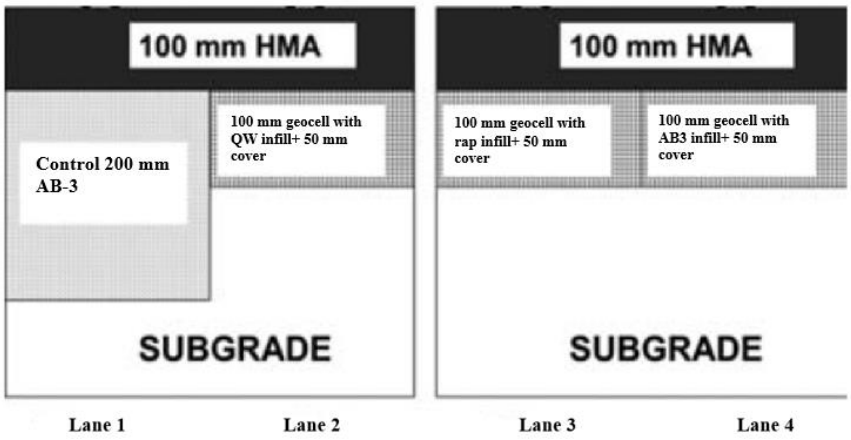

Figure 2.17 Pavement cross sections for the second test (adapted from Bortz et al., 2012).

The results of the first test showed that the thickness of the pavement layers was not enough to carry the traffic load. This is shown in Figure 2.18, which is a plot of the average rut depth versus the number of wheel passes for lanes 1 and 2, for the first and second tests. Figure 2.19 shows the development of rut depth with increasing number of passes for lanes 3 and 4, for the second test. All the reinforced and unreinforced pavement sections with the increased thicknesses achieved a rut depth smaller than 10 mm after 1,200,000 repetitions of the load. This fact shows that 100 mm of HMA is the minimum thickness that can carry the load. In addition, 100 mm geocell with infill material such as quarry waste, RAP or crushed limestone covered by 50 mm of infill can effectively replace a 200 mm crushed limestone layer. Thus, with the use of geocell reinforcement in the base course not only good quality materials such as crushed limestone AB-3 can be replaced by marginal materials, but also a reduction of 25% in the thickness of the base layer can be achieved.

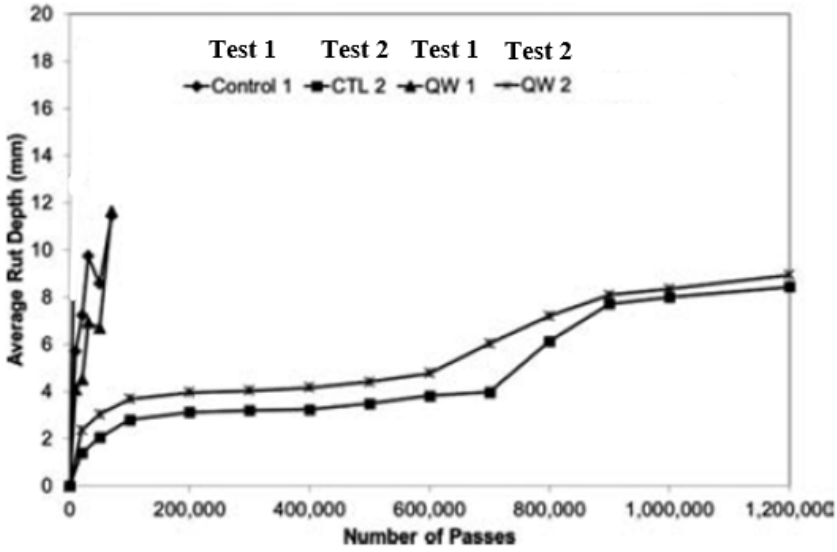

Figure 2.18 Development of the average rut depth with increasing number of wheel passes for lanes 1 and 2 of the two tests (adapted from Bortz et al., 2012).

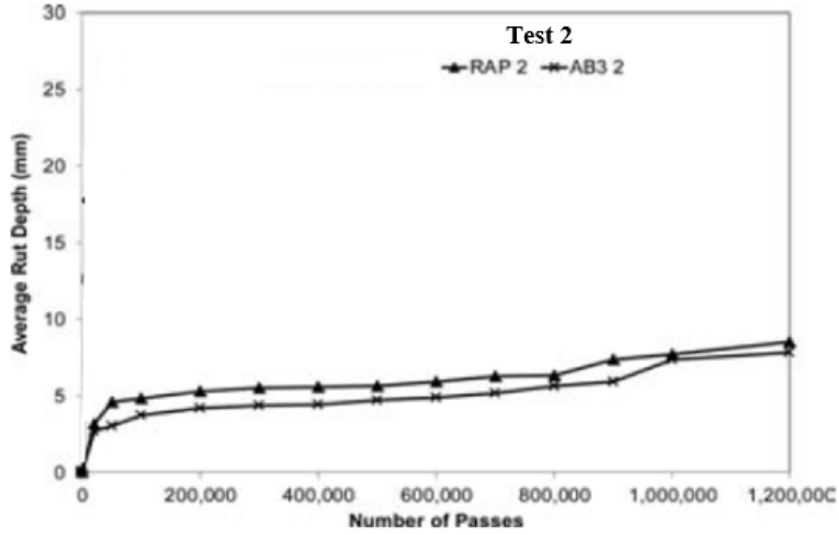

Figure 2.19 Development of the average rut depth with increasing number of wheel passes for lanes 3 and 4 of the second test (adapted from Bortz et al., 2012).

2.3.3 Load distribution

As discussed, a thinner geocell-reinforced base can lead to similar or even better performance in terms of rutting compared to an unreinforced base in unpaved and paved road systems. Another important factor that helps understand and quantify the benefits of geocell

reinforcement is how the vertical stress is transmitted to the subgrade. In the study of Pokharel et al. (2011), the vertical stresses on the subgrade were measured by pressure cells located at the subgrade–base interface. The authors noticed that the 17 cm geocell-reinforced AB-3 section had stresses similar to those of the unreinforced section with 30 cm aggregate AB-3. This implies that the thinner reinforced base achieved a stress reduction on the subgrade by distributing the load to a wider area. The calculated stress distribution angle for the unreinforced section was 29.2° while for the reinforced RAP and AB-3 section was 40.8° and 43.6°, respectively. According to Figure 2.20, the stress distribution angle, after 100-wheel passes, is obtained as:

$$p_i = \frac{P}{\pi(r + htan\alpha)^2} \tag{2.7}$$

where p_i is the distributed vertical stress on top of the subgrade (kPa);

P is the wheel load (kN);

r is the radius of tire contact area;

h is the thickness of base course; and

α is the distribution angle

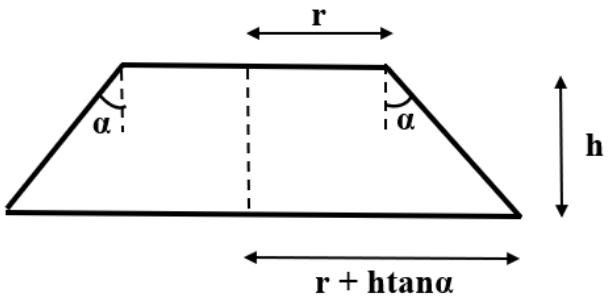

Figure 2.20 Vertical stress dispersion effect in the base course layer.

Different observations were made by Berg et al. (2012) for the paved road systems. They observed that the unreinforced pavement sections resulted in the lowest stresses on the subgrade due to their larger thickness compared to the geocell-reinforced pavement sections.

2.4 Geosynthetic-reinforced embankments over weak foundations

Excessive differential settlements and instabilities are the major concerns when designing embankments over soft foundation soils. Geosynthetics have been utilized as reinforcement below embankments on weak soils since the late 60s (John, 1987). Until then, the traditional methods to improve the foundation had been to drive piles through the weak soil, excavate and replace the weak foundation materials with suitable soil, inject additives for soil stabilization, or surcharge and wait until consolidation happens (Koerner, 2005). All these foundation improvements are time-consuming and expensive compare to geosynthetic-reinforcement methods.

Geosynthetic-reinforcement may be used to improve the bearing capacity of a foundation on soft soil. The reinforcement is placed at the base of the embankment. It is important to mention that, although geosynthetics can improve short-term performance, i.e. bearing capacity, immediate settlements, resilience under repeated loading and constructability, they will not reduce long-term settlements due to consolidation or creep of the underlying soil. Reinforcement is only required to maintain stability during construction and during primary consolidation until the foundation soil has gained shear strength (Jewell, 1988). As one can see from Figure 2.21, geosynthetic-reinforcement can be used to maintain the factor of safety above one for the reinforced embankment until the soft foundation has consolidated sufficiently. It can also be seen that the factor of safety with reinforcement decays with time during construction and during the subsequent consolidation, which might be caused by the creep behavior of geosynthetics.

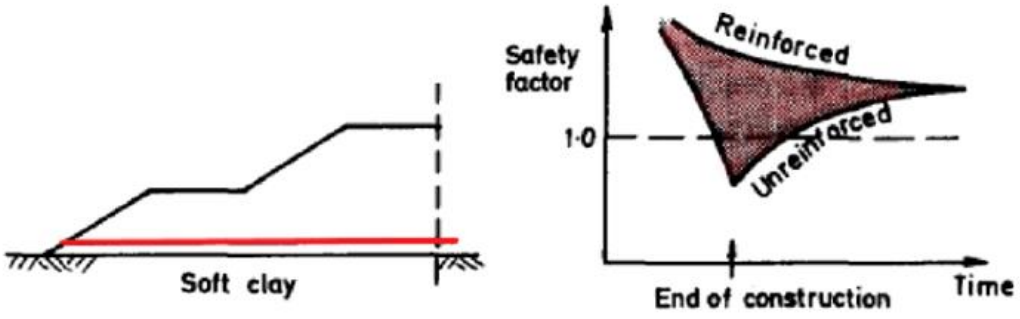

Figure 2.21 Geosynthetic-reinforced embankment over soft soil (adapted from Jewell, 1988).

When embankments are constructed over soft soils, the outward lateral thrust created by the horizontal stresses in the embankment fill results in outward shear stresses at the base of the embankment that reduce the bearing capacity of the foundation and hence the embankment stability. Basal reinforcement can support part or all of the embankment outward shear stresses, and, as a result, improve the bearing capacity of the foundation and restrain the lateral deformations of the embankment. If the reinforcement interlocks well with the foundation surface, then it provides inward (resisting) shear stresses which improve further the bearing capacity. The forces resisting failure can only be beneficial if either the soil strength increases with depth or the soil is of limited depth, or a combination of these (Jewell, 1988).

In general, a geogrid placed between an embankment and its foundation can reinforce the embankment in the following four ways: (1) Increasing the stability against bearing capacity failure of the embankment; (2) Increasing the stability against slope failure; (3) Bridging over weak zones in the foundation; and (4) Restricting the lateral movement of the embankment (Wu et al., 1992). The four functions of reinforcement are depicted in Figure 2.22.

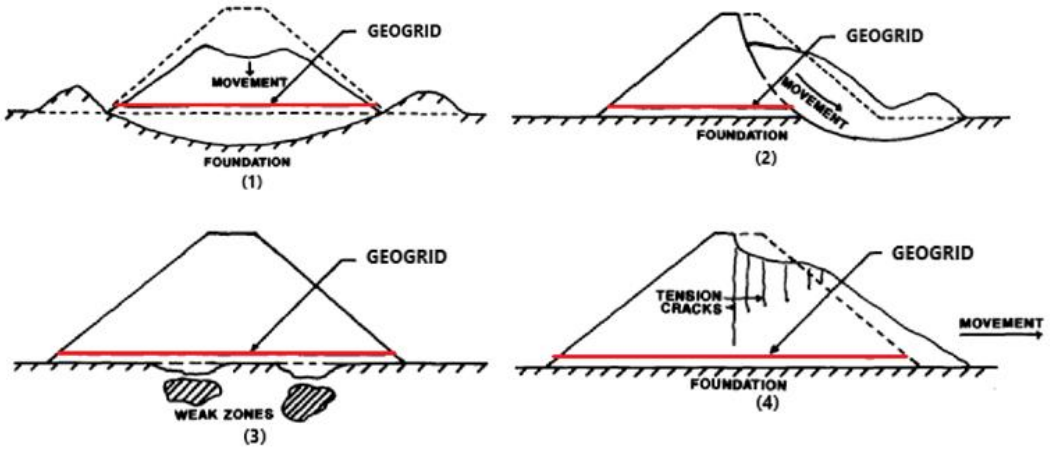

Figure 2.22 Functions of geogrid in reinforced embankments: (1) Increasing bearing capacity; (2) Increasing stability against slope failure; (3) Bridging over weak foundation zones; and (4) Reducing lateral spreading (adapted from Wu et al., 1992).

A study by Rowe and Soderman (1984) showed the beneficial effects of geotextile-reinforcement on an embankment constructed over a clay deposit. Two test embankments, an unreinforced and a geotextile-reinforced, were constructed over a 3.3 m thick soft clay deposit underlain by a dense sand layer at Almere in The Netherlands. A woven geotextile with a tensile

stiffness of 2000 kN/m was placed at the base of the embankment. The reinforced embankment experienced a failure at a height of 2.75 m, while the unreinforced embankment failed rapidly at a height of 1.75 m. A 60% increase in failure height with reinforcement was observed. Results from finite element analyses provided a good agreement with the field observed behavior. The analyses showed that the reinforcement restricted the extent of the plastic region in the soil, and hence increased the failure height of the embankment.

Humphrey and Holtz (1986) presented a review of 37 case histories of reinforced embankments. All the embankments, having heights greater than 1 m, were constructed over soft organic soils underlain by a stronger soil layer. In many cases, a combination of geosynthetics with other measures such as wick or sand drains, staged construction, or berms was used to maintain stability. The causes of failure for the reinforced embankments were reported to be excessive deformation when low modulus reinforcement was used, tensile failure of the reinforcement, and the pulling apart of overlapped joints or sewn seams in the geotextile. One of the major findings of this study was that, in many cases, the failure height of the embankment predicted by the classical bearing capacity theory was significantly less than the actual failure height. Moreover, in four cases, the failure heights of the reinforced embankments were 0.9 to 2 m greater than the heights of the unreinforced embankments, which shows the beneficial effect of reinforcement on stability.

The benefits of basal reinforcement on the stability of embankments constructed over soft clays are also highlighted by Bergado et al. (1994). Two test embankments were constructed to failure: an unreinforced embankment and an embankment reinforced with a high-strength, nonwoven geotextile as base reinforcement. It was shown that the high-strength geotextile considerably increased the failure height of the embankment on soft clay. A 50% increase in failure height was observed.

A study undertaken by Wu et al. (1992) discussed the effectiveness of tensile reinforcement for reducing settlements of an embankment constructed over a weak foundation. They found that when an embankment deforms significantly in the lateral direction, then tensile reinforcement is effective in reducing differential settlements and in increasing embankment stability. If small lateral deformations are expected, then tensile reinforcement has a minor beneficial effect.

In an earlier JTRP research study by Ludlow et al. (1992), a number of case histories were summarized, and numerical modeling was performed. The synthesis of the case histories

confirmed the role of geosynthetic base reinforcement in improving the bearing capacity of embankments on soft foundation soil, and the numerical models were consistent with this finding.

2.4.1 Geocell-reinforced embankments

Geocells are geosynthetic products that can be used as a reinforcement layer at the base of an embankment constructed over a soft foundation. A detailed description of geocell materials, the reinforcement mechanisms that govern their behavior, and their application in pavements were presented in Section 2.3. The performance of geocell-reinforced embankments on soft soils has been investigated through laboratory, field, and numerical studies for the past three decades.

Bush et al. (1990) presented case histories of monitored performance for geocell-reinforced embankments that showed the effectiveness of a geocell mattress in reducing differential settlements and in increasing bearing capacity of the soft foundation. The inclusion of a geocell mattress at the base of an embankment provides a restraining effect against the deformation of the soft foundation due to the two following characteristics of the geocell: (1) a rough interface between the fill material in the geocell and the soft foundation; and (2) a stiff platform that helps to even the distribution of the load onto the foundation (Bush et al., 1990).

Cowland and Wong (1993) presented a case study of a geocell-reinforced embankment on soft clay. A geocell mattress foundation, together with pre-fabricated wick drains to facilitate consolidation of the clay, was used to support the embankment. The geocell, formed using high-density polyethylene (HDPE) geogrids, was filled with angular rockfill allowing good interlocking between the rockfill and the geogrids. Instrumentation monitoring of the geocell layer showed that it was elongated by less than 1%, which is much smaller than typical observations for geotextiles, in the range of 3-6%. The small lateral extension and deflected shape of geocell led to the conclusion that the geocell mattress behaved like a stiff raft foundation of the embankment.

Rajagopal et al. (1999) studied the improvement in strength and stiffness of geocell-reinforced soils. They conducted a series of triaxial compression tests on granular soil encased in single and multiple geocells, which were fabricated from different types of geotextiles and mesh elements. It was observed that the granular soil developed an apparent cohesive strength due to the confinement by the geocell. This cohesive strength was found to be dependent on the stiffness of the geosynthetic used to form the geocell. The frictional strength of the encased soil remained unaffected by the confinement. The development of apparent cohesion was attributed to the

increased confining stress created in the soil due to the membrane stresses in the geocell walls. Mohr circles were used for the calculation of the apparent cohesion of the geocell-soil composite. The following relation was obtained:

$$c_r = \frac{\Delta\sigma_3}{2}\sqrt{\frac{1+sin\varphi}{1-sin\varphi}} \qquad (2.8)$$

where $\Delta\sigma_3$ is the additional confining stress; and

φ is the friction angle of the soil

The additional confining pressure ($\Delta\sigma_3$) was estimated from the rubber membrane theory of Henkel and Gilbert (1952), and is given by:

$$\Delta\sigma_3 = \frac{2M}{d_o}\left[\frac{1-\sqrt{1-\varepsilon_a}}{1-\varepsilon_a}\right] \qquad (2.9)$$

where ε_a is the axial strain at failure;

d_o is the initial diameter of individual cell pockets (m); and

M is the secant modulus of the membrane of the cell at an axial strain of ε_a (kN/m)

The improvement in the performance of embankments constructed over soft clays due to the inclusion of a geocell reinforcement layer was also investigated by Krishnawamy et al. (2000). Results from a series of load tests on model embankments with and without geocell-reinforcement were presented. The increase in the surcharge capacity at the crest of the embankment and decrease in settlements were used to ascertain the improvement of performance of the embankment. In general, the geocell-reinforced embankments had higher surcharge capacities and lower settlements compared to unreinforced embankments. This can be seen in Figure 2.23, where the embankment (with a height of 400 mm) supported on a 100-mm-thick geocell layer made of uniaxial geogrid had almost twice the surcharge capacity of the unreinforced embankment. The influence of the type of geogrid used to form the geocell was also investigated and the results are shown in Figure 2.23. It was found that geogrids with higher stiffness were more effective in reducing settlements than those with lower stiffness. The aspect ratio (height to diameter ratio) of the geocell pocket was also found to have a significant influence. An increase in the height of the geocell layer, keeping the diameter of the geocell pocket constant, resulted in higher surcharge

capacity. The optimum height to diameter ratio, above which changes in surcharge capacity were not significant, was found to be 0.5.

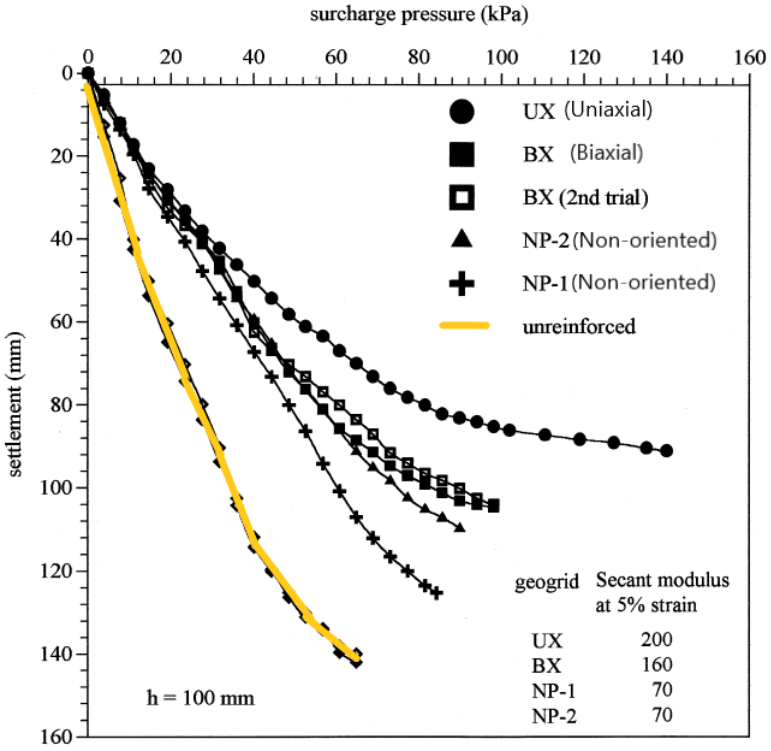

Figure 2.23 Influence of geogrid stiffness on the pressure-settlement curve (adapted from Krishnawamy et al., 2000).

A two-dimensional model for the geocell-soil composite, that can replicate the behavior of a three-dimensional system, was proposed by Rajagopal et al. (2001). The model was validated against experiments on geocell-reinforced embankments constructed over soft clay. Rajagopal et al. (2001) developed simple equations to correlate the shear strength and stiffness of the geocell with the geocell properties. The apparent cohesion of the geocell-soil composite due to single geocell encasement is given by Equation 2.8. It was also found that the stiffness of the geocell-soil composite increases with an increase in the confining pressure exerted in the soil by the geocell walls. Madhavi Latha (2000) proposed the following empirical equation for the Young's modulus of the geocell encased soil (E_g), following the hyperbolic equation by Duncan and Chang (1970):

$$E_g = K_r P_a \left(\frac{\sigma_3}{P_a}\right)^{0.7} \qquad (2.10)$$

where P_a is the atmospheric pressure (≈ 101.3 kPa);

σ_3 is the confining pressure (kPa); and

K_r is the dimensionless modulus parameter of the reinforced sand, given by

$$K_r = K_u + 200M^{0.16} \quad (2.11)$$

where M is the secant modulus of the geocell material (kN/m); and

K_u is the dimensionless modulus parameter of the unreinforced sand

The model by Rajagopal et al. (2001) was verified through a finite element analysis of model embankments tested in the laboratory by Madhavi Latha and Rajagopal (2007). Parametric finite element analyses on full-scale geocell-reinforced embankments were carried out to investigate the effect of parameters such as the dimensions of the geocell layer, the tensile strength of the geocell material, the properties of the infill soil, and the depth of the soft foundation soil. The model used for the parametric analysis is depicted in Figure 2.24. The optimum aspect ratio (height to diameter ratio) of the geocell pocket was found to be 1. The influence of the stiffness of the geocell material was also investigated and the results agreed with those of Krishnawamy et al. (2000). An increase in the modulus of the geocell resulted in a reduction of the settlements at the crest of the embankment. An increase of the modulus above 200 kN/m did not significantly increase the surcharge capacity of the embankment. The lateral deformations in the embankment, where granular soil fill was used for the geocell, were 20% less than those with cohesive soil fill. Thus, granular soils were proposed as the optimum material for fill inside the geocell. Finally, the performance of the geocell-reinforced embankment deteriorated with the increase of the depth of the foundation soil.

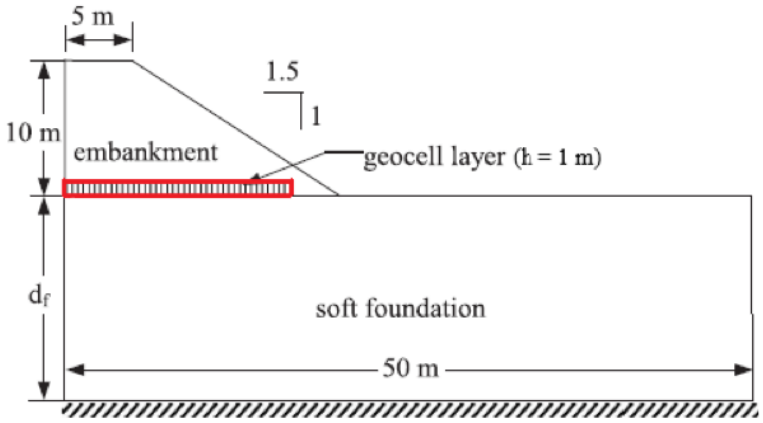

Figure 2.24 Embankment model used for parametric analysis (adapted from Madhavi Latha and Rajagopal, 2007).

The model described by the Equations 2.8 to 2.11 simplifies the geocell-reinforced soil to a homogenous composite material with improved strength and stiffness properties. Although this model led to a better understanding of the parameters affecting the performance of geocell-reinforced embankments, researchers in the past decade have questioned the validity of this two-dimensional (2-D) approach. Yang et al. (2010) identified as a limitation of the 2-D model the case where a geocell-reinforced layer is subjected to a concentrated vertical force, such as the wheel load. In this case, the confining stress provided by the geocell, and thus the stiffness of the layer, may not be the same throughout the geocell layer. For this reason, researchers attempted to study the geocell-soil interaction by modeling the complex three-dimensional (3-D) structure of the geocells (Han et al., 2008; Yang et al., 2010; Hegde and Sitharam, 2015). However, due to the complexity of the honeycomb shape of geocells, many of them have used simplified shapes to model the geocell pockets. According to Yang et al. (2010), the characteristics of geocell-reinforcement that can be simulated by modeling the geocell and soil separately are: (1) the increase in strength of the geocell-soil composite due to geocell confinement; (2) the confining effect of geocell on the infill soil; and (3) the interface friction between geocell and soil.

2.5 Use of geosynthetics by DOTs

This section focuses on the practices of selected state DOTs regarding the use of geosynthetics in roadway applications. The practices regarding the use of geosynthetics for the

functions of separation, stabilization and reinforcement of the pavement layers are thoroughly studied.

Washington State DOT (WSDOT) uses geosynthetics in roadways for two main functions: separation and soil stabilization. A geotextile can be used as a separator in roadway applications where the subgrade can be prepared and compacted as required in the Standard Specifications. Removal of the subgrade and replacement with granular material defeat the purpose of the geotextile separator. In general, WSDOT notes that separation geotextile is needed if the subgrade resilient modulus is between 5,800 psi and 15,000 psi. WSDOT follows the requirements of AASHTO M 288, Class 2, for separators. Geotextiles used for soil stabilization must function as a separator, a filtration layer, and a reinforcement layer. Soil stabilization geotextiles are used in roadway applications if the subgrade is too soft and wet to be prepared and compacted as required in the Standard Specifications. Soil stabilization geotextiles are placed directly on the soft subgrade material, even if some over-excavation of the subgrade is performed. In general, a soil stabilization geotextile is needed if the subgrade resilient modulus is less than or equal to 5,800 psi, or if a saturated fine sandy, silty, or clayey subgrade is present. Soil stabilization geotextiles should not be used under roadway fills greater than 5 ft high or on extremely soft subgrades. WSDOT follows the requirements of AASHTO M 288, Class 1, for stabilization geotextiles (WSDOT Design Manual, 2009).

New York State DOT (NYSDOT) follows the guidelines by Holtz et al. (2008) published by FHWA. Geotextiles are used in roadway applications for the function of separation and soil stabilization. The geotextile requirements are based on AASHTO M 288 Specification for Geotextiles and material properties listed in National Transportation Product Evaluation Program (NTPEP)'s DataMine. In NYSDOT Geotechnical Design Manual (2018), it is stated that it is not the practice of the NYSDOT to consider the reinforcing effect of the geotextile in pavement design. In that case, a geogrid is used as reinforcement and the geotextile, if used, is assumed to act only as a separator. Another use of geogrids, that is mentioned in the NYSDOT GDM, is as embankment base reinforcement.

California DOT (Caltrans) uses the following three methods for improvement of low-quality subgrade: (1) mechanical stabilization (compaction and blending); (2) chemical stabilization, or (3) subgrade enhancement geosynthetics. Caltrans Highway Design Manual (2020) mentions that, on soft subgrade soils, the geosynthetic may replace some or all stabilizing material such as lime

or cement used solely as a working platform for the construction of subsequent layers. The geosynthetics used for this purpose are geotextiles and geogrids, which are placed between the pavement structure and the subgrade, which is usually untreated. Subgrade stabilization is the primary function for geogrids installed between an aggregate base and subgrade layer. The primary functions of geotextiles are separation, stabilization, filtration, reinforcement, and drainage. Caltrans Highway Design Manual (2020) refers to the following criteria for the selection of subgrade enhancement geosynthetic, which are also depicted as a flowchart in Figure 2.25:

- Geogrids are most applicable for subgrades with resilient modulus $M_r < 5{,}000$ psi. For Mr between 5,000 and 9,500 psi the engineer may consider using geogrids for base reinforcement.
- Geotextiles are most applicable for subgrades with resilient modulus $M_r < 4{,}500$ psi. For Mr between 4,500 and 9,500 psi, the engineer may consider using a geotextile as a separator.
- On very soft subgrade conditions ($M_r < 3{,}000$ psi), consider placing a thicker initial lift (minimum of 6 inches) of subbase or aggregate base material on top of the geosynthetic to effectively bridge the soft soils and avoid bearing capacity failure under construction traffic loading.
- Use of geogrid is not recommended unless the materials meet the following natural filter criteria:

  $(D_{15}\text{Aggregate Base}/D_{85}\text{Subgrade}) \leq 5$ and $(D_{50}\text{Aggregate Base}/D_{50}\text{Subgrade}) \leq 25$, where D_{15}, D_{85}, and D_{50} are grain sizes of the soil particles for which 15 percent, 85 percent, and 50 percent of the material is smaller than these sieve sizes.
- If the aggregate base material does not meet the above natural filter criteria, geotextiles that meet both separation and stabilization requirements are recommended.
- Do not use geosynthetics for subgrade with $M_r > 9{,}500$ psi, because stabilization of the subgrade is not required and application of geosynthetics will not impart significant benefit to the pavement.

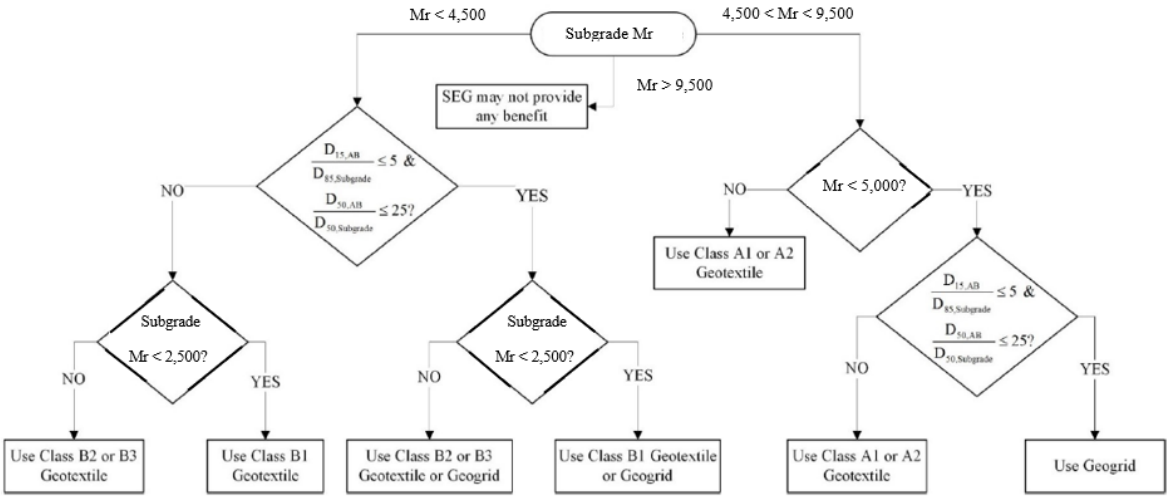

Figure 2.25 Flowchart for the selection of SEG, Subgrade Enhancement Geosynthetic (M_r is the resilient modulus) (adapted from Caltrans Highway Design Manual, 2020).

Pennsylvania DOT (PennDOT) specifies geosynthetics for separation, stabilization and reinforcement in roadway applications. Specifically, biaxial geogrids and high-strength woven geotextiles are used for subgrade stabilization and reinforcement. Non-woven geotextiles are used for separation. In contrast with other DOTs, PennDOT uses geocells in subgrade stabilization applications where soft or unstable subgrades are anticipated or identified during construction. PennDOT Geotechnical Design Manual (2018) notes that geocells filled with coarse aggregate is an effective method for carrying the wheel loads over soft subgrade with resilient modulus less than or equal to 4,500 psi. For subgrades with resilient modulus greater than 4,500 psi, it may be more appropriate and cost effective to increase the aggregate thickness and/or use a geogrid in the subbase layer. For that purpose, an economic analysis needs to be performed to prove that it is cost effective to use a geocell layer instead of a biaxial geogrid in the subbase layer or simply increase the subbase thickness (PennDOT GDM, 2018). PennDOT specifies three different types of geocells based on the cell area: Type A (44.8 in^2), Type B (71.3 in^2), and Type C (187.0 in^2). Types A and B are used in practice for subgrade stabilization applications. The following guidelines are used by the department for the selection of an appropriate geocell to stabilize the unstable subgrade:

- The geocell should be placed as close as possible to the applied load to be more effective. A minimum of 1 in of aggregate surface should be placed above the geocell to protect it. If the required thickness of subbase is greater than the thickness of the geocell, then the additional thickness of subbase should be placed below the geocell, as seen in Figure 2.26.
- Aggregate infill material such as PennDOT No. 2A coarse aggregate should be used.
- A separation geotextile is always placed under the geocell to prevent fines migrating into and contaminating the geocell infill.
- The required geocell height increases as the resilient modulus of the subgrade decreases. Standard available geocell heights range from 3 to 8 in for each geocell type.

Figure 2.26 depicts a typical PennDOT pavement section with a geocell stabilization layer.

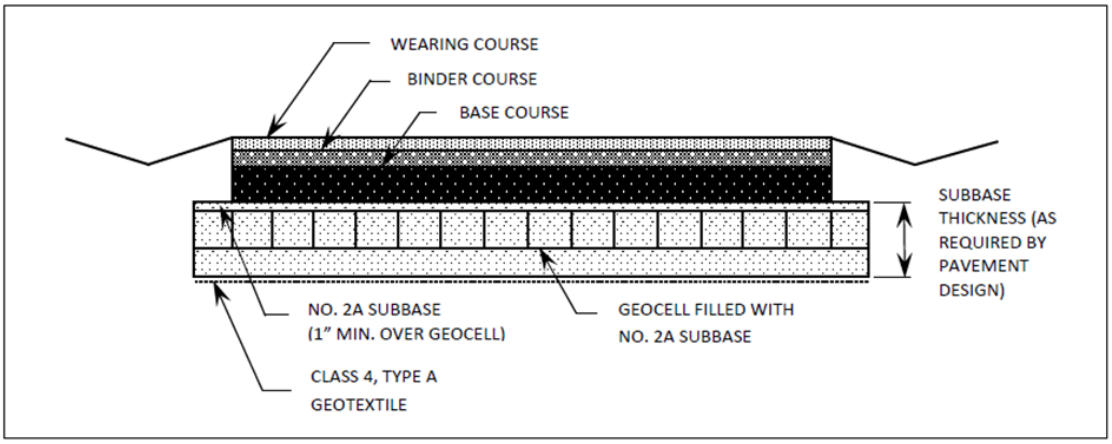

Figure 2.26 Typical pavement section with geocell layer (adapted from PennDOT GDM, 2018).

Illinois DOT (IDOT) specifies geosynthetics for stabilization of subgrades and embankment foundations. IDOT Standard Specifications for Road and Bridge Construction (2016) refers to the use of woven or nonwoven geotextile fabric for ground stabilization. In 2005, IDOT adopted a Subgrade Stability Manual as a guide on the stability of subgrades in the construction of highways. Geosynthetics are mentioned as a subgrade treatment option and guidelines for the aggregate thickness reduction when geosynthetic is used are specified. Table 2.6 summarizes the guidelines for the required aggregate cover with or without the use of geosynthetic. The table indicates that

the use of geosynthetics should only be considered when the subgrade IBV/CI is 3/120 or less. Immediate Bearing Value (IBV) is a measure of soil strength, obtained by conducting the standard bearing ratio test, according to AASHTO T 193, on the molded soil sample immediately after compaction (without soaking). Cone Index (CI) is a strength value determined by the SCP (Static Cone Penetrometer) test (IDOT SSM, 2005). The CI value is equal to the penetrometer load (pounds) divided by the cone base area (in.) and has units of psi (IDOT SSM, 2005). As it is noted, geosynthetics could reduce the aggregate cover by as much as 30%. The amount of thickness reduction depends on the type and strength characteristics of the geosynthetic, aggregate, and subgrade soil.

Texas DOT (TxDOT) specifies geosynthetics for both restraint of pavement materials and separation of materials. TxDOT Pavement Manual (2019) mentions that there is no specific guidance regarding the use of geosynthetics as reinforcement of unbound materials in pavements due to the insufficient research at this moment. When soft subgrades are present, both geogrids and geotextiles have been used providing restraint of pavement materials and creating a working platform for subsequent layers. Also, the Pavement Manual refers to the use of geogrids as a substitute of lime treatment.

Massachusetts DOT mentions that geotextiles used for separation and stabilization in pavement applications should conform to requirements of AASHTO M 288 for the intended application (MassDOT, 2020). Kentucky Transportation Cabinet (KYTC) also uses geotextiles for subgrade or embankment foundation stabilization and geotextiles must meet the requirements of AASHTO M 288 for the specific applications (KYTC, 2019). On the other hand, Ohio DOT has developed its own geotextile standard specifications and doesn't follow AASHTO M 288 (ODOT, 2019). Their use of geosynthetics is limited for subgrade-base separation and stabilization in pavement applications. Finally, Wisconsin DOT is another department that uses geosynthetics for subgrade separation, stabilization, and reinforcement (WisDOT, 2020).

Table 2.6 Guidelines for aggregate cover with or without geosynthetics (adapted from IDOT SSM, 2005).

IBV/CI	Aggregate Cover		
	without Geosynthetics in (mm)	with Geotextile in (mm)	with Geogrid in (mm)
1/40	22 (560)	16 (405)	15 (375)
1.5/60	18 (450)	12 (300)	12 (300)
2/80	16 (400)	12 (300)	10 (250)
3/120	12 (300)	12 (300)	9 (230)

2.5.1 Use of geosynthetics by Indiana DOT

Indiana DOT (INDOT) specifies geosynthetics such as geotextiles, geogrids, and geocells confining systems for use in pavement applications. Specifically, geotextiles are used as a separator layer between aggregate and subgrade soils and geogrids as a subgrade treatment and foundation improvement for embankments over soft soils. Geogrids are preferred as a subgrade treatment in places like urban areas or where shallow utilities or an unstable subgrade exists. INDOT also allows geocells filled with coarse aggregate as an option of subgrade treatment. Among all the DOTs studied, only PennDOT and INDOT suggest the use of geocells infilled with coarse aggregate as subgrade enhancement. However, PennDOT provides more detailed guidelines for the selection of the appropriate geocell depending on the strength of the subgrade. In general, INDOT uses one of the following methods for subgrade improvement: (1) chemical modification; (2) coarse aggregate layer; (3) geogrid placed under coarse aggregate layer; and (4) soil compaction to 100% maximum dry density (INDOT, 2020). If the original ground cannot be compacted to the required strength because of soft or unstable soils in the foundation of embankments, the use of stabilizing materials consisting of coarse aggregate No. 5 encapsulated in geotextile or soil drying with a chemical modifier shall be used (INDOT, 2020). A detailed description of the types of subgrade treatment used by INDOT is shown in Table 2.7.

Table 2.7 Types of subgrade treatment (INDOT, 2020).

Type	Subgrade Description
I	24 in. of soil compacted in accordance with 203.23
IA	[blank]
IBC	14 in. chemical soil modification using cement
IBL	14 in. chemical soil modification using lime
IC	12 in. coarse aggregate No. 53 in accordance with 301
ID	12 in. coarse aggregate with Type 2B geotextile in accordance with 918.02(c)
II	6 in. coarse aggregate No. 53 in accordance with 301
III	In-place compaction in accordance with 203.23
IV	12 in. coarse aggregate No. 53 with Type IB geogrid in accordance with 214
IVA	12 in. coarse aggregate with Geocell confining system in accordance with 214
V	3 in. of subgrade excavated and replaced with 3 in. coarse aggregate No. 53

2.6 Summary and discussion

The literature review completed highlights the benefits of using: geogrid-reinforcement in the base course of flexible pavements, geocell-reinforced bases in unpaved and paved roads, and geosynthetic-reinforcement at the base of embankments constructed over weak foundations. In addition, this chapter summarizes the best practices of INDOT and other DOTs regarding the use of geosynthetics in roadway applications. The following are the major findings:

- An improved performance of a flexible pavement, reinforced with a geogrid at the interface between subgrade and base, can be expected for weaker subgrades, thinner base course layers or for higher tensile modulus geogrids. It has been reported that, with the use of geogrids, a 40% or larger increase in the resilient modulus of a base course layer may be achieved. Also, a similar increase of CBR value, in geogrid-reinforced working platforms, could be attained. These findings show how the benefits of including geosynthetic-reinforcement could be integrated into pavement design, in particular by using the notion of enhanced resilient modulus.
- The benefits of using a geocell-reinforced base in terms of rut depth reduction could be significant for both unpaved and paved road systems. For unpaved roads, the thickness of the aggregate layer could be reduced by approximately 43% with the use of geocells infilled with materials such as well-graded aggregate (AB-3) or RAP. The geocell-reinforced base not only could allow to decrease the thickness of the base layer but also

could prolong the life of the pavement by as much as 3.5 times (for a reinforced RAP pavement), as mentioned by Pokharel et al. (2011). In paved roads, geocell-reinforcement infilled with RAP, crushed limestone or quarry waste could allow a 25% reduction of the base layer thickness, as long as the minimum requirement for the thickness of HMA layer is satisfied. In terms of load distribution, geocell-reinforced bases in unpaved roads can lead to an increase in load distribution angles of 13.4° and 11.6° for crushed limestone and RAP infill materials, respectively, compared to unreinforced sections. Although these observations emphasize the benefits of using geocell-reinforcement in pavements, further laboratory and field testing is still required to prove that geocells can effectively prolong the life of pavements and that they can be used instead of other reinforcement methods.

- The use of geosynthetics to support embankments constructed over soft foundations has been proven to be beneficial in increasing bearing capacity. The failure heights of embankments can be increased by up to 60% with the use of basal reinforcement. A geocell-reinforcement layer, when used at the base of an embankment constructed on a soft soil, has been shown to improve the bearing capacity of the foundation and reduce the vertical and lateral deformations of the embankment. Planar reinforcement improves the performance of the embankment by friction and interlocking between the geosynthetic and soil, while geocell improves the performance by friction, interlocking, and vertical and lateral confinement of the soil. Numerical studies have confirmed these findings and have contributed to a better understanding of the mechanisms of geocell-reinforcement and the factors affecting the performance of geocell-reinforced embankments. However, these studies have used equivalent composite properties without modeling the detail of geocell-soil interaction, have assumed a geocell shape that is inaccurate, or used unrealistic soil models (e.g. linearly elastic-perfectly plastic) when such interaction was considered. Although these studies emphasized the benefits of using geocell-reinforcement in embankments, a further understanding of the load- and displacement- transfer mechanisms between geocells and fill and an investigation of the conditions in which geocell-reinforcement can be optimized is required.
- Most DOTs follow AASHTO M 288 for geotextiles applications, often enhanced with modifications. The majority of the DOTs consider the option of using geosynthetics such

as geotextiles and geogrids for separation and stabilization applications. AASHTO M 288 defines three classes of material strength: Class 1 refers to severe or harsh survivability conditions; Class 2 refers to typical conditions; and Class 3 refers to applications where there is little or no potential for geosynthetic damage. AASHTO M 288, Class 2 geotextile, is usually specified for separation and AASHTO M 288, Class 1 geotextile, for subgrade stabilization. As mentioned in AASHTO M288, a geotextile functions as a separator for subgrades with a CBR value equal to or greater than 3 (or resilient modulus, M_r, equal to or greater than 4,500 psi). For subgrade with 1<CBR<3 (or 1,500<M_r<4,500 psi), the geotextile provides the function of stabilization. There is no specific guidance regarding the upper limit of CBR (or M_r) for using a geotextile as separator. The upper limit can vary from a resilient modulus M_r of 9,500 psi (Caltrans) to 15,000 psi (WSDOT). Table 2.8 summarizes geosynthetics applications from several state DOTs. The applications of geosynthetics in roadways mentioned in the table are: (1) subgrade separation; (2) subgrade stabilization; (3) subgrade reinforcement; and (4) embankment foundation reinforcement. It should be noted that the information presented is based on DOTs technical documentation. It is indicative of available design options including geosynthetics but does not necessarily reflect how frequently these options are used.

Table 2.8 Summary of state DOT use of geosynthetics in roadways based on application.

State	Application of Geosynthetics in Roadways			
	Subgrade Separation	**Subgrade Stabilization**	**Subgrade Reinforcement**	**Embankment Foundation Reinforcement**
Washington	X	X		X
New York	X	X		X
California	X	X	X	X
Pennsylvania	X	X	X	
Illinois		X		X
Texas	X	X		
Massachusetts	X	X		
Kentucky		X		X
Ohio	X	X		
Wisconsin	X	X	X	
Indiana	X	X		X

3. QUANTIFYING THE BENEFIT OF GEOSYNTHETIC-REINFORCEMENT IN PAVED ROADS

3.1 Introduction

The purpose of this chapter is to discuss the benefits of geosynthetics reinforcement on paved roads. As discussed in the literature review section, the reinforcement mechanisms (i.e. lateral restraint and tensile membrane actions) translate into stiffening the pavement structure. A way to quantify this effect is to compute the enhanced moduli of base or subgrade layers, due to the reinforcement, that would be applicable to an unreinforced structure. The interest of this approach is the possibility to input the resulting moduli in a design method, readily available for unreinforced pavement, and observe the potential benefit in comparison to the original design without geosynthetic. The computer program "Composite Geosynthetic-Base Course Model" (Luo et al., 2017) allows us to assess the apparent increase in the layers moduli, as a result of geosynthetic-reinforcement. Then, potential benefits can be evaluated with the input of the enhanced moduli into the AASHTOWare Pavement ME Design software, this benefit being quantified by the computed improvement in pavement life. The AASHTOWare Pavement ME predicts the performance of pavement distresses (cracking, permanent deformation, etc.) over the design life of a pavement structure. In this way, Pavement ME facilitates the comparison of the predicted performance of pavements with and without geosynthetics embedded in the base courses. The pavement life for a specific distress category is defined as the pavement age at which the specific distress category reaches the allowable limit. Increase in the pavement life for a distress category can be a potential benefit of the reinforcement and is investigated in this chapter.

The AASHTOWare Pavement ME software builds upon the NCHRP Mechanistic-Empirical Pavement Design Guide (MEPDG) (AASHTO, 2008) which includes the following three parts: (1) mechanistic, where theory is used to predict critical pavement responses (strains, stresses, deflections, etc.) as a function of traffic and climatic loading; (2) material characterization; and (3) empirical, which includes defined relationships between the critical pavement response parameter and field-observed distress. First, designers consider the site conditions, such as traffic, climate, subgrade, and existing pavement conditions in creating a trial design for a pavement. Then, the software predicts the pavement distresses and smoothness, which are evaluated against

performance criteria and reliability values. If the design does not meet the required performance criteria, it is revised and the evaluation process is repeated (AASHTO, 2008).

In 2009, the Indiana Department of Transportation (INDOT) adopted the MEPDG method. Current application of the Pavement ME in Indiana neglects the modulus improvement of chemically treated soils (Jung and Bobet, 2008). In addition, INDOT does not take into account the stiffness improvement due the inclusion of a geogrid in the base course. An increase in modulus of pavement materials can result in an increase in pavement life, which is currently neglected.

In addition, the design method of the Tensar's Spectrapave software: Biaxial Grid Pavement Analysis (Tensar, 2019), was utilized as an alternative to the Composite Geosynthetic-Base Course Model. As explained in the following sections, Spectrapave follows a different theoretical approach than that of Luo et al. (2017) to assess the reinforced layers improvement; comparison of their respective outputs informed on the consistency of the two methods.

Throughout the following analysis the reinforcement was a simplified representation of a biaxial geogrid placed at the interface between the subgrade and base course of a flexible pavement structure.

3.2 Reinforcement-enhanced moduli of pavement layers

Data from three asphalt pavement sites in Indiana were used for the analysis. The characteristics of each pavement structure are summarized in Subsection 3.2.1. The reinforcement-enhanced moduli that were input in AASHTOWare Pavement ME Design software were, at first, determined using the computer programs "Composite Geosynthetic-Base Course Model" and Tensar's Spectrapave.

3.2.1 Description of the pavements

The following three roadway structures with asphalt pavement were used as example cases: (1) SR 46 Clay County; (2) US 31 St. Joseph County; and (3) SR 37 Martinsville. The pavement structures and resilient moduli (M_R) of the untreated and cement-treated subgrades for the three sites are summarized in Table 3.1. These values were available from earlier laboratory resilient modulus tests (K. Gupta, personal communication, 2021).

Table 3.1 Pavement structures for the 3 example case sites.

SITE 1: SR 46 Clay County				
Layer	**Layer Type**	**Material Type**	**Thickness (in)**	**M_R (ksi)**
1	Flexible	Asphalt Concrete	1.5	-
2	Flexible	Asphalt Concrete	2.5	-
3	Flexible	Asphalt Concrete	6.0	-
4	Unbound	Crushed Gravel	12.0	-
5	Subgrade	A-6 (untreated)	Semi-Infinite*	15.66
SITE 2: US 31 St. Joseph County				
Layer	**Layer Type**	**Material Type**	**Thickness (in)**	**M_R (ksi)**
1	Flexible	Asphalt Concrete	1.5	-
2	Flexible	Asphalt Concrete	2.5	-
3	Flexible	Asphalt Concrete	12.5	-
4	Unbound	Crushed Stone	6.0	-
5	Subgrade	A-1-a (treated)	14.0	40.30
6	Subgrade	A-1-a (untreated)	Semi-Infinite*	12.30
SITE 3: SR 37 Martinsville				
Layer	**Layer Type**	**Material Type**	**Thickness (in)**	**M_R (ksi)**
1	Flexible	Asphalt Concrete	1.5	-
2	Flexible	Asphalt Concrete	2.5	-
3	Flexible	Asphalt Concrete	10.5	-
4	Unbound	Crushed Stone	6.0	-
5	Subgrade	A-2-4 (treated)	14.0	48.06
6	Subgrade	A-2-4 (untreated)	Semi-Infinite*	14.07

Notes: 1 ksi ≈ 6.89 MPa, 1 in ≈ 25.4 mm

* Assumed for modeling purposes

3.2.2 Composite geosynthetic-base course model

The computer program "Composite Geosynthetic-Base Course Model" developed by Luo et al. (2017) was used to determine the reinforcement-enhanced moduli of base and subgrade. The computer program was created by Luo et al. (2017) to supplement the Pavement ME Design software by making it possible to predict the performance of geosynthetic-reinforced pavements. The geosynthetic-reinforced pavement structure data, such as layer thickness and material properties, are required as input and the program generates as output an unreinforced pavement structure maintaining the same layer thicknesses, but with equivalent material properties (e.g. enhanced base modulus and enhanced subgrade modulus) so that both pavement responses, i.e. geosynthetic-reinforced and unreinforced, are identical.

In this study, the three pavement structures described previously were analyzed with this program without considering the chemical treatment of subgrades. Also, because the maximum thickness of the asphalt-concrete layer allowed by the software is 9.9 in., the value of 9 in. was chosen for the three examples. In all the cases, a biaxial geogrid with an elastic modulus of 39 ksi (equivalent to Tensar's biaxial geogrid BX1100), placed at the interface between subgrade and base course, was included. Table 3.2 shows the data input in the program for each of the three sites.

Table 3.2 Pavement structure data used in the Composite Geosynthetic-Base Course Model.

Pavement Structure	**SITE 1 Untreated**	**SITE 2 Untreated**	**SITE 3 Untreated**
Asphalt Thickness (in)	9	9	9
Base Thickness (in)	12	6	6
Asphalt Resilient Modulus (ksi)	300	300	300
Base Resilient Modulus (ksi)	20	20	20
Geosynthetic Sheet Stiffness (ksi)	39	39	39
Subgrade Resilient Modulus (ksi)	15.66	12.30	14.07
Geogrid Type	Biaxial Geogrid	Biaxial Geogrid	Biaxial Geogrid

Notes: 1 ksi ≈ 6.89 MPa, 1 in ≈ 25.4 mm

The results of these analyses showed that only the subgrade modulus was affected by the presence of the geogrid at the interface between the subgrade and base course. The base modulus remained practically unaffected. The enhanced subgrade moduli that resulted from the analyses of the three pavement structures are listed in Table 5.3.

Table 3.3 Enhanced subgrade modulus.

SITE	**Enhanced Subgrade Modulus (ksi)**
1	45.4
2	24.4
3	29.1

Note: 1 ksi ≈ 6.89 MPa

3.2.3 Tensar's Spectrapave software

Tensar's Spectrapave software, Biaxial Grid Pavement Analysis, is based on the pavement design methodology incorporated in AASHTO 1993 pavement design procedure (AASHTO, 1993). The AASHTO 1993 flexible pavement design procedure assigns layer coefficients (instead of modulus) to each layer above the subgrade. The layer coefficient represents the relative contribution of each layer material to the pavement overall performance under traffic. These layer coefficients are introduced in design equations as weighting factors to the respective thickness of each layer, in order to obtain the overall effective (or equivalent) thickness of the proposed structure design. This value is then compared to the required effective thickness, based on expected traffic and subgrade conditions. In the Spectrapave software, the inclusion of a geogrid at the interface between the subgrade and base course allows to increase the layer coefficient of the reinforced base with the expectation that stiffness and durability are improved. According to this concept, the benefits of including geosynthetic-reinforcement in unbound, granular layers would be a possible reduction in the amount of material needed for these layers or an increase in the service life of the pavement.

In this study, all the three pavement structures (untreated) had a subgrade modulus of 8.8 ksi, since this is the maximum value of the subgrade modulus that the software allows. Tensar's biaxial geogrid class 1, with a planar tensile stiffness of 1166 lb/in., was considered for the analyses. Table 3.4 shows the pavement structure data that were input in Spectrapave for each of the three sites. Results of the three analyses are summarized in Table 3.5. Specifically, Table 3.5 illustrates the enhanced base coefficient due to the presence of the geogrid, the percentage increase in base coefficient, and the enhanced base modulus, which represents the initial base modulus increased according to the increase in base coefficient. An initial resilient modulus of the base equal to 20 ksi was considered. As observed from Table 3.5, regardless of the thickness of the asphalt layer and base course, the percentage increase in the base coefficient was the same for all the three pavement structures.

Table 3.4 Pavement structure used for Spectrapave.

Pavement Structure	SITE 1	SITE 2	SITE 3
Asphalt Thickness (in)	9	9	9
Base Thickness (in)	12	6	6
Asphalt Coefficient	0.42	0.42	0.42
Base Coefficient	0.14	0.14	0.14
Geosynthetic Sheet Stiffness (lb/in)	1166	1166	1166
Subgrade Resilient Modulus (ksi)	8.8	8.8	8.8
Geogrid Type	Biaxial Class 1	Biaxial Class 1	Biaxial Class 1

Notes: 1 ksi ≈ 6.89 MPa, 1 in ≈ 25.4 mm

Table 3.5 Reinforcement-induced improvement in base coefficients and moduli.

SITE	Initial Base Coefficient	Enhanced Base Coefficient	Percentage increase in base coefficient (%)	Initial Base Modulus (ksi)	Enhanced Base Modulus (ksi)
1	0.14	0.165	18	20	23.6
2	0.14	0.165	18	20	23.6
3	0.14	0.165	18	20	23.6

Note: 1 ksi ≈ 6.89 Mpa

To compare the result from Spectrapave and Composite Geosynthetic-Base Course Model, it was necessary to compute, using the Composite Geosynthetic-Base Course Model, the improved moduli of the pavement layers for the three sites, while considering a subgrade modulus of 8.8 ksi. As mentioned previously, 8.8 ksi is the maximum value of the subgrade modulus that the Spectrapave software allows. The pavements with the same data shown in Table 3.2 were analyzed, except that the subgrade resilient modulus was 8.8 ksi in all cases. The enhanced subgrade moduli for the three pavement structures are shown in Table 3.6.

Table 3.6 Enhanced subgrade modulus.

SITE	Enhanced Subgrade Modulus (ksi)
1	20.3
2	15.2
3	15.2

Note: 1 ksi ≈ 6.89 MPa

3.3 Analysis of example cases with the MEPDG

A number of analyses of pavement structures, based on the example cases described above, were carried out using the AASHTOWare Pavement ME Design software. The purpose was to quantify the potential benefit of geogrid-reinforcement of the base course and to compare performances with those of designs where chemical treatment of the subgrade would be the sole improvement. For each of the example sites three cases were considered: untreated pavement; geogrid-reinforced pavement; and chemically treated pavement (Sites 2 and 3 only). In addition, to compare the solutions derived from the Composite Geosynthetic-Base Course Model and from Tensar's Spectrapave, three more cases were considered for each site: untreated pavement (8.8 ksi subgrade modulus); geogrid-reinforced pavement (Composite Geosynthetic-Base Course Model); and geogrid-reinforced pavement (Tensar's Spectrapave software).

For Site 1, the following cases were considered: Case 1-1 Pavement with untreated subgrade; Case 1-2 Pavement of Case 1-1 with 14-in. improved subgrade layer due to geogrid-reinforcement; Case 1-3 Pavement with untreated subgrade (8.8 ksi subgrade modulus); Case 1-4 Pavement of Case 1-3 with 14-in. improved subgrade layer due to geogrid-reinforcement; and Case 1-5 Pavement of Case 1-3 with improved base course due to geogrid-reinforcement. For the Sites 2 and 3, the following cases of pavement structure were considered: Cases 2-1 and 3-1 Pavement with untreated subgrade; Cases 2-2 and 3-2 Pavement of Cases 2-1 and 3-1, respectively, with 14-in. improved subgrade layer due to geogrid-reinforcement; Cases 2-3 and 3-3 Pavement of Cases 2-1 and 3-1, respectively, with 14-in. chemically treated subgrade layer; Cases 2-4 and 3-4 Pavement with untreated subgrade (8.8 ksi subgrade modulus); Cases 2-5 and 3-5 Pavement of Cases 2-4 and 3-4, respectively, with 14-in. improved subgrade layer due to geogrid-reinforcement; and Cases 2-6 and 3-6 Pavement of Cases 2-4 and 3-4, respectively, with improved base course due to geogrid-reinforcement. Table 3.7 lists all the cases analyzed with Pavement ME.

Table 3.7 Pavement structures analyzed using the MEPDG.

SITE 1				
Case 1-1				
Layer	**Layer Type**	**Material Type**	**Thickness (in)**	**M_R (ksi)**
1	Flexible	Asphalt Concrete	1.5	-
2	Flexible	Asphalt Concrete	2.5	-
3	Flexible	Asphalt Concrete	6.0	-
4	Unbound	Crushed Gravel	12.0	20
5	Subgrade	A-6 (untreated)	Semi-Infinite	15.66
Case 1-2				
Layer	**Layer Type**	**Material Type**	**Thickness (in)**	**M_R (ksi)**
1	Flexible	Asphalt Concrete	1.5	-
2	Flexible	Asphalt Concrete	2.5	-
3	Flexible	Asphalt Concrete	6.0	-
4	Unbound	Crushed Gravel	12.0	20
5	Subgrade	A-6 (enhanced)	14	45.4
6	Subgrade	A-6 (untreated)	Semi-Infinite	15.66
Case 1-3				
Layer	**Layer Type**	**Material Type**	**Thickness (in)**	**M_R (ksi)**
1	Flexible	Asphalt Concrete	1.5	-
2	Flexible	Asphalt Concrete	2.5	-
3	Flexible	Asphalt Concrete	6.0	-
4	Unbound	Crushed Gravel	12.0	20
5	Subgrade	A-6 (untreated)	Semi-Infinite	8.8
Case 1-4				
Layer	**Layer Type**	**Material Type**	**Thickness (in)**	**M_R (ksi)**
1	Flexible	Asphalt Concrete	1.5	-
2	Flexible	Asphalt Concrete	2.5	-
3	Flexible	Asphalt Concrete	6.0	-
4	Unbound	Crushed Gravel	12.0	20
5	Subgrade	A-6 (enhanced)	14	20.3
6	Subgrade	A-6 (untreated)	Semi-Infinite	8.8
Case 1-5				
Layer	**Layer Type**	**Material Type**	**Thickness (in)**	**M_R (ksi)**
1	Flexible	Asphalt Concrete	1.5	-
2	Flexible	Asphalt Concrete	2.5	-
3	Flexible	Asphalt Concrete	6.0	-
4	Unbound	Crushed Gravel (enh.)	12.0	23.6
5	Subgrade	A-6 (untreated)	Semi-Infinite	8.8
SITE 2				
Case 2-1				
Layer	**Layer Type**	**Material Type**	**Thickness (in)**	**M_R (ksi)**
1	Flexible	Asphalt Concrete	1.5	-
2	Flexible	Asphalt Concrete	2.5	-
3	Flexible	Asphalt Concrete	12.5	-
4	Unbound	Crushed Stone	6.0	20
5	Subgrade	A-1-a (untreated)	Semi-Infinite	12.3

Table 3.7 continued

Case 2-2				
Layer	**Layer Type**	**Material Type**	**Thickness (in)**	**M_R (ksi)**
1	Flexible	Asphalt Concrete	1.5	-
2	Flexible	Asphalt Concrete	2.5	-
3	Flexible	Asphalt Concrete	12.5	-
4	Unbound	Crushed Stone	6.0	20
5	Subgrade	A-1-a (enhanced)	14.0	24.4
6	Subgrade	A-1-a (untreated)	Semi-Infinite	12.3
Case 2-3				
Layer	**Layer Type**	**Material Type**	**Thickness (in)**	**M_R (ksi)**
1	Flexible	Asphalt Concrete	1.5	-
2	Flexible	Asphalt Concrete	2.5	-
3	Flexible	Asphalt Concrete	12.5	-
4	Unbound	Crushed Stone	6.0	20
5	Subgrade	A-1-a (treated)	14.0	40.3
6	Subgrade	A-1-a (untreated)	Semi-Infinite	12.3
Case 2-4				
Layer	**Layer Type**	**Material Type**	**Thickness (in)**	**M_R (ksi)**
1	Flexible	Asphalt Concrete	1.5	-
2	Flexible	Asphalt Concrete	2.5	-
3	Flexible	Asphalt Concrete	12.5	-
4	Unbound	Crushed Stone	6.0	20
5	Subgrade	A-1-a (untreated)	Semi-Infinite	8.8
Case 2-5				
Layer	**Layer Type**	**Material Type**	**Thickness (in)**	**M_R (ksi)**
1	Flexible	Asphalt Concrete	1.5	-
2	Flexible	Asphalt Concrete	2.5	-
3	Flexible	Asphalt Concrete	12.5	-
4	Unbound	Crushed Stone	6.0	20
5	Subgrade	A-1-a (enhanced)	14.0	15.2
6	Subgrade	A-1-a (untreated)	Semi-Infinite	8.8
Case 2-6				
Layer	**Layer Type**	**Material Type**	**Thickness (in)**	**M_R (ksi)**
1	Flexible	Asphalt Concrete	1.5	-
2	Flexible	Asphalt Concrete	2.5	-
3	Flexible	Asphalt Concrete	12.5	-
4	Unbound	Crushed Stone (enh.)	6.0	23.6
5	Subgrade	A-1-a (untreated)	Semi-Infinite	8.8
SITE 3				
Case 3-1				
Layer	**Layer Type**	**Material Type**	**Thickness (in)**	**M_R (ksi)**
1	Flexible	Asphalt Concrete	1.5	-
2	Flexible	Asphalt Concrete	2.5	-
3	Flexible	Asphalt Concrete	10.5	-
4	Unbound	Crushed Stone	6.0	20
5	Subgrade	A-2-4 (untreated)	Semi-Infinite	14.07

Table 3.7 continued

Case 3-2				
Layer	**Layer Type**	**Material Type**	**Thickness (in)**	**M_R (ksi)**
1	Flexible	Asphalt Concrete	1.5	-
2	Flexible	Asphalt Concrete	2.5	-
3	Flexible	Asphalt Concrete	10.5	-
4	Unbound	Crushed Stone	6.0	20
5	Subgrade	A-2-4 (enhanced)	14.0	29.1
6	Subgrade	A-2-4 (untreated)	Semi-Infinite	14.07
Case 3-3				
Layer	**Layer Type**	**Material Type**	**Thickness (in)**	**M_R (ksi)**
1	Flexible	Asphalt Concrete	1.5	-
2	Flexible	Asphalt Concrete	2.5	-
3	Flexible	Asphalt Concrete	10.5	-
4	Unbound	Crushed Stone	6.0	20
5	Subgrade	A-2-4 (treated)	14.0	48.06
6	Subgrade	A-2-4 (untreated)	Semi-Infinite	14.07
Case 3-4				
Layer	**Layer Type**	**Material Type**	**Thickness (in)**	**M_R (ksi)**
1	Flexible	Asphalt Concrete	1.5	-
2	Flexible	Asphalt Concrete	2.5	-
3	Flexible	Asphalt Concrete	10.5	-
4	Unbound	Crushed Stone	6.0	20
5	Subgrade	A-2-4 (untreated)	Semi-Infinite	8.8
Case 3-5				
Layer	**Layer Type**	**Material Type**	**Thickness (in)**	**M_R (ksi)**
1	Flexible	Asphalt Concrete	1.5	-
2	Flexible	Asphalt Concrete	2.5	-
3	Flexible	Asphalt Concrete	10.5	-
4	Unbound	Crushed Stone	6.0	20
5	Subgrade	A-2-4 (enhanced)	14.0	15.2
6	Subgrade	A-2-4 (untreated)	Semi-Infinite	8.8
Case 3-6				
Layer	**Layer Type**	**Material Type**	**Thickness (in)**	**M_R (ksi)**
1	Flexible	Asphalt Concrete	1.5	-
2	Flexible	Asphalt Concrete	2.5	-
3	Flexible	Asphalt Concrete	10.5	-
4	Unbound	Crushed Stone (enh.)	6.0	23.6
5	Subgrade	A-2-4 (untreated)	Semi-Infinite	8.8

Notes: 1 ksi ≈ 6.89 Mpa, 1 in ≈ 25.4 mm

The soil index properties, such as Liquid Limit (LL), Plasticity Index (PI), percent fines and soil class, for the untreated and cement-treated subgrades used are summarized in Table 3.8. These data were obtained from laboratory tests (K. Gupta, personal communication, 2021). According to the findings of Sandoval et al. (2019), for cement-treated subgrades, the PI of the original soil was

decreased by 30%, the LL was increased by 10%, and the fines were reduced by 15%. The soil classification was assumed to be unchanged by the treatment.

Table 3.8 Index soil properties for untreated and treated subgrades used for analysis in Pavement ME.

Case	Soil Properties Untreated Subgrade				Soil Properties Treated Subgrade			
	LL (%)	PI (%)	Fines (%)	Class	LL (%)	PI (%)	Fines (%)	Class
1.1-1.5	34.3	12	50.66	A-6	-	-	-	-
2.1, 2.2, 2.4, 2.5, 2.6	23.6	6.3	19.70	A-1	-	-	-	-
2.3	23.6	6.3	19.70	A-1	26	4.4	16.75	A-1
3.1, 3.2, 3.4, 3.5, 3.6	20.4	5.7	28.97	A-2-4	-	-	-	-
3.3	20.4	5.7	28.97	A-2-4	22.4	4	24.62	A-2-4

3.4 Results of pavement performances analyses

The analyses of all the cases were carried out using Pavement ME software. Pavement ME is a pavement design software, which predicts performances in terms of pavement distresses, namely the International Roughness Index (IRI), rutting (or permanent deformation), Asphalt-Concrete (AC) bottom-up fatigue cracking, and AC thermal cracking, and the related confidence level (called reliability) over the design life of the proposed pavement structure design. In this study, the design life for the pavement structures of Sites 1, 2, and 3 was chosen as 50, 50, and 20 years, respectively. The design reliability level was selected to be 90%. The threshold value of a particular distress category is the value above which the pavement would likely fail according to this specific mode. The threshold values for IRI, rutting, AC bottom-up cracking, and AC thermal cracking were chosen to be 172, 0.75, 25, and 1000, respectively.

Figure 3.1 shows the development of each distress mode with the pavement age for Cases 1-1 (untreated) and 1-2 (geogrid-reinforced), while Figure 3.2 shows the development of each distress mode with the pavement age for Cases 1-3 (untreated with 8.8 ksi subgrade modulus), 1-4 (geogrid-reinforced, Composite Geosynthetic-Base Course Model), and 1-5 (geogrid-reinforced, Tensar's Spectrapave software).

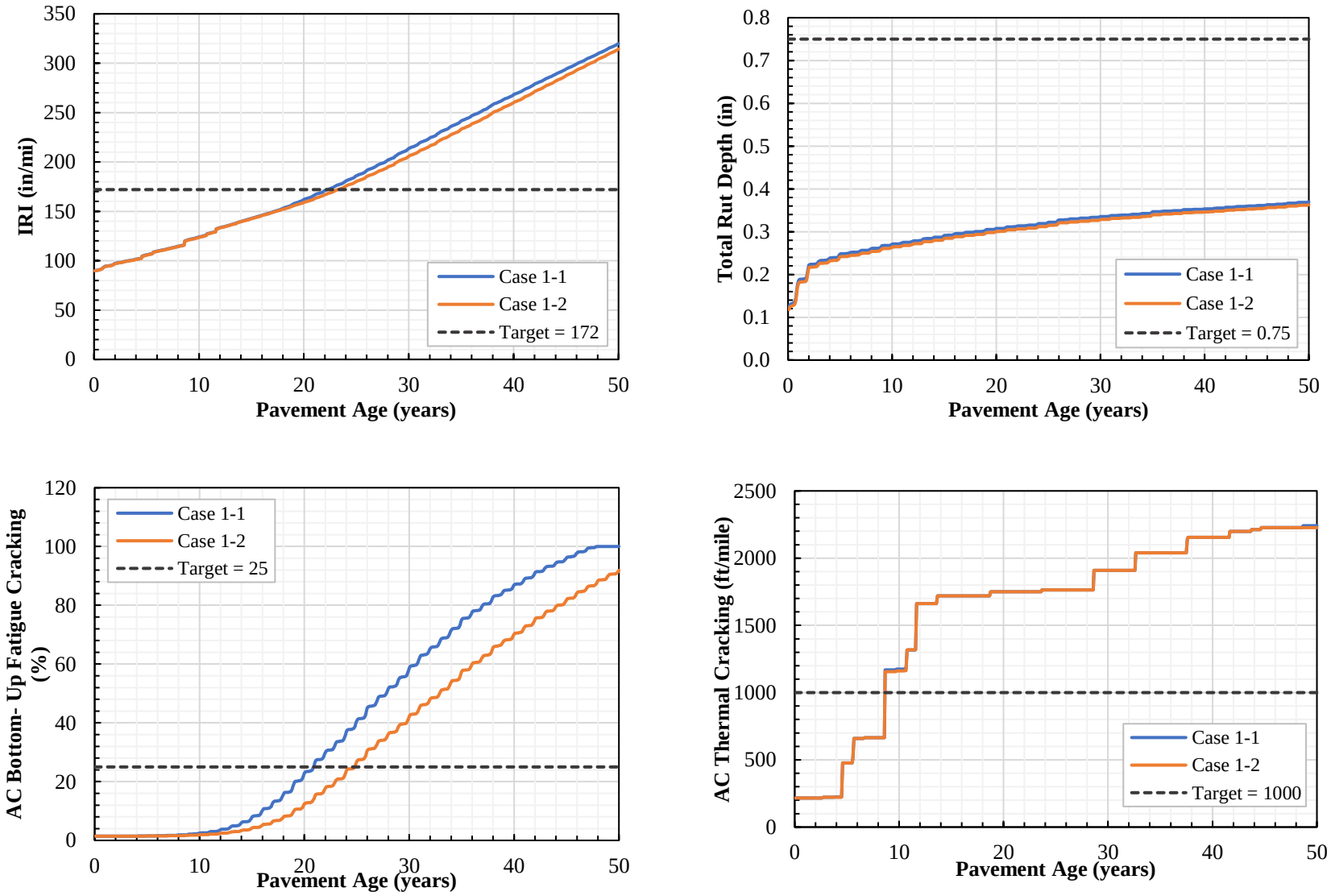

Figure 3.1 Development of IRI, rut depth, AC bottom-up cracking, and AC thermal cracking with pavement age (Cases 1-1 and 1-2).

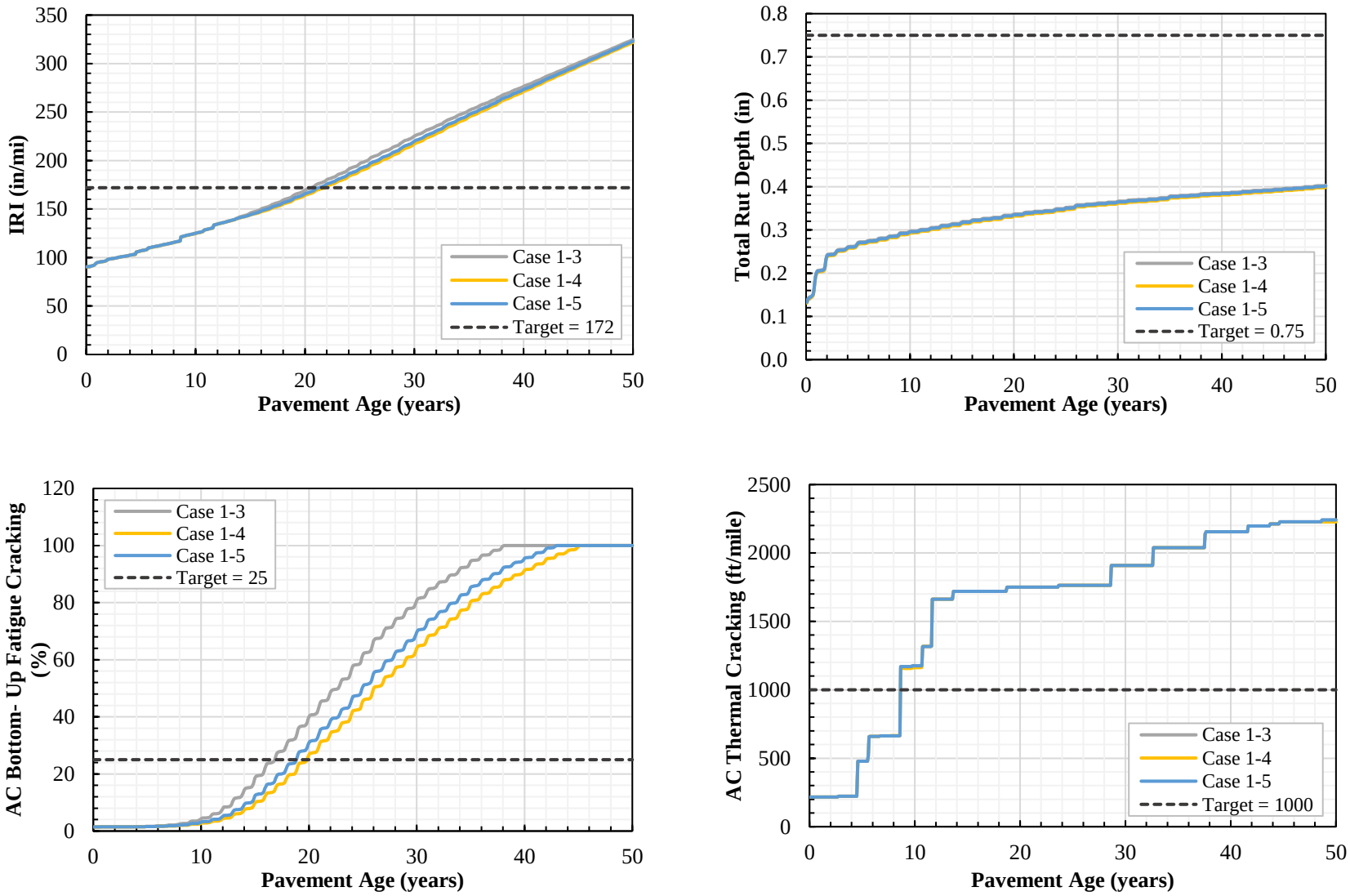

Figure 3.2 Development of IRI, rut depth, AC bottom-up cracking, and AC thermal cracking with pavement age (Cases 1-3 to 1-5)

Table 3.9 summarizes the pavement expected life for all the distress categories and for Cases 1-1 to 1-5. The same results are presented under the form of bar charts in Figures 3.3 and 3.4. As can be seen, the IRI and AC cracking are the critical modes of pavement distress, since they reach their threshold values before the end of the design life (50 years). The results in Table 3.9 show that the placement of a geogrid on top of the untreated subgrade (Case 1-2) increased the pavement life, based on the IRI, by 1 year, i.e. by 4.5%. The largest gain in the pavement life is observed for AC bottom-up cracking, which is increased by approximately 4 years, i.e. by 18.7%. The increased pavement life for AC bottom-up cracking with the use of Tensar's approach (Case 1-5) was predicted to be 18.8 years (i.e. 12% increase), while the increased pavement life from the Composite Geosynthetic-Base Course Model (Case 1-4) was 19.8 years (i.e. 18% increase). Tensar's approach for quantifying the benefit of geogrid-reinforcement is shown to be the most conservative of the two methods. Finally, the total rut depth and AC thermal cracking remain practically unaffected by the relatively small improvements in subgrade or base resilient modulus.

Table 3.9 Pavement life for each distress category (Cases 1-1 to 1-5).

Case	**Life of Pavement (years)**			
	Distress Category			
	IRI	**Permanent Deformation**	**AC Bottom-Up Cracking**	**AC Thermal Cracking**
1-1	22.2	50	20.9	8.6
1-2	23.2	50	24.8	8.6
1-3	20.6	50	16.8	8.6
1-4	21.8	50	19.8	8.6
1-5	21.2	50	18.8	8.6

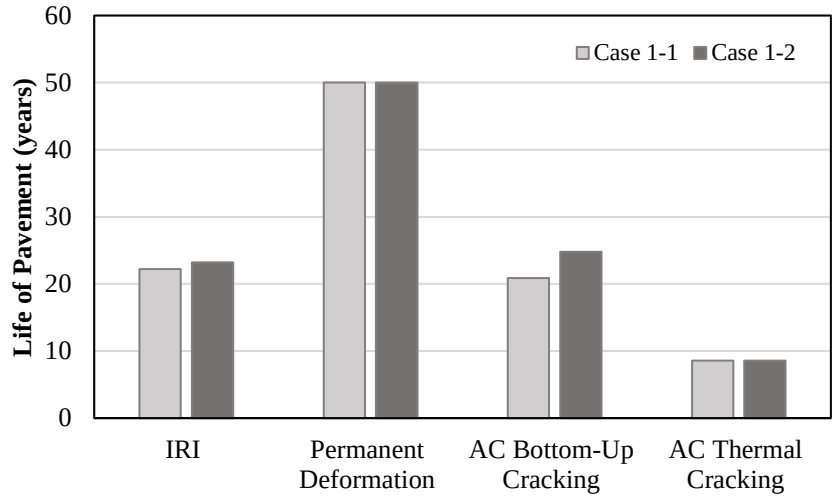

Figure 3.3 Pavement life for each distress category (Cases 1-1 and 1-2).

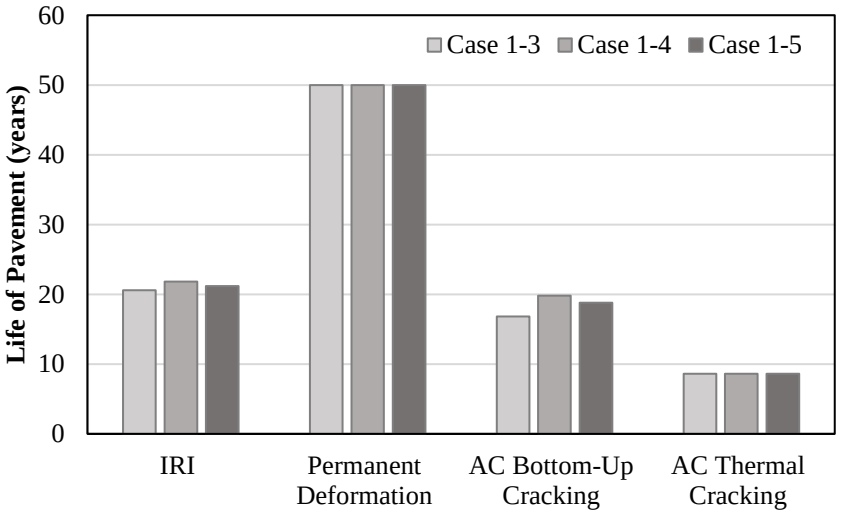

Figure 3.4 Pavement life for each distress category (Cases 1-3 to 1-5).

Figure 3.5 shows the evolution of each distress parameter with pavement aging, and for Cases 2-1 (untreated), 2-2 (geogrid-reinforced), and 2-3 (chemically treated), while Figure 3.6 is a similar plot for Cases 2-4 (untreated with 8.8 ksi subgrade modulus), 2-5 (geogrid-reinforced, Composite Geosynthetic-Base Course Model) and 2-6 (geogrid-reinforced, Tensar's Spectrapave software). All the pavement structures considered for Site 2 are shown to be failing, though only according to the IRI distress mode, before the end of the design life (50 years).

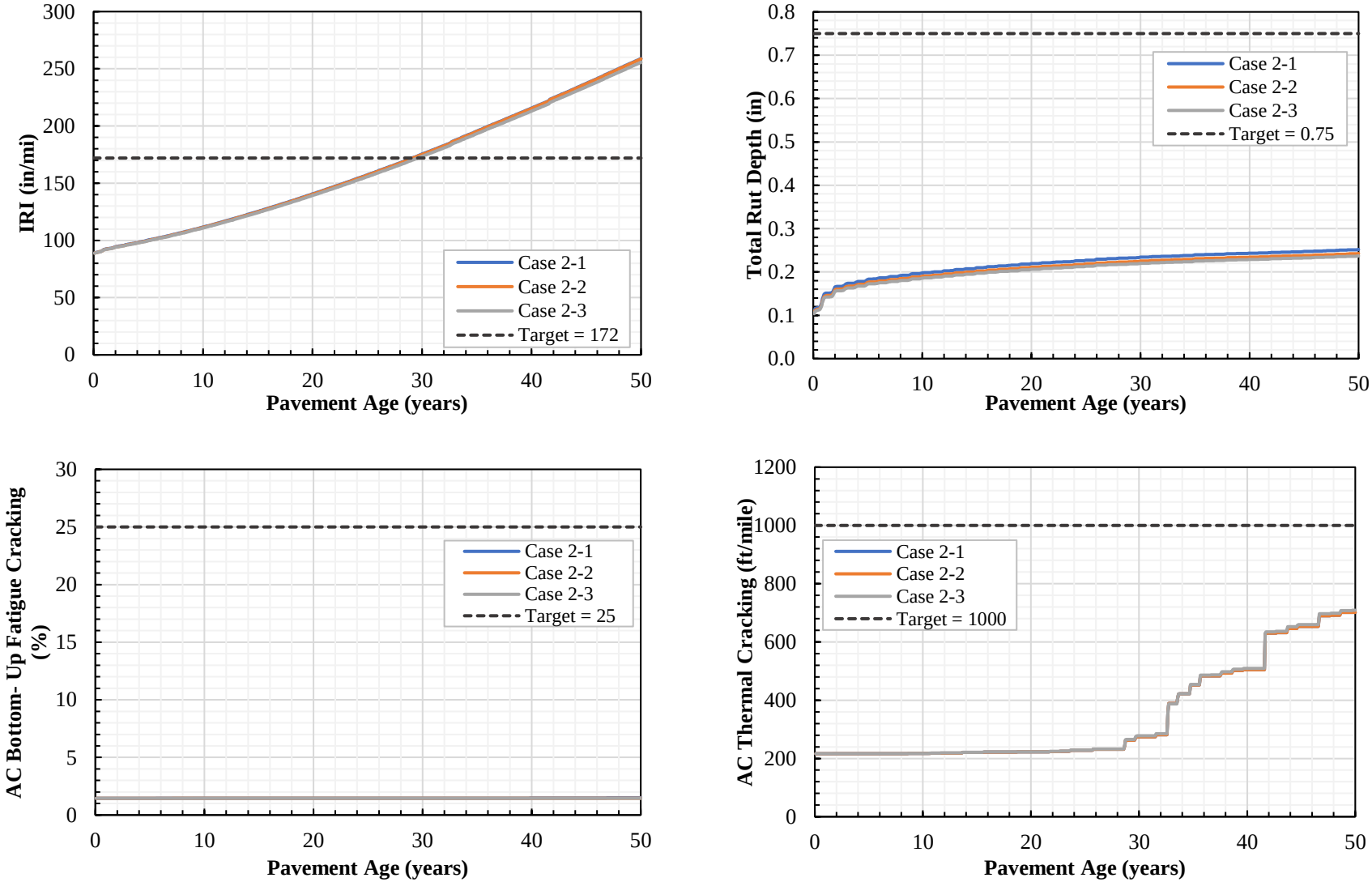

Figure 3.5 Development of IRI, rut depth, AC bottom-up cracking, and AC thermal cracking with pavement age (Cases 2-1 to 2-3).

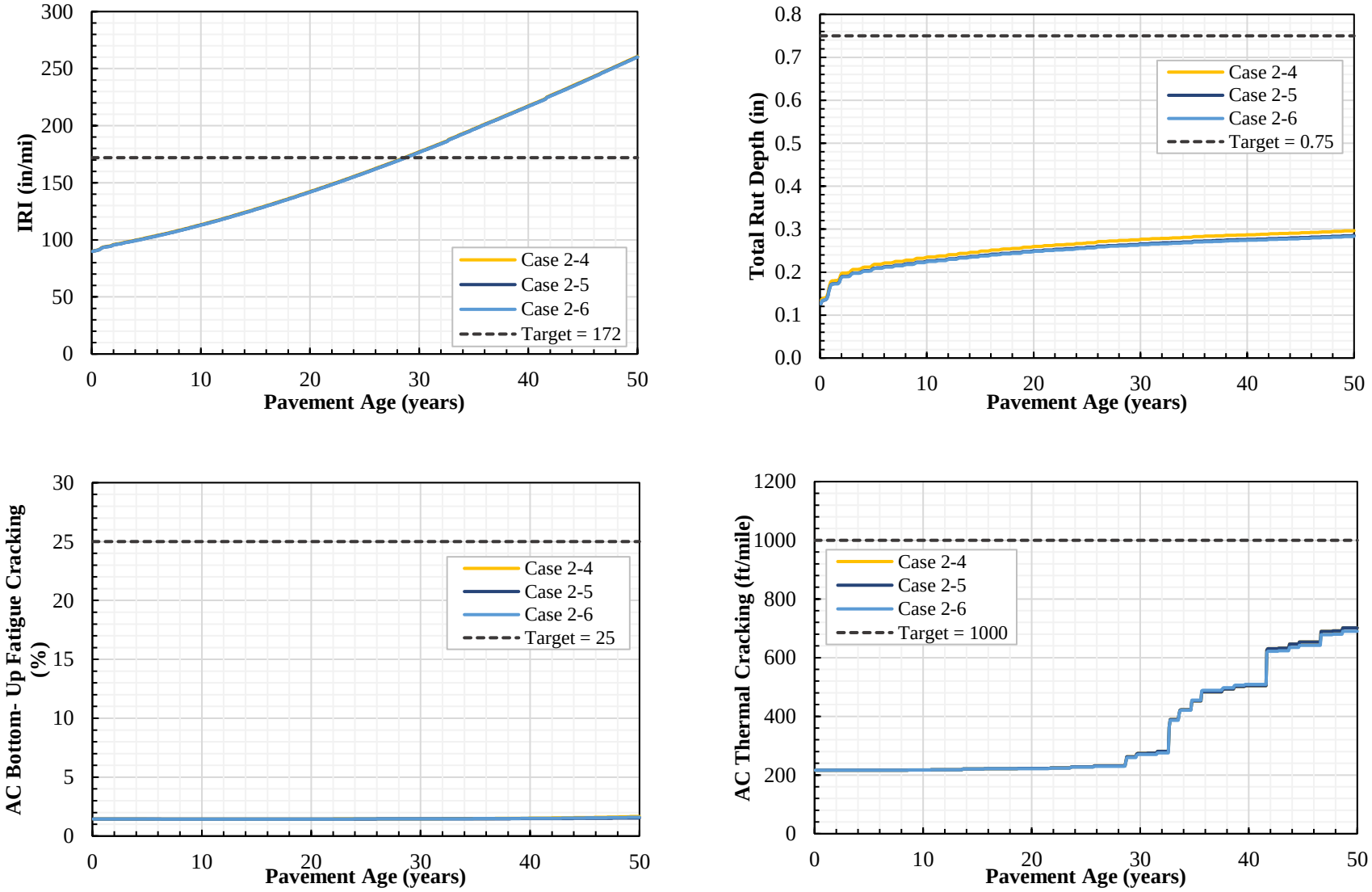

Figure 3.6 Development of IRI, rut depth, AC bottom-up cracking, and AC thermal cracking with pavement age (Cases 2-4 to 2-6).

Table 3.10 summarizes the pavement life for Cases 2-1 to 2-6. It is shown that the placement of a geogrid on top of the untreated subgrade (Case 2-2) increased the pavement expected life, based on the IRI mode, by approximately 0.3%, while the chemical treatment of the subgrade increased it by approximately 1.7%. Both methods of reinforcement resulted in an insignificant reduction of IRI or increase in pavement life. It has to be noted that the pavement of Site 2 included a 1.7 times thicker asphalt-concrete layer than Site 1, which could have hidden the relatively smaller benefits of subgrade reinforcement. In addition, there is no difference between Cases 2-5 and 2-6, whether the Composite Geosynthetic-Base Course Model is used or the Tensar method.

Table 3.10 Pavement life for each distress category (Cases 2-1 to 2-6).

Case	Life of Pavement (years)			
	Distress Category			
	IRI	Permanent Deformation	AC Bottom-Up Cracking	AC Thermal Cracking
2-1	29.1	50	50	50
2-2	29.2	50	50	50
2-3	29.6	50	50	50
2-4	28.6	50	50	50
2-5	28.7	50	50	50
2-6	28.7	50	50	50

Figures 3.7 and 3.8, similarly to Figures 3.5 and 3.6, show the evolution of each distress parameter with pavement age, for Cases 3-1 to 3-6. None of the cases of Site 3 failed before the end of the design life (20 years). None of the two types of improvement (geogrid or cement treatment) brought significant reduction in predicted pavement distress. The performance of this pavement structure is shown to be almost identical to that of Site 2 for the first 20 years of its life and thus was not investigated further.

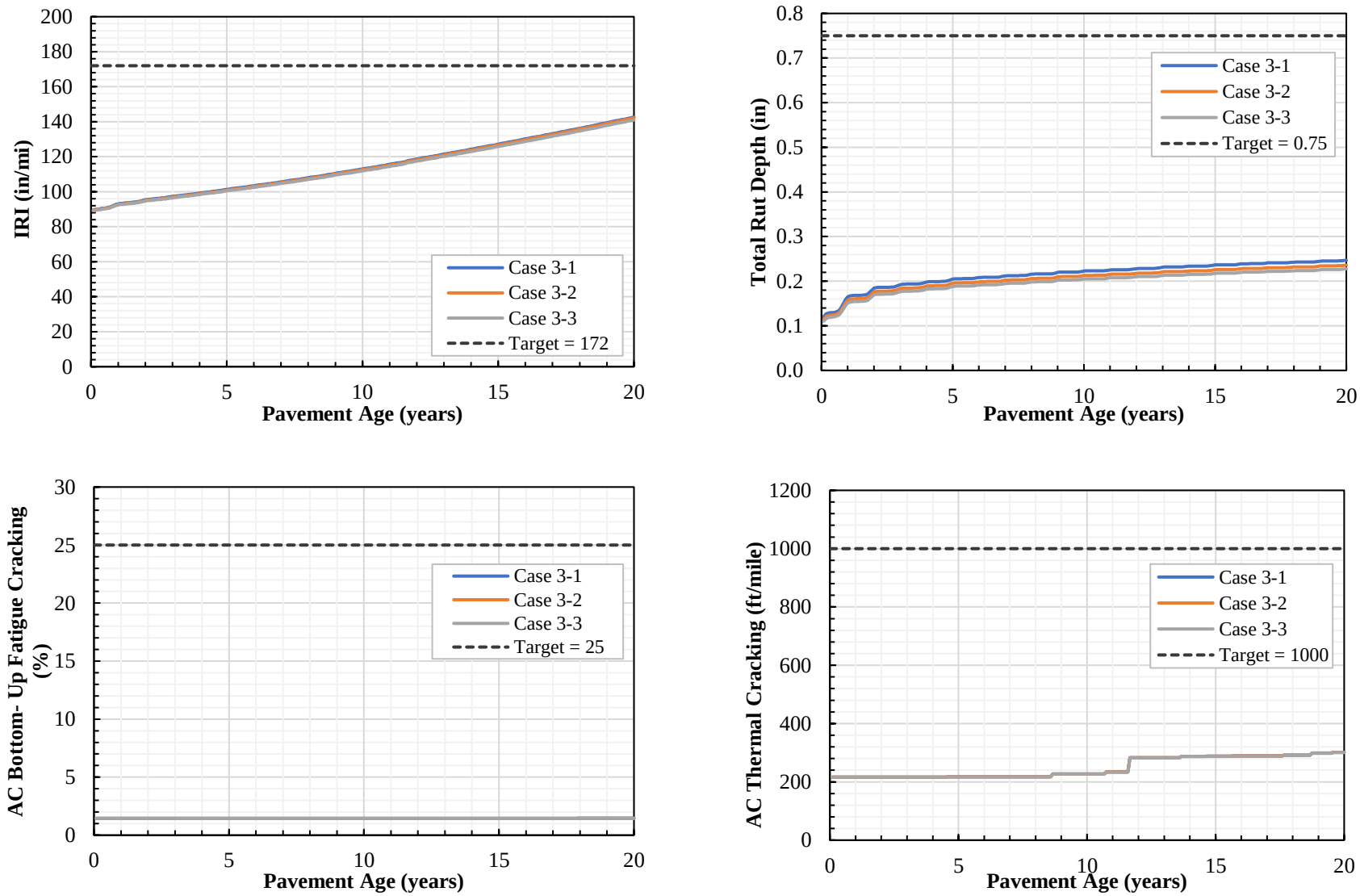

Figure 3.7 Development of IRI, rut depth, AC bottom-up cracking, and AC thermal cracking with pavement age (Cases 3-1 to 3-3).

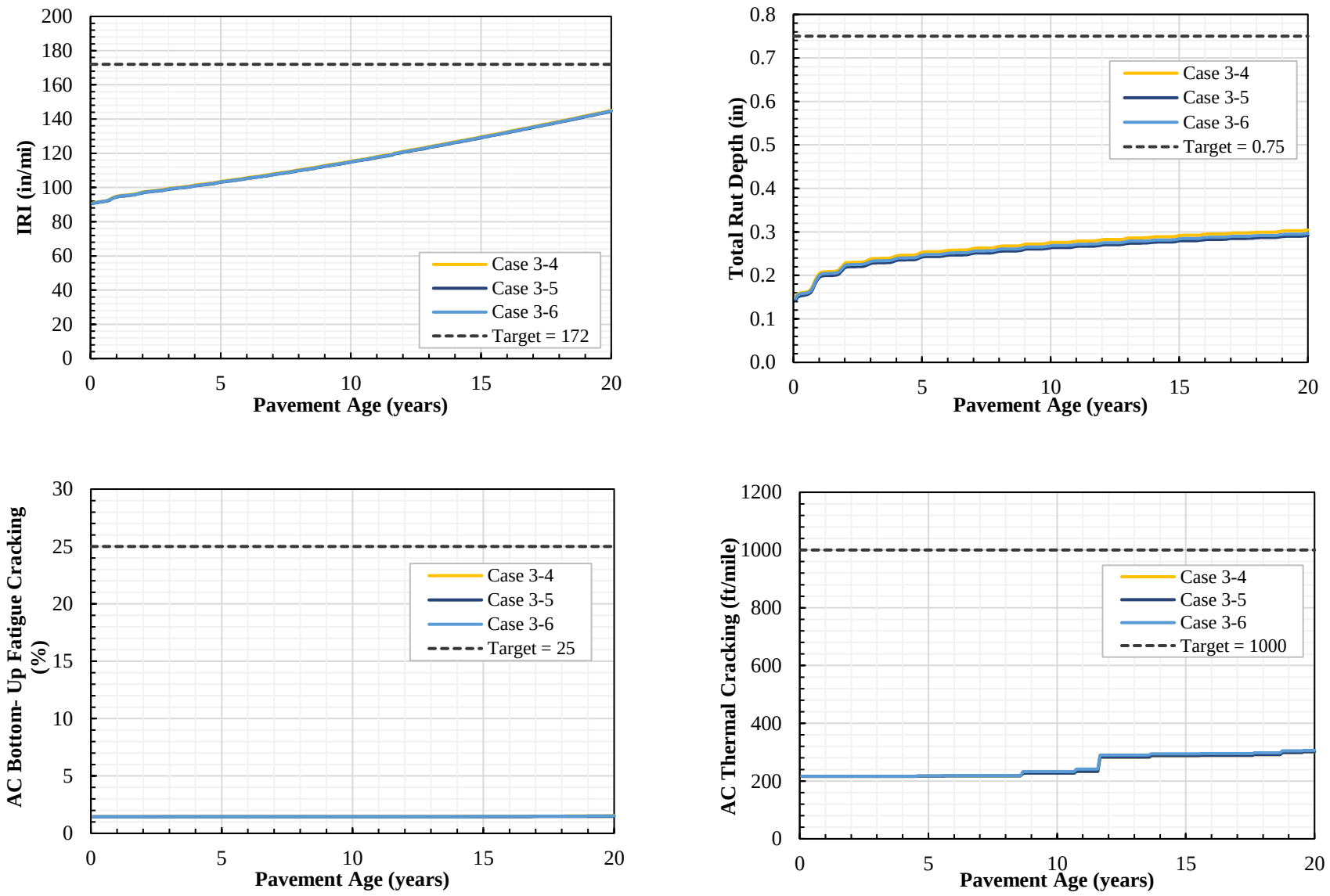

Figure 3.8 Development of IRI, rut depth, AC bottom-up cracking, and AC thermal cracking with pavement age (Cases 3-4 to 3-6).

3.5 Summary and discussion

In this chapter, the potential for structural benefits of placing a geogrid at the interface between subgrade and base course of a flexible pavement was quantified for select design examples, using methods and software readily available to DOT engineers and practitioners. The analysis was conducted in two steps: First, apparent increases in resilient moduli of the pavement layers, resulting from geogrid-reinforcement, were determined using the Composite Geosynthetic-Base Course Model and Tensar's Spectrapave software packages. In a second phase, the enhanced moduli values were input in the AASHTOWare Pavement ME software, which predicted the pavement expected performance relative to potential distress modes (i.e., cracking, rutting, and roughness) over the desired design life of the structure.

Analyzed examples included untreated, chemically treated and geogrid-reinforced pavement structures. These were based on three asphalt pavements previously constructed (without geogrid-reinforcement) in Indiana: (1) SR 46 in Clay County; (2) US 31 St. in Joseph County; and (3) SR 37 in Martinsville. To quantify the benefits of geogrid-reinforcement in pavements and compare pavement performance using geogrids with that using chemically treated subgrades three cases were considered for each site: untreated pavement; geogrid-reinforced pavement; and chemically treated pavement (Sites 2 and 3 only). In addition, to compare the results from the Composite Geosynthetic-Base Course Model and Tensar's Spectrapave software three more cases were considered for each site: untreated pavement (8.8 ksi subgrade modulus); geogrid-reinforced pavement (Composite Geosynthetic-Base Course Model); and geogrid-reinforced pavement (Tensar's Spectrapave software).

The following observations were made:

(1) For the pavement of Site 1 which has the thinnest asphalt layer (10 in.), the geogrid-reinforcement reduced fatigue cracking and pavement roughness. In such a case, a geogrid placed over untreated subgrade would increase the pavement life, based on fatigue cracking, by almost 18%.

(2) For pavements with thicker asphalt layers, such as those at Sites 2 and 3, the subgrade reinforcement did not result in significant improvement.

(3) For all the pavements designs analyzed in this study, rutting and thermal cracking remained unaffected by the presence of the geosynthetic reinforcement.

(4) Overall, inclusion of a geogrid as subgrade reinforcement did not appear highly beneficial, as only modest increase in pavement life was indicated by the analysis.

(5) Results obtained using the two modulus assessment methods were generally consistent.

Finally, it is important to recognize the limitations of the study presented in this chapter:

- The analyses were performed for a limited number of design situations, in terms of subgrade conditions, layer thicknesses, material properties, geogrid tensile stiffness, environmental and traffic conditions. Conclusions should not be extrapolated outside the ranges of parameters that have been considered here.
- In all cases, it was assumed the geogrid would be placed at the interface between subgrade and aggregate layer. This is the most practical option with respect to construction consideration. However, depending on the thickness of overlaying layers and loading conditions as discussed in the literature review, this might not be the optimal location for reinforcing effect to be maximized.
- Potential mechanisms of improvement due to the presence of a geogrid during the placement and compaction of the aggregate layer are not modeled in the software used herein. For instance, interlocking between the aggregate and the grid apertures could restraint lateral deformation of the material being compacted and result in better stability and quality of compaction. This, however, might be only temporary because of creep taking place in the geogrid polymer. Another potential benefit, unaccounted here, is the support a geogrid could provide in order to establish a stable working platform on soft, high-water content subgrade. The situation would, temporarily, be equivalent to that of an unpaved road, and is outside the scope of this study. This problem was addressed in an earlier JTRP investigation by Huang et al. (2010). Conclusions drawn at the time are still valid.

4. NUMERICAL ANALYSIS OF GEOSYNTHETIC-REINFORCED EMBANKMENT CONSTRUCTED OVER A WEAK FOUNDATION ZONE

4.1 Introduction

One of the most challenging problems with the construction of road embankments over a locally weak foundation zone is induced differential settlement. In addition to detrimental effects to the embankment and supported roadway, differential settlement can cause undesirable change in the transverse slope of the pavement and its surficial drainage function. In the presence of a weak foundation zone of finite extent during the embankment construction, the weight of embankment fill, under its self-weight, tends to settle more above the weak soil than above the firmer foundation. This tendency is resisted by shear strength in the contact zone between the moving mass of soil above the weak zone and the stationary mass of soil above the stiff foundations. As a result, stresses applied by the embankment fill to the weak foundation zone are reduced and stresses acting on the stiff foundation are increased. This load transfer mechanism is known as soil arching (Terzaghi, 1943). The use of geogrid-reinforcement at the base of such embankment as a potential mean of further reducing differential settlement is investigated in this chapter. It is postulated that, when a geogrid is placed at the base of an embankment constructed over a locally weak foundation zone, the resulting differential settlement mobilizes tension in the geogrid, which then behaves like a tensioned membrane and restricts the downward movement of the fill. In this way, the addition of a geogrid is expected to supplement soil arching by reducing further any differential settlement and unwanted geometric defects.

It is noted that the geogrid application considered herein, to mitigate the effects of localized weak foundation zone, is different from the well-known use of geogrid reinforcement to control the bearing capacity of embankments on overall weak foundation soils. The later has been investigated extensively, including in JTRP past projects (Ludlow et al. 1992), its mechanism as well as benefits are well-understood (e.g. Jewell 1988; Rowe and Li 2005) and it is not addressed in this study.

To investigate the potential benefits of using geogrid-reinforcement at the base of an embankment constructed of a localized weak foundation zone, numerical analyses were carried out using the ABAQUS finite element software package. A 2D plane strain finite element model

was developed to simulate the embankment and its foundation, and a sensitivity study was performed in order to identify the most influential parameters.

4.2 ABAQUS software

ABAQUS is a commercial software package for finite element analysis. ABAQUS can be used to model a wide range of engineering situations including linear and non-linear problems. The ABAQUS product suite consists of three main modules: ABAQUS/STANDARD, ABAQUS/EXPLICIT and ABAQUS/CAE. ABAQUS/CAE provides the environment for pre- and post-processing. During the stage of pre-processing, the model is graphically created, and an ABAQUS input file is generated. The post-processing stage involves evaluation of the results once simulation has been completed. ABAQUS/STANDARD or ABAQUS/EXPLICIT is used in the simulation stage. ABAQUS/STANDARD is a general-purpose finite element program, which uses an implicit integration scheme while ABAQUS/EXPLICIT uses an explicit integration scheme. ABAQUS/STANDARD and ABAQUS/CAE were used in this study.

The following information is required to define an analysis model in ABAQUS: discretized geometry (elements and nodes), element section properties, material data, loads and boundary conditions, and analyses type (static or dynamic) (ABAQUS, 2016). More details about the components of an ABAQUS analysis model can be found in the ABAQUS Online Documentation (2016).

4.3 Model geometry and finite element mesh

The present study examines the construction of an example road embankment with 2:1 (horizontal:vertical) slope. Due to the assumed symmetry, only the right half of the problem was modeled. Figure 4.1(a) represents the right half of embankment having 3 m height and 5.5 m crest width and its foundation represented by a 30 m thick soil deposit resting on a rigid bedrock. A model width of 30.5 m was chosen in order to minimize boundary effects. That is, the horizontal limit of the discretization is far enough from the area of interest such that its presence does not affect the results. Figure 4.1(a) depicts the reference scenario where the embankment is placed over a homogeneous, stiff foundation soil. To address the benefits of a geogrid-reinforced embankment over a weak foundation zone of finite size, the foundation soil is divided into two

parts: weak and stiff. The width of weak zone was initially chosen to be equal to 30% of the total embankment base width (0.3B). Figure 4.1(b) shows the unreinforced embankment, which is the same as in Figure 4.1(a), except for the inclusion of the weak zone. The half width of the weak zone is 3.45 m.

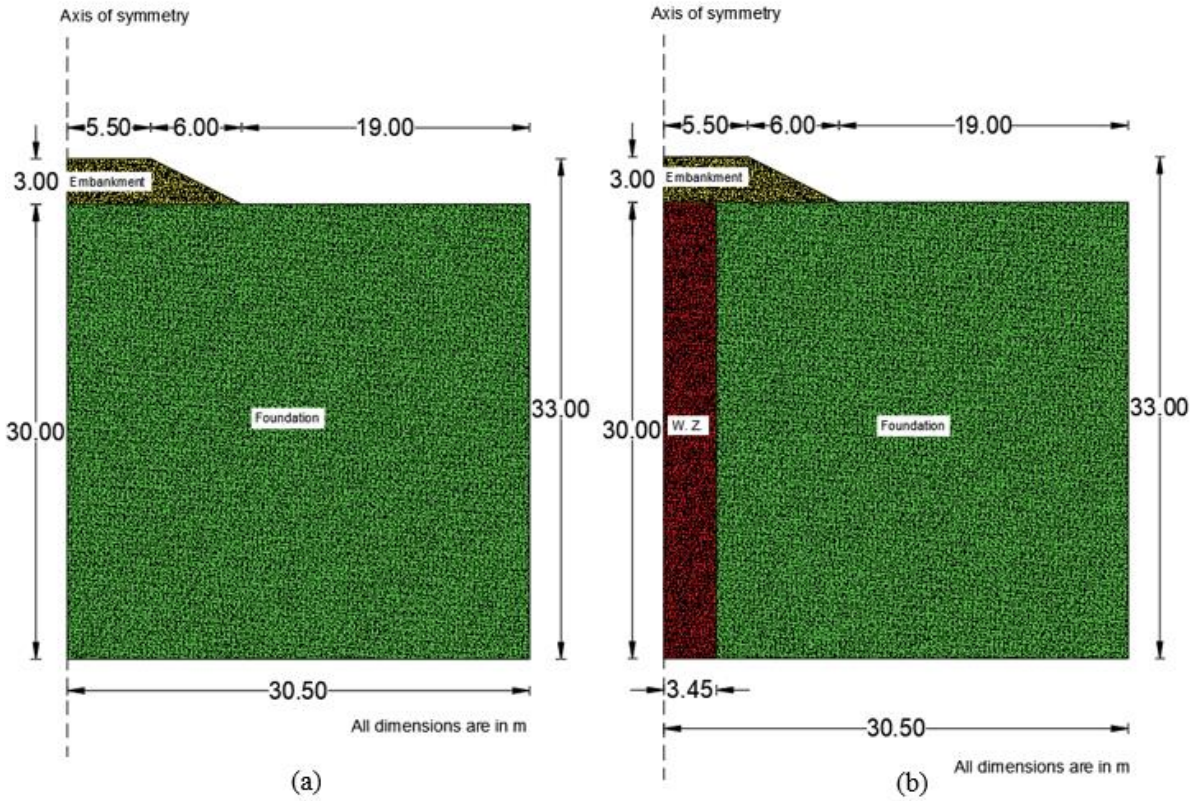

Figure 4.1 Cross-section of the unreinforced embankment model with: (a) no weak zone; and (b) weak zone width equal to 0.3B.

The geogrid-reinforced embankment model includes: (1) a 0.3-m-thick granular base layer on top of the foundation; and (2) the geogrid on top of the granular layer. The detailed geometry of the geogrid-reinforced embankment is depicted in Figure 4.2. Total of 13,770 linear plane strain triangle elements (CPE3) (for a total of 7,169 nodes) were used to discretize the embankment and foundation soil. Another 54 linear 2D truss elements with cross-sectional area of 0.001 m^2 were used to discretize the geogrid. The finite element model is illustrated in Figure 4.3.

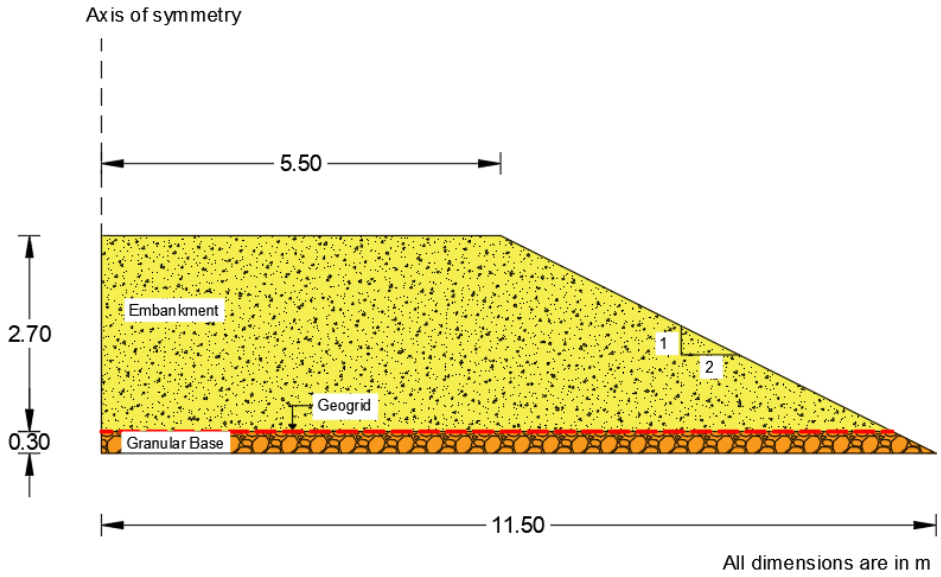

Figure 4.2 Cross-section of the geogrid-reinforced embankment.

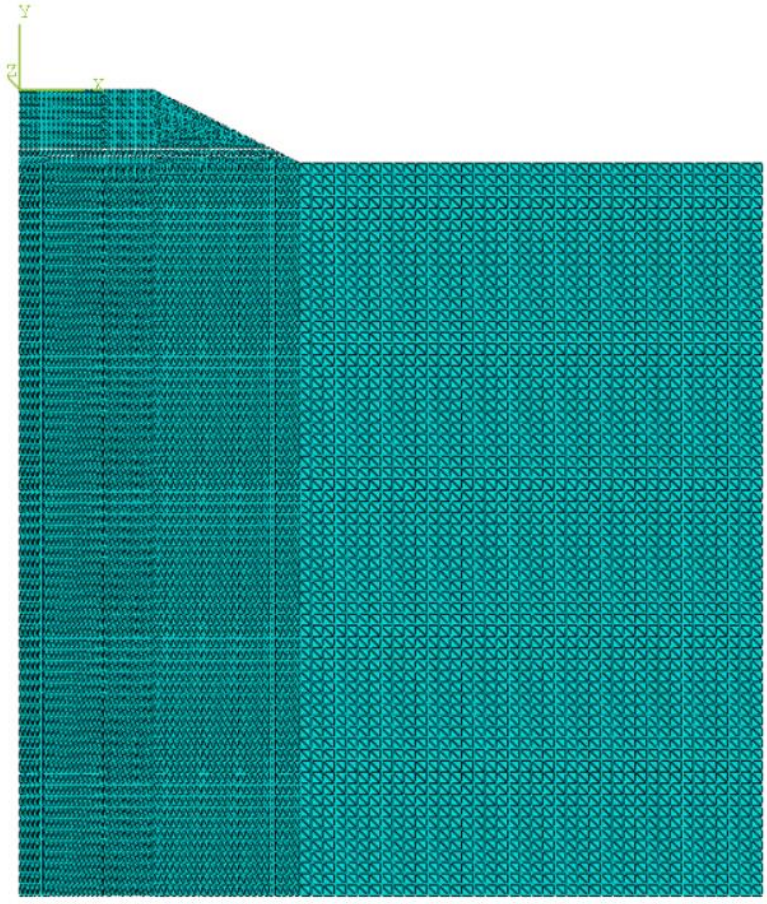

Figure 4.3 Finite element model for the embankment.

4.4 Loading and boundary conditions

The loading included application of gravity to the foundation soils during the first step of the analysis. During the second step, the construction of the embankment was simulated by applying gravity to the elements forming the embankment. In the reinforced model, the gravity in the embankment, granular base and geogrid was applied simultaneously. In addition, during the first step, a linear horizontal pressure distribution was applied to the right boundary of the model to simulate the far-field geostatic stresses in the foundation soil for at-rest conditions. Density of the soil was assumed to be 2,050 kg/m^3 and its coefficient of earth pressure, at-rest, Ko = 0.5, which gives the lateral stress along the boundary increasing linearly with depth from 0 to 302 kPa.

The left boundary is the axis of symmetry and allows vertical displacement only. Normal displacement was not allowed on the bottom boundary of the model. Finally, the top boundary of the model was free of restrain. The loading and boundary conditions for the embankment model are illustrated in Figure 4.4.

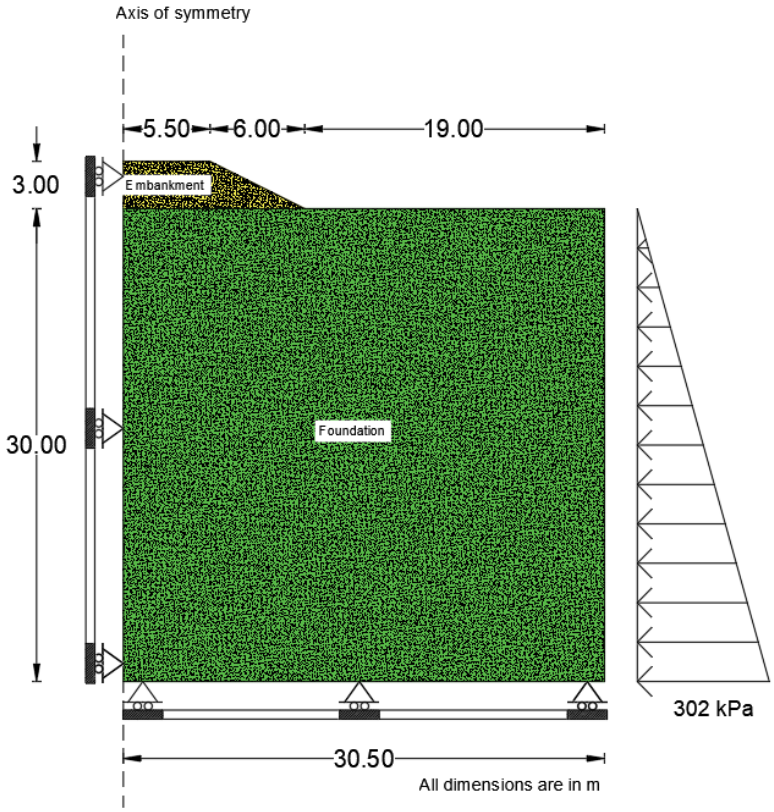

Figure 4.4 Loading and boundary conditions for the embankment model.

4.5 Material models and parameters

In this study, the Mohr-Coulomb (M-C) linear elastic-perfectly plastic model was used for the embankment, foundation, and granular base. This constitutive model is already implemented in ABAQUS.

The Mohr-Coulomb criterion is used to model the material yielding condition. Yielding occurs when the state of stress at a material point reaches the condition:

$$\tau_f = c + \sigma' tan\varphi \qquad (4.1)$$

where τ_f is the shear strength on the yielding plane; c is the cohesion; σ' is the normal effective stress, and φ is the friction angle of the material. The M-C criterion can also be described in terms of principal stresses as:

$$F = (\sigma_1' - \sigma_3') + (\sigma_1' + \sigma_3')\, sin\varphi - 2c\, cos\varphi = 0 \qquad (4.2)$$

where σ_1' and σ_3' are the major and minor principal effective stresses, respectively.

The following parameters are needed in ABAQUS to employ the Mohr-Coulomb plasticity model, with non-associated flow rule: friction angle (φ), dilation angle (ψ), cohesion (c), and absolute plastic strain (ε^p). Furthermore, the criterion was applied in conjunction with linear isotropic elasticity for non-yielding states of stress, which requires the definition of the following parameters: Young's modulus (E), Poisson's ratio (ν). The model parameters for the soils used in this study are summarized in Table 4.1.

Linear elasticity was used to describe the behavior of the geogrid. As the detail of the grid geometry could not be represented in a two-dimensional model, its cross-section was converted into an equivalent, continuous sheet of thickness (t), 1 mm, and the Young's modulus (E) was adjusted accordingly, the tensile stiffness per unit width (J) of the geogrid being defined as $J = E\, t$. An initial value of J = 350 kN/m was considered, which results in a value of 350 MPa for the Young's modulus of the geogrid. Interface conditions between the reinforcement and surrounding materials are non-slippage, full contact.

Table 4.1 Model parameters of embankment fill, stiff foundation soil, weak zone, and granular base.

Parameter	**Embankment fill**	**Stiff foundation soil**	**Weak zone**	**Granular base**
Material model	M-C	M-C	M-C	M-C
Young's modulus, E (MPa)	100	100	5	200
Poisson's ratio, ν	0.3	0.3	0.3	0.3
Friction angle, φ (°)	28	28	20	32
Dilation angle, ψ (°)	0	0	0	2
Cohesion, c (MPa)	0.01	0.01	10^{-3}	10^{-3}

4.6 Numerical results

Figure 4.5 shows the vertical displacement (i.e. in the Y direction) contours in the unreinforced model with no weak zone (W.Z. = 0). This is the base case used as reference in further discussion and the parametric study. The displacements shown in the Figure correspond to the end of the second load step (end of embankment construction). Figure 4.6 shows the vertical displacement (Y direction) contours in the unreinforced and reinforced models with W.Z.= 0.3B (30% of the base width of the embankment). A comparison between Figures 4.5 and 4.6 shows, in both unreinforced and reinforced cases, a large differential settlement at the crest of the embankment constructed over the weak zone. The results from the reinforced and unreinforced models do not show any significant difference. The benefit of adding a geogrid-reinforcement with Young's modulus of 350 MPa in the embankment for this case was not significant. However, it is noted that this value (350 MPa) represents the lower end in the range of available geogrid tensile stiffness (350kN/m). The influence of this parameter will be discussed later.

These observations were confirmed by the results shown in Tables 4.2 and 4.3. Table 4.2 summarizes the results of vertical displacements (positive downwards) at the center and edge of embankment crest, differential settlement between the center and edge, transverse slope induced by the differential settlement between the two points, and percentage decrease in transverse slope with the addition of geogrid. Table 4.3 shows the same results as Table 4.2, but in this case the two points of comparison are the center of the embankment crest and the edge of weak zone projected on the crest. The Table shows that a maximum transverse slope of 4.7% was induced by the existence of the weak zone in the foundation soil, which is more than two orders of magnitude greater than the transverse slope in the embankment model without the weak zone. The geogrid reinforcement contributes only a 5.4% decrease in the transverse slope.

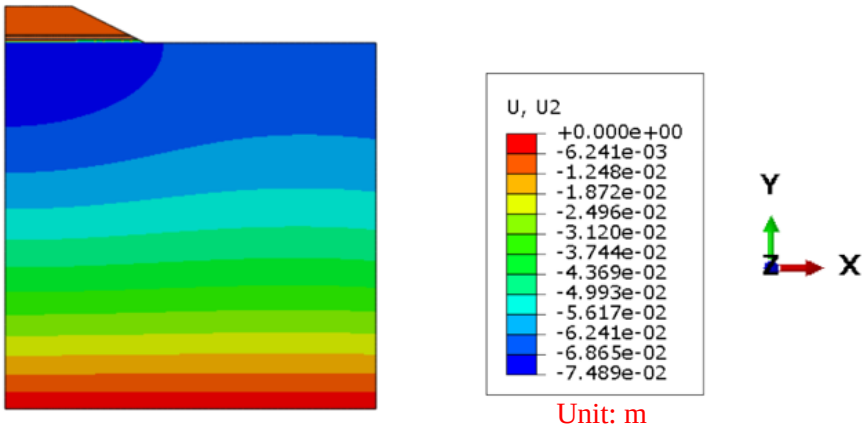

Figure 4.5 Vertical displacement contours for the unreinforced model with W.Z.= 0.

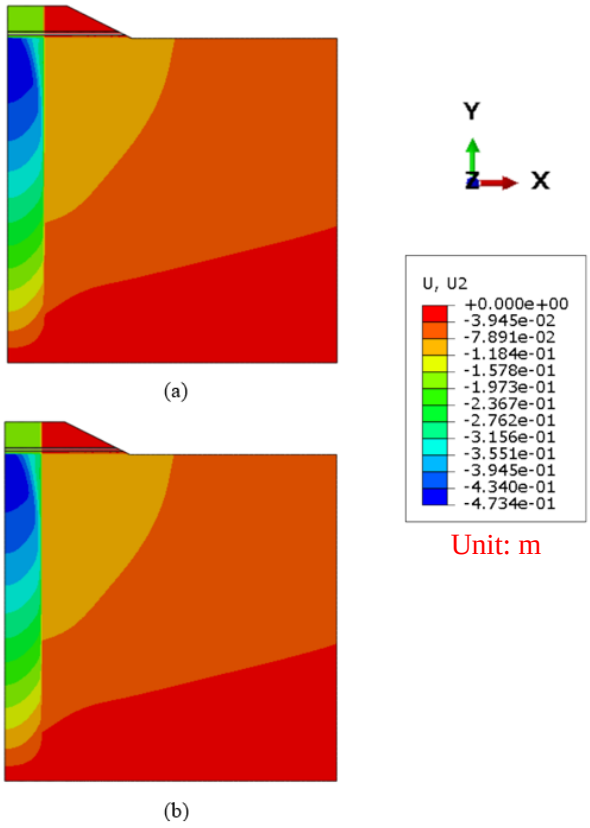

Figure 4.6 Vertical displacement contours for: (a) unreinforced model with W.Z.= 0.3B; and (b) reinforced model with W.Z.= 0.3B.

Table 4.2 Crest settlements and transverse slope deformations for unreinforced and reinforced embankments (W.Z.= 0 and 0.3B).

W.Z. width (B)	**Reinforced/Unreinforced**	u_y^{center} **(mm)**	u_y^{edge} **(mm)**	$\Delta u_y = u_y^c - u_y^e$ **(mm)**	$\frac{\Delta u_y}{L_{c-e}}$ **(%)**	**Percentage decrease in transverse slope with reinforcement**
0	Unreinforced	11.52	10.17	1.35	0.025	
0.3	Unreinforced	191.15	23.61	167.54	3.046	
	Reinforced	182.69	23.69	159	2.891	-5.1

Table 4.3 Crest settlements and transverse slope deformations for unreinforced and reinforced embankments (W.Z.= 0.3B).

W.Z. width (B)	**Reinforced/Unreinforced**	u_y^{center} **(mm)**	$u_y^{edge\ of W.Z.}$ **(mm)**	$\Delta u_y = u_y^c - u_y^e$ **(mm)**	$\frac{\Delta u_y}{L_{c-e}}$ **(%)**	**Percentage decrease in transverse slope with reinforcement**
0.3	Unreinforced	191.15	28.21	162.94	4.723	
	Reinforced	182.69	28.62	154.07	4.466	-5.4

4.7 Parametric study

In the analysis described above, only the case of a weak zone equal to 0.3B with a Young's modulus of 5 MPa was considered. It is of interest to investigate the potential benefit of geogrid reinforcement in embankment models with different weak zone and reinforcement configurations. A parametric study was performed in order to investigate the respective influence of these factors, namely the modulus of weak zone, its width and location, and the tensile stiffness of the geogrid reinforcement.

4.7.1 Effect of modulus and width of the weak zone

Based on the initial model with W.Z.= 0.3B, the following values for the Young's modulus of weak zone were considered: 5, 7, 10, 15, 25 MPa. The effect of the modulus of weak zone was also investigated for W.Z.= 0.1B and W.Z.= 0.48B. Figure 4.7 represents the cross-sections of the unreinforced embankment model with W.Z.= 0.1B and W.Z.= 0.48B. The following values for the modulus of the weak zone were investigated for the model with W.Z.= 0.1B: 5 and 10 MPa. For

the model with W.Z.= 0.48B, the following stiffnesses were used: 7, 12, 15, 20, 25 MPa. In contrast with the initial reinforced model, a geogrid with a Young's modulus of 400 MPa, instead of 350 MPa, was used for the reinforced model with W.Z.= 0.48B, due to numerical convergence issues in ABAQUS.

Table 4.4 summarizes the results of the vertical displacements at the center and edge of embankment crest, the differential settlement between the center and edge, transverse slope induced by the differential settlement between these two points, and percentage decrease in transverse slope with the addition of the geogrid for the cases with W.Z.= 0.1B, 0.3B, and 0.48B. Table 4.5 shows the same results as Table 4.4, but in this case the two points of comparison are the center of the embankment crest and the edge of weak zone projected on the crest, for the model with W.Z.= 0.3B. The reinforced model with two geogrids layers which is included in both tables, will be discussed later. As one can see from Table 4.4, there was practically no contribution of the geogrid-reinforcement to the decrease of transverse slope induced in the model with W.Z.= 0.1B. The width of weak zone was small and thus the induced transverse slope was close to that of the case with no weak zone. In this case, the geogrid was not mobilized, and soil arching in the embankment was a dominant mechanism.

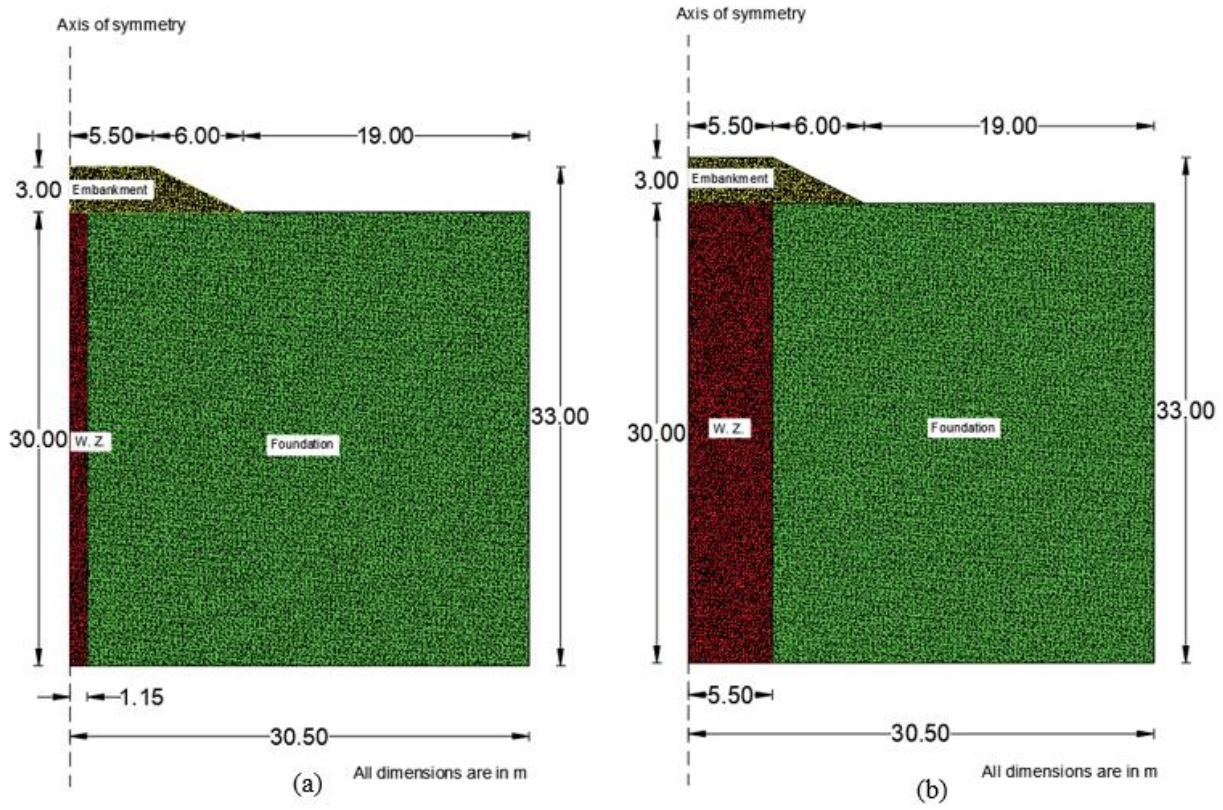

Figure 4.7 Cross-section of the unreinforced embankment model with: (a) W.Z.= 0.1B; and (b) W.Z.=0.48B.

Table 4.4 Crest settlements and transverse slope deformations for unreinforced and reinforced embankments (W.Z.= 0, 0.1B, 0.3B, and 0.48B).

W.Z. width (B)	**W.Z. Young's modulus (MPa)**	**Type of reinforcement**	u_y^{center} **(mm)**	u_y^{edge} **(mm)**	$\Delta u_y = u_y^c - u_y^e$ **(mm)**	$\frac{\Delta u_y}{L_{c-e}}$ **(%)**	**Percentage decrease in transverse slope with reinforcement**
0		Unreinforced	11.52	10.17	1.35	0.025	
0.10	5	Unreinforced	14.26	11.52	2.74	0.050	
		1 Geogrid	14.19	11.46	2.73	0.050	-0.4
		2 Geogrids	14.13	11.41	2.72	0.049	-0.7
0.10	10	Unreinforced	13.77	11.28	2.49	0.045	
		1 Geogrid	13.68	11.22	2.46	0.045	-1.2
		2 Geogrids	13.61	11.16	2.45	0.045	-1.6
0.30	5	Unreinforced	191.15	23.61	167.54	3.046	
		1 Geogrid	182.69	23.69	159.00	2.891	-5.1
		2 Geogrids	174.69	23.88	150.81	2.742	-10
0.30	7	Unreinforced	124.58	22.15	102.43	1.862	
		1 Geogrid	121.68	22.18	99.50	1.809	-2.9
		2 Geogrids	119.15	22.30	96.85	1.761	-5.4
0.30	10	Unreinforced	80.26	20.17	60.09	1.093	

Table 4.4 continued

W.Z. width (B)	W.Z. Young's modulus (MPa)	Type of reinforcement	u_y^{center} (mm)	u_y^{edge} (mm)	$\Delta u_y = u_y^c - u_y^e$ (mm)	$\frac{\Delta u_y}{L_{c-e}}$ (%)	Percentage decrease in transverse slope with reinforcement
0.30	10	1 Geogrid	79.54	20.17	59.37	1.079	-1.2
		2 Geogrids	79.44	20.20	59.24	1.077	-1.4
0.30	15	Unreinforced	48.41	17.40	31.01	0.564	
		1 Geogrid	48.25	17.36	30.89	0.562	-0.4
		2 Geogrids	48.74	17.31	31.43	0.571	1.4
0.30	25	Unreinforced	24.19	14.16	10.03	0.182	
		1 Geogrid	24.29	14.08	10.21	0.186	1.8
0.48	7	Unreinforced	225.37	36.08	189.29	3.442	
0.48	12	Unreinforced	130.28	23.28	107.00	1.945	
		1 Geogrid	127.6	24.28	103.32	1.879	-3.4
0.48	15	Unreinforced	103.57	19.73	83.84	1.524	
		1 Geogrid	101.60	20.94	80.66	1.467	-3.8
		2 Geogrids	100.49	20.91	79.58	1.447	-5.1
0.48	20	Unreinforced	76.37	16.46	59.91	1.089	
		1 Geogrid	75.13	17.71	57.42	1.044	-4.2
		2 Geogrids	74.67	17.88	56.79	1.033	-5.2
0.48	25	Unreinforced	59.59	15.34	44.25	0.805	
		1 Geogrid	58.74	15.91	42.83	0.779	-3.2
		2 Geogrids	58.54	16.14	42.40	0.771	-4.2

Table 4.5 Crest settlements and transverse slope deformations for unreinforced and reinforced embankments (W.Z.= 0.3B).

W.Z. width (B)	W.Z. Young's modulus (MPa)	Type of reinforcement	u_y^{center} (mm)	$u_y^{edge\ of\ W.Z.}$ (mm)	$\Delta u_y = u_y^c - u_y^e$ (mm)	$\frac{\Delta u_y}{L_{c-e}}$ (%)	Percentage decrease in transverse slope with reinforcement
0.30	5	Unreinforced	191.15	28.21	162.94	4.723	
		1 Geogrid	182.69	28.62	154.07	4.466	-5.4
		2 Geogrids	174.69	29.09	145.60	4.220	-10.6
0.30	7	Unreinforced	124.58	26.49	98.09	2.843	
		1 Geogrid	121.68	26.65	95.03	2.754	-3.1
		2 Geogrids	119.15	26.93	92.22	2.673	-6.0
0.30	10	Unreinforced	80.26	24.26	56.00	1.623	
		1 Geogrid	79.54	24.31	55.23	1.601	-1.4
		2 Geogrids	79.44	24.41	55.03	1.595	-1.7
0.30	15	Unreinforced	48.41	21.14	27.27	0.790	
		1 Geogrid	48.25	21.09	27.16	0.787	-0.4
		2 Geogrids	48.74	21.02	27.72	0.803	1.7
0.30	25	Unreinforced	24.19	17.42	6.77	0.196	
		1 Geogrid	24.29	17.30	6.99	0.203	3.2

Figure 4.8 is a plot of the transverse slope between the center and edge of the embankment as a function of the Young's modulus of the weak zone, for the model with W.Z.= 0.3B and 0.48B. Figure 4.9 focusses on the data of Figure 4.8 for the case of W.Z.= 0.3B. As it can be seen from Figures 4.8 and 4.9, there is a decreasing benefit of geogrid-reinforcement with increasing modulus of the weak zone. This is quite apparent in the case of W.Z.= 0.3B, where the maximum percentage decrease of the transverse slope with a single reinforcement was approximately 5% and for the softest weak zone, i.e. for 5 MPa Young's modulus. As the weak zone becomes stiffer (from 5 to 10 MPa), the transverse slope, in the unreinforced case, is decreased by a factor of 3, and the benefit of geogrid becomes negligible. For a weak zone with modulus greater than 15 MPa, the percentage decrease in transverse slope with geogrid-reinforcement was almost 0%. For the case of W.Z.= 0.48B, there was no clear trend observed in the effect of the modulus of the weak zone on the benefit of geogrid-reinforcement. The percentage decrease in transverse slope with reinforcement was constant, around 3-4% for all the modulus values above 12 MPa (the case of 5 MPa with geogrid did not numerically converge and thus results are not available).

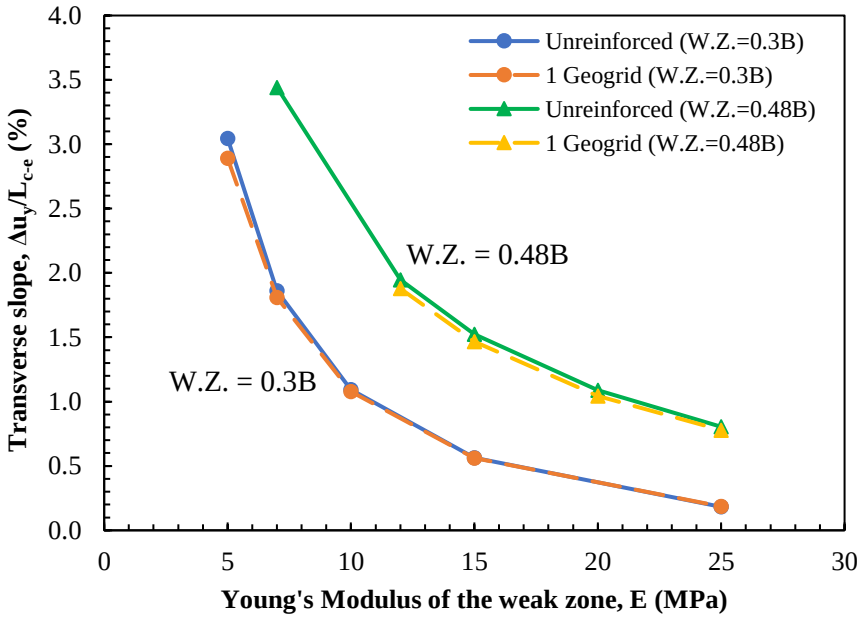

Figure 4.8 Dependence of transverse slope between edge and center of embankment on the Young's modulus of the weak zone for unreinforced and reinforced models with W.Z.= 0.3B and 0.48B.

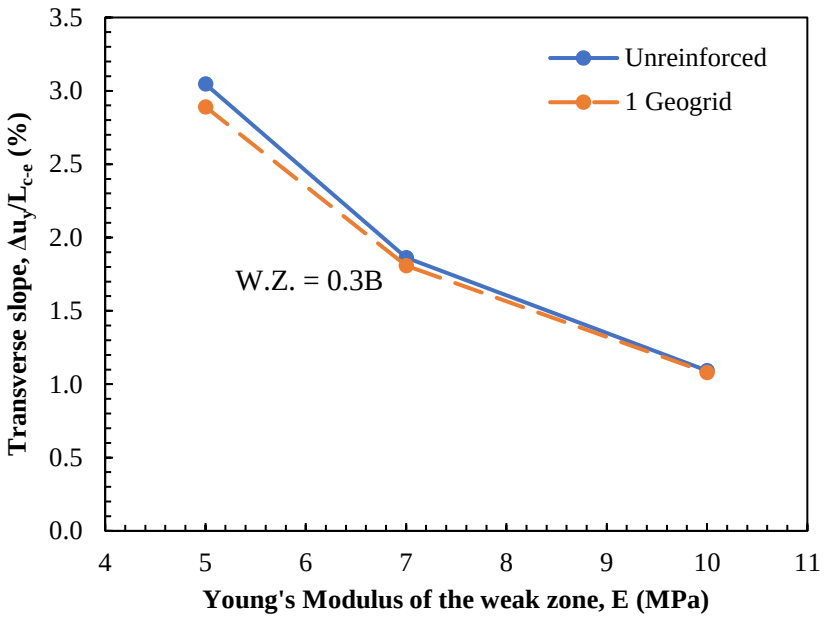

Figure 4.9 Dependence of transverse slope between edge and center of embankment on the Young's modulus of the weak zone for unreinforced and reinforced models with W.Z.= 0.3B.

As mentioned above, the geogrid-reinforcement in the case of W.Z.= 0.1B didn't contribute to the decrease of transverse slope at the embankment crest. For instance, a total width of the weak zone equal to 2.3 m, it was effectively bridged by the embankment fill arching and only a transverse slope of 0.05% was induced by the existence of the weak zone. In the case of W.Z.= 0.3B, the largest benefit of geogrid reinforcement was seen for a modulus of the weak zone equal to 5 MPa. The addition of a geogrid layer with 350 MPa modulus decreased the transverse slope by 5%. Finally, for the case of W.Z= 0.48B, there was no computation result that could be obtained with the 5 MPa modulus.

4.7.2 Effect of type of geogrid-reinforcement

In the initial reinforced embankment model, only one layer of geogrid with tensile stiffness 350 kN/m or equivalent Young's modulus of 350 MPa was considered. This subsection presents the results of a modified model where a second layer of geogrid is included. For this reason, a 0.3-m-thick granular base layer was added to the top of the first geogrid and then a second geogrid was placed on the top of the second granular base layer. The cross-section of the reinforced embankment with two geogrid layers is depicted in Figure 4.10.

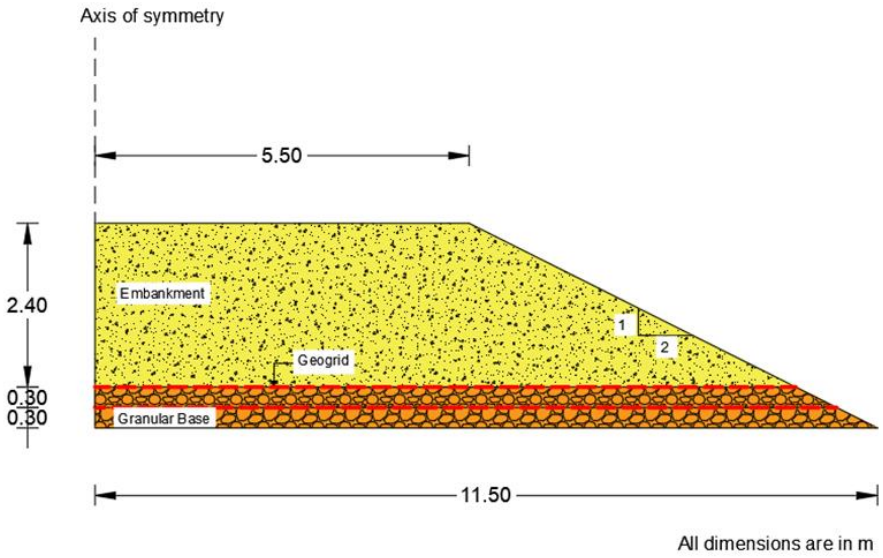

Figure 4.10 Cross-section of the reinforced embankment with two layers of geogrid.

Another modification was made to the unreinforced and reinforced models to account for the staged construction of the embankment. Two models simulating staged construction were created. In the first model, the load of the embankment was applied in the three stages: (1) Activation of gravity for the first granular base layer and geogrid; (2) Activation of gravity for the second granular base layer and geogrid; and (3) Activation of gravity for the remaining part of the embankment. The three stages of construction were simulated for the unreinforced and for the two reinforced models (single and double geogrid reinforcement). In the second model, the weight of the embankment was applied in four stages: (1) Activation of gravity for the first granular base layer and geogrid; (2) Activation of gravity for the second granular base layer and geogrid; and (3) Activation of gravity for the first half of the embankment; and (4) Activation of gravity for remaining part of the embankment. The four stages of construction were simulated for the unreinforced and for the two reinforced models.

The effect of the number of geogrid layers on the results of the transverse slope of the embankment with W.Z.= 0.3B and modulus ranging from 5 to 10 MPa was investigated. The results of the first loading model are included in Tables 4.4 and 4.5. The model that simulated the embankment construction in three stages was also used to investigate the effect of geogrid modulus on the transverse slope of the embankment. For this purpose, the following values of geogrid modulus were considered: 350, 1000, and 2000 MPa. The equivalent modulus values 1000 and

2000 MPa (or tensile stiffnesses of 1000kN/m and 2000kN/m, respectively) are typical of high-end uniaxial geogrids. Table 4.6, which is analogous to Table 4.4, lists the results for the model with three stages of embankment construction, W.Z.= 0.3B and weak zone modulus ranging from 5 to 10 MPa. Also, the results for the following types of reinforcement are shown: one layer of geogrid (E= 350, 1000, and 2000 MPa), and two layers of geogrid (E= 350 and 1000 MPa).

Figure 4.11 illustrates the results presented in Table 4.6 and shows the dependence of the transverse slope on the Young's modulus of the weak zone for the unreinforced and reinforced models with W.Z.= 0.3B. It can be observed that the addition of a second geogrid layer with the same modulus as the first one improved the results approximately by a factor of 2. The maximum decrease in transverse slope (19%) was achieved when double geogrid reinforcement with a modulus of 1000 MPa was used for the softest weak zone (modulus 5 MPa). In addition, when the modulus of the single geogrid was increased 2.9 times and 5.7 times, the benefit increased only by a factor of 1.4 and 1.7, respectively. This makes the case of double geogrid-reinforcement the most beneficial.

Table 4.6 Crest settlements and transverse slope deformations for unreinforced and reinforced embankments (embankment construction in 3 stages).

W.Z. width (B)	W.Z. Young's modulus (MPa)	Type of reinforcement	u_y^{center} (mm)	u_y^{edge} (mm)	$\Delta u_y = u_y^c - u_y^e$ (mm)	$\frac{\Delta u_y}{L_{c-e}}$ (%)	Percentage decrease in transverse slope with reinforcement
0.30	5	Unreinforced	171.60	18.89	152.71	2.78	
		1 Geogrid (E=350 MPa)	160.07	18.98	141.09	2.57	-7.6
		1 Geogrid (E=1000 MPa)	155.78	19.09	136.69	2.49	-10.5
		1 Geogrid (E=2000 MPa)	152.52	19.20	133.32	2.42	-12.7
		2 Geogrids (E=350 MPa)	149.27	19.15	130.12	2.37	-14.8
		2 Geogrids (E=1000 MPa)	predicted by linear regression			2.25	-19.0
0.30	7	Unreinforced	111.21	17.66	93.55	1.70	
		1 Geogrid (E=350 MPa)	106.33	17.72	88.61	1.61	-5.3
		1 Geogrid (E=1000 MPa)	104.81	17.79	87.02	1.58	-7.0
		1 Geogrid (E=2000 MPa)	103.03	17.87	85.16	1.55	-9.0
		2 Geogrids (E=350 MPa)	101.74	17.84	83.90	1.53	-10.3
		2 Geogrids (E=1000 MPa)	99.58	18.03	81.55	1.48	-12.8
0.30	10	Unreinforced	70.39	16.05	54.34	0.99	
		1 Geogrid (E=350 MPa)	68.79	16.04	52.75	0.96	-2.9
		1 Geogrid (E=1000 MPa)	68.32	16.08	52.24	0.95	-3.9
		1 Geogrid (E=2000 MPa)	67.69	16.13	51.56	0.94	-5.1
		2 Geogrids (E=350 MPa)	67.56	16.08	51.48	0.94	-5.3
		2 Geogrids (E=1000 MPa)	66.46	16.24	50.22	0.91	-7.6

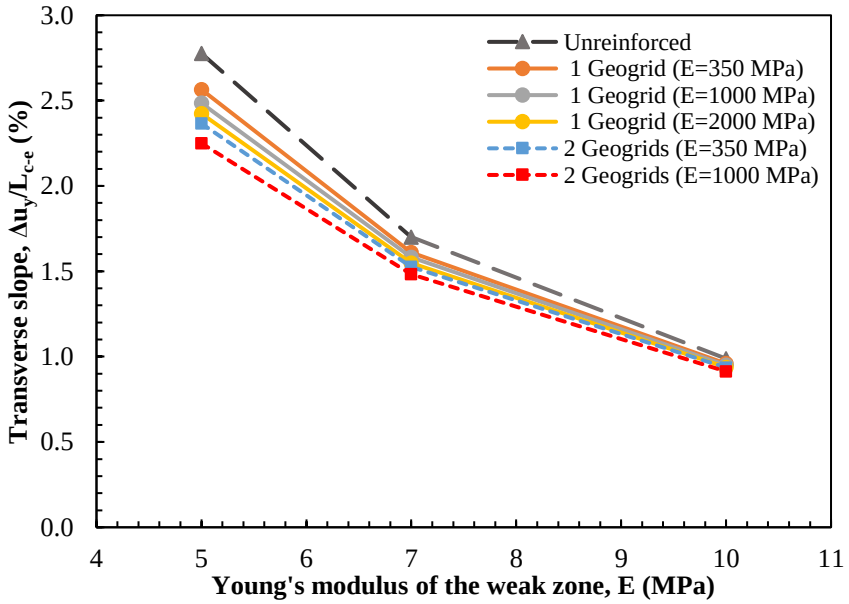

Figure 4.11 Dependence of transverse slope on the Young's modulus of the weak zone for unreinforced and reinforced models with W.Z.= 0.3B (embankment construction in 3 stages).

Table 4.7 summarizes the results of the transverse slope and relative reduction with the addition of geogrid for the models with 4 stages of embankment construction. Similarly to the models with 3 stages of embankment construction, the addition of a second geogrid layer with the same modulus as the first one improves the results approximately by a factor of 2. This observation was also confirmed by the results in Table 4.7. Figure 4.12 shows the dependence of the transverse slope on the Young's modulus of the weak zone for the unreinforced and reinforced models. In all cases, the maximum decrease in slope was observed for the case of double geogrid reinforcement with 350 MPa modulus. The percentage decrease in transverse slope with the addition of two geogrid layers for the three loading models was 11%, 15% and 16%, respectively.

Table 4.7 Crest settlements and transverse slope deformations for unreinforced and reinforced embankments (embankment construction in 4 stages).

W.Z. width (B)	**W.Z. Young's modulus (MPa)**	**Type of reinforcement**	u_y^{center} **(mm)**	u_y^{edge} **(mm)**	$\Delta u_y = u_y^c - u_y^e$ **(mm)**	$\frac{\Delta u_y}{L_{c-e}}$ **(%)**	**Percentage decrease in transverse slope with reinforcement**
0.30	5	Unreinforced	95.18	8.98	86.20	1.57	
		1 Geogrid (E=350 MPa)	88.47	9.05	79.42	1.44	-7.9
		2 Geogrids (E=350 MPa)	predicted by linear regression			1.32	-15.8
0.30	7	Unreinforced	63.33	8.44	54.89	1.00	
		1 Geogrid (E=350 MPa)	59.37	8.51	50.86	0.92	-7.3
		2 Geogrids (E=350 MPa)	55.46	8.62	46.84	0.85	-14.7
0.30	10	Unreinforced	41.48	7.66	33.82	0.61	
		1 Geogrid (E=350 MPa)	39.44	7.70	31.74	0.58	-6.2
		2 Geogrids (E=350 MPa)	37.50	7.74	29.76	0.54	-12.0

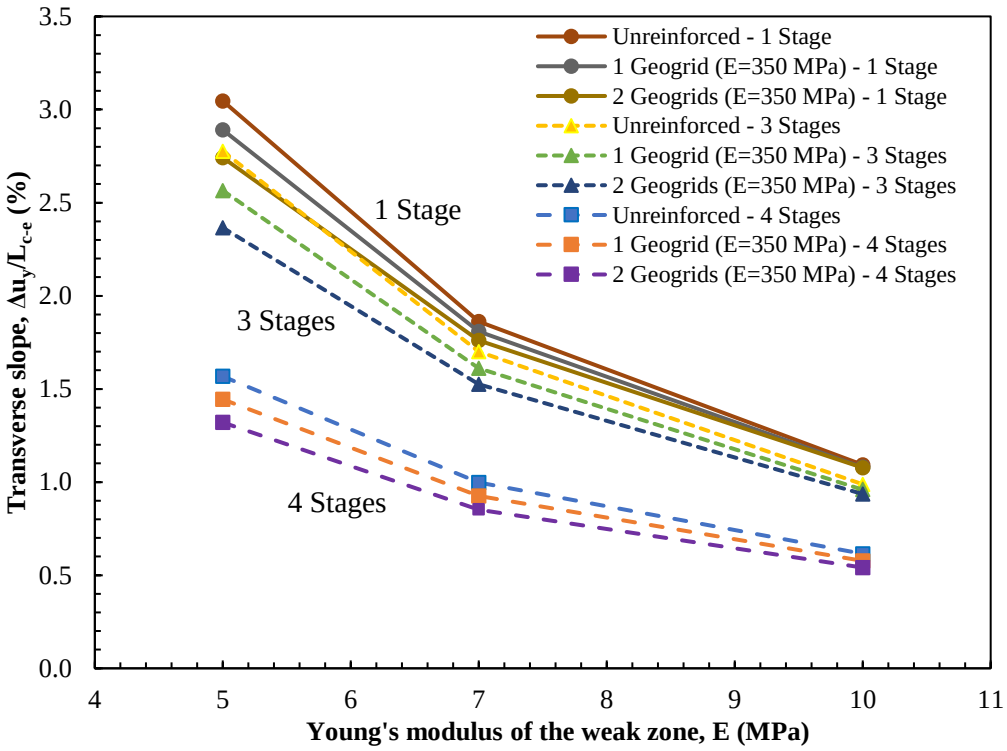

Figure 4.12 Dependence of transverse slope on the Young's modulus of the weak zone for the unreinforced and reinforced models with W.Z.= 0.3B (embankment construction in 1, 3, and 4 stages).

4.7.3 Effect of location of the weak zone

Modeling was performed (for the 3-stage construction sequence) to investigate the effect of the location of the weak zone on the potential benefits of using geogrid-reinforcement. In all the previous models, the weak zone was placed symmetrically below the center of the embankment. Three cases were considered: weak zone of width 0.15B under each edge of the embankment, and weak zone with width 0.15B or 0.30B under the right edge of the embankment.

Figure 4.13 shows the cross-section of the unreinforced model with noncentral and symmetric weak zone of width 0.15B under each edge of the embankment.

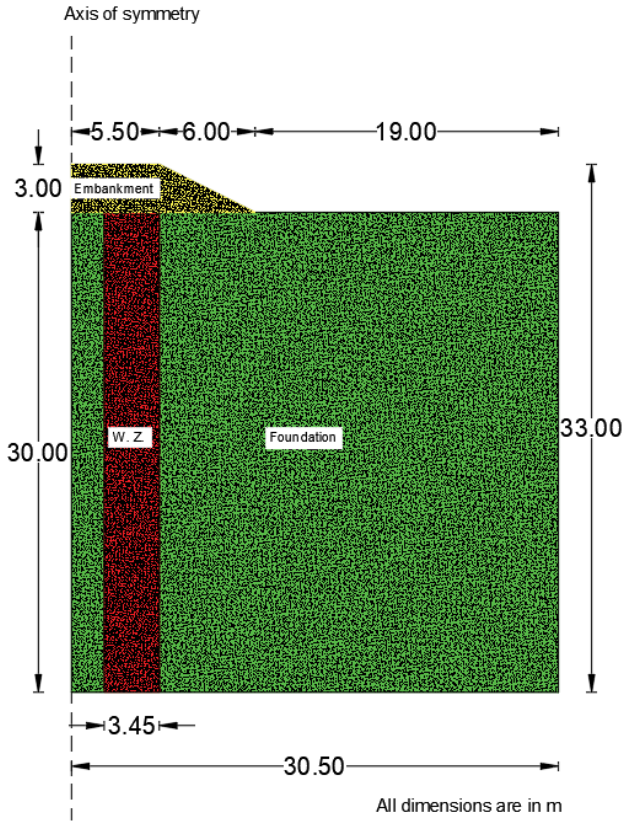

Figure 4.13 Cross-section of the unreinforced embankment model with non-central W.Z.= 0.3B.

Table 4.8 summarizes the results for the transverse slope and its relative reduction with the addition of geogrid for the models with non-central W.Z.= 0.3B. The following values for the Young's modulus of the weak zone were used: 7 and 10 MPa. The results show that the point of maximum settlement is not at the center of the embankment crest. Because of that, the two points of comparison are the points with maximum and minimum vertical displacement (the edge of the embankment crest remains the point with minimum settlement). The results in Table 4.8 show that the location of the weak zone did not significantly affect the conclusions previously obtained when considering a central weak zone. In all cases, the reduction in transverse slope due to the presence of reinforcement was less than 10%. Figure 4.14 shows the vertical displacement (in the Y direction) contours in the unreinforced and reinforced models (2 geogrids) with non-central W.Z.= 0.3B and for a weak zone modulus of 7 MPa.

Table 4.8 Crest settlements and transverse slope deformations for unreinforced and reinforced embankments (noncentral W.Z.=0.3B).

W.Z. width (B)	**W.Z. Young's modulus (MPa)**	**Type of reinforcement**	u_y^{max} **(mm)**	u_y^{min} **(mm)**	$\Delta u_y = u_y^{max} - u_y^{min}$ **(mm)**	$\frac{\Delta u_y}{L_{max-min}}$ **(%)**	**Percentage decrease in transverse slope with reinf.**
0.30	7	Unreinforced	107.56	17.93	89.63	3.26	
		1 Geogrid (E=400 MPa)	103.94	18.41	85.53	3.11	-4.6
		1 Geogrid (E=1000 MPa)	102.12	17.83	84.29	3.07	-6.0
		2 Geogrids (E=400 MPa)	101.45	18.08	83.37	3.03	-7.0
0.30	10	Unreinforced	72.93	14.02	58.91	2.14	
		1 Geogrid (E=350 MPa)	71.19	14.56	56.63	2.06	-3.9
		1 Geogrid (E=1000 MPa)	70.20	14.37	55.83	2.03	-5.2
		1 Geogrid (E=2000 MPa)	69.20	14.43	54.77	1.99	-7.0
		2 Geogrids (E=350 MPa)	70.39	14.35	56.04	2.04	-4.9
		2 Geogrids (E=1000 MPa)	68.57	14.75	53.82	1.96	-8.6

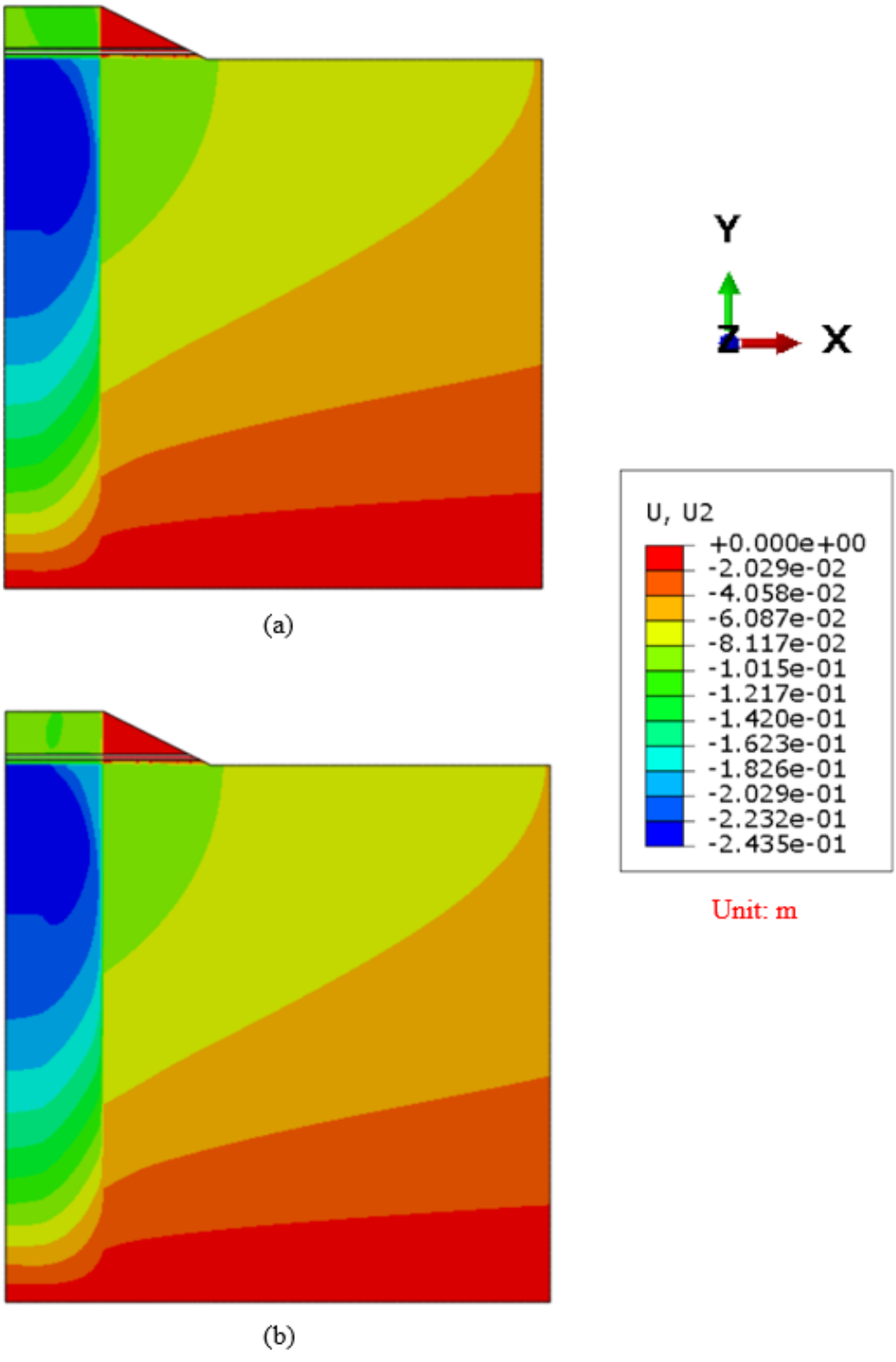

Figure 4.14 Vertical displacement contours for: (a) unreinforced; and (b) reinforced models with 2 geogrids (E = 400 MPa) (noncentral W.Z.= 0.3B, $E_{w.z.}$= 7 MPa).

Figures 4.15(a) and 4.15(b) show the cross-sections of the unreinforced model with dissymmetrical weak zones with width 0.15B and 0.29B, respectively. Embankment construction was simulated in 3 stages.

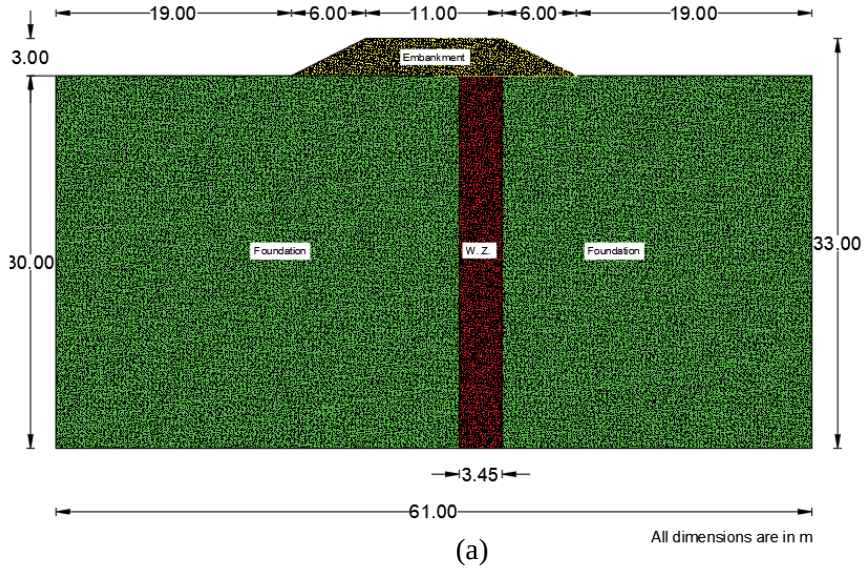

(a)

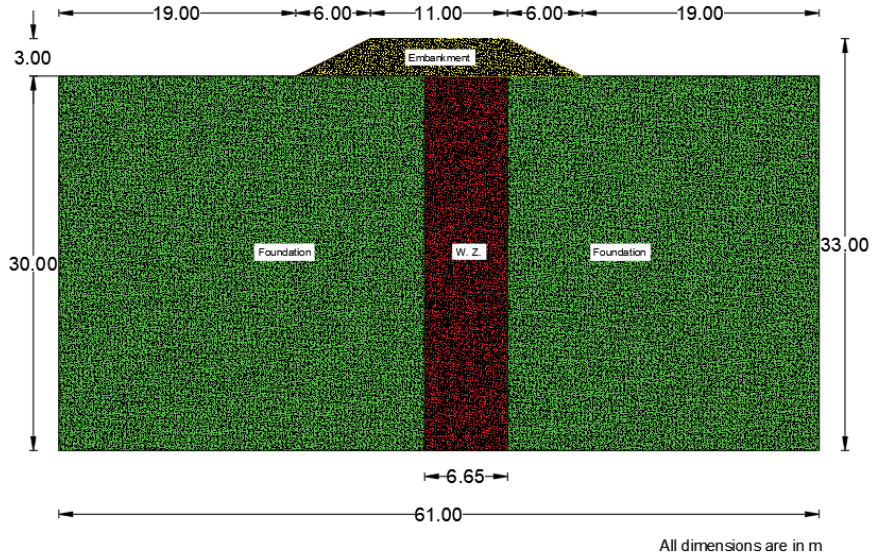

(b)

Figure 4.15 Cross-section of the unreinforced embankment model with: (a) W.Z.= 0.15B; and (b) W.Z.=0.29B.

Table 4.9 summarizes the results for the transverse slope and relative reduction in transverse slope with the addition of geogrid for W.Z.= 0.15B and W.Z.= 0.29B. Similarly to previous cases,

there was practically no benefit from geogrid-reinforcement on the embankment constructed over the weak zone with width of 0.15B. A weak zone width of 0.15B was not large enough to induce significant differential settlement at the crest of embankment and as a result the geogrid was not mobilized. On the other hand, the results of the reinforced models with W.Z.= 0.29B and weak zone modulus 10 MPa showed a small reduction in transverse slope which ranged from 3.6 to 6.2%, depending on the type of geogrid-reinforcement. For comparison, and for the case of W.Z.= 0.3B at the center of the embankment, a similar decrease in slope, from 2.9 to 7.6%, occurred for a weak zone modulus of 10 Mpa (Table 4.6). The results show that the location of the weak zone in the foundation has only minor effect on the potential benefits of using geogrid-reinforcement at the base of an embankment.

Table 4.9 Crest settlements and transverse slope deformations for unreinforced and reinforced embankments (W.Z.= 0.15B and 0.29B).

W.Z. width (B)	**W.Z. Young's modulus (MPa)**	**Type of reinforcement**	u_y^{max} **(mm)**	u_y^{min} **(mm)**	$\Delta u_y = u_y^{max} - u_y^{min}$ **(mm)**	$\frac{\Delta u_y}{L_{max-min}}$ **(%)**	**Percentage decrease in transverse slope with reinf.**
0.15	5	Unreinforced	14.49	9.79	4.70	0.23	
		1 Geogrid (E=350 MPa)	14.44	9.69	4.75	0.23	1.1
		1 Geogrid (E=1000 MPa)	14.44	9.69	4.75	0.23	1.1
		2 Geogrids (E=350 MPa)	14.44	9.69	4.75	0.23	1.1
0.29	10	Unreinforced	60.37	13.03	47.34	1.79	
		1 Geogrid (E=350 MPa)	58.90	13.25	45.65	1.72	-3.6
		1 Geogrid (E=1000 MPa)	58.39	13.44	44.95	1.70	-5.0
		1 Geogrid (E=2000 MPa)	58.10	13.70	44.40	1.68	-6.2
		2 Geogrids (E=350 MPa)	58.88	13.26	45.62	1.72	-3.6
		2 Geogrids (E=1000 MPa)	58.31	13.54	44.77	1.69	-5.4

4.8 Summary and discussion

This chapter discussed the results of a numerical model of a geosynthetic-reinforced embankment over a localized weak foundation zone. A parametric study was performed to investigate the effects of various factors, namely the modulus of weak zone, its width, the type of geogrid reinforcement, and the location of the weak zone, on the potential benefit of using geogrid-reinforcement placed at the base of the embankment. The following conclusions were drawn:

(1) The benefits of geogrid-reinforcement decrease when the modulus of the weak zone is increased. This was clearly observed when the total width of the weak zone was 30% of the total width of the embankment base (W.Z.= 0.3B). The largest improvement was achieved for a weak zone modulus equal to 5 MPa, i.e. when the ratio between the firm foundation soil and the weak zone moduli is the largest. In other words, the weakest the zone is, the largest the benefits of using geogrids.

(2) There was no contribution of the geogrid-reinforcement to the decrease of transverse slope in the embankment model with W.Z.= 0.1B. The geogrid was not mobilized, and arching of the embankment fill over the weak zone was the controlling mechanism. The largest benefit of geogrid-reinforcement was seen for the case of W.Z.= 0.3B. That is, the use of geogrids as a deformation-controlling method seems to be justified only when the size of the weak zone is large, relative to the embankment width.

(3) The addition of a second geogrid layer decreases differential deformation by a factor of 2, for the input data used in the model. In addition, the higher the value of the geogrid modulus the larger the benefit of the geogrid-reinforcement.

(4) In all the cases considered, the largest improvement resulting from geogrid-reinforcement was a 20% relative reduction in the transverse slope induced by the existence of a weak foundation zone. Thus, it is unlikely that the sole use of geogrids to mitigate differential settlements would be sufficient.

(5) The position of the weak zone in the foundation has only a minor effect on the benefit of using geogrid-reinforcement at the base of the embankment.

5. SUMMARY AND CONCLUSIONS

5.1 Summary of the work done

The objectives of this study are to advance the knowledge on the use of geosynthetics as reinforcement elements and provide recommendations for their use in embankment foundations and in pavements. The objectives have been accomplished through the following tasks:

(1) An extensive literature review to compile the information and experience that already exists on the use of geosynthetics on problems that are relevant to the improvement of the foundation of fills in low-bearing capacity materials, where the water table is close to the surface, and on the improvement of the subgrade in pavements. Specifically, the literature review highlighted the benefits of using geogrid-reinforcement in the base course of flexible pavements, geocell-reinforced bases in unpaved and paved roads, and geosynthetic-reinforcement at the base of embankments constructed over weak foundations. The best practices of INDOT and other DOTs regarding the use of geosynthetics in roadway applications were also reviewed.

(2) Assessment of the potential benefits of placing a geogrid at the interface between the subgrade and base course of a flexible pavement. This was done for select design cases, using methods and software readily available to DOT engineers and practitioners. The Composite Geosynthetic-Base Course Model and Tensar's Spectrapave software packages were used to determine the apparent increases in resilient moduli of the pavement layers, resulting from geogrid-reinforcement. In the study, the enhanced moduli were input in the AASHTOWare Pavement ME software to estimate the pavement performance relative to potential distress modes (i.e., cracking, rutting, and roughness) over the desired design life of the structure. The cases analyzed included untreated, chemically-treated and geogrid-reinforced pavements. These were based on three sections constructed in Indiana: (1) SR 46 in Clay County; (2) US 31 St. in Joe County; and (3) SR 37 in Martinsville.

(3) Numerical analyses to investigate the potential benefits of using geogrid-reinforcement at the base of an embankment constructed over a localized weak foundation zone. A parametric study, using the ABAQUS finite element software package, was performed to investigate the effects of factors such as the modulus of the weak zone, its width, the type of geogrid-reinforcement, and the location of the weak zone, on the potential benefit of using geogrid-reinforcement placed at the base of the embankment.

5.2 Conclusions

The main conclusions drawn from this study are as follows:

- The majority of the DOTs consider using geosynthetics such as geotextiles and geogrids for subgrade separation and stabilization. In general, the geotextile requirements are based on AASHTO M 288 Specification for Geotextiles. As mentioned in AASHTO M288, for subgrades with $1 < CBR < 3$ (or $1{,}500 < M_r < 4{,}500$ psi), the geotextile provides the function of stabilization. A geotextile functions as a separator for subgrades with $CBR \geq 3$ (or $M_r \geq$ 4,500 psi). There is no specific guidance regarding the upper limit of CBR (or M_r) for using a geotextile as separator. The upper limit can vary from a resilient modulus M_r of 9,500 psi (Caltrans) to 15,000 psi (WSDOT). Only few DOTs (3 out of 11 selected DOTs) consider using geosynthetics as reinforcement in pavements. However, they don't provide any specific guidance regarding the use of geosynthetics as reinforcement of unbound materials in pavements. The benefits of using geosynthetics as foundation improvement for embankments over soft soils have been identified by many DOTs.
- Geosynthetics such as geogrids can provide base reinforcement when they are placed within or at the bottom of unbound aggregate layers in a flexible pavement. Previous studies on base reinforcement have shown that the benefit of geogrid-reinforcement to reduce pavements' permanent deformation is more significant for weaker subgrades (CBR < 3), thinner base course layers (< 200 mm {or 8 in.}), or with higher tensile modulus geogrids, in designs that include a thin hot-mix asphalt (HMA) layer (50 – 75 mm {or 2 – 3 in.}) as the wearing course. In this study, analyses of pavement designs using Pavement ME, while considering geogrid-enhanced base or subgrade resilient

modulus values, showed that geogrid-reinforcement, when placed at the interface between subgrade and base, did not produce significant benefits, as only a modest increase in pavement life was predicted. The analyses were performed for a limited number of cases, in terms of subgrade conditions, layer thicknesses (thick HMA layer {≥ 10 in}), material properties, geogrid tensile stiffness, environmental and traffic conditions. While the trends were consistent across all the cases analyzed, it is possible that different conclusion may be reached for cases outside those investigated.

- Parametric finite element analyses, to investigate the potential benefits of placing a geogrid at the base of a fill over a localized weak foundation zone, showed that: (1) the benefits of geogrid-reinforcement decrease when the modulus of the weak zone increases (i.e. the weakest the zone, the largest the benefits of using geogrids); (2) the use of geogrids is beneficial when the stiffness of the weak zone is at least 5 to 10 times smaller than the foundation soil; (3) the use of geogrids as a deformation-controlling method seems to be justified only when the size of the weak zone is large relative to the embankment foundation width (i.e. weak zone width > 0.3 × embankment base width); (4) the addition of a second geogrid layer could decrease differential deformations of the fill surface by a factor of 2, at most; (5) the higher the value of the geogrid tensile modulus, the larger the benefit of the geogrid reinforcement; (6) the largest improvement resulting from geogrid-reinforcement was less than 20% in differential settlements at the surface of the fill; and (7) it is unlikely that the sole use of geogrids would be sufficient to mitigate differential settlements.
- Geocells are three-dimensional geosynthetics that can be filled with different types of materials and, thus, can be used as a strengthening mechanism. Geocell mattresses can be used as base course reinforcement over weak subgrades in unpaved and paved roads and as basal reinforcement for embankments constructed over weak foundations. Previous studies have shown that the rut depth on a pavement with a geocell-reinforced base, even with the geocell infilled with poorly graded or recycled material, may be similar or even smaller than that of a pavement with an unreinforced high-quality aggregate base layer. The inclusion of a geocell-reinforced base could lead to a 50% reduction of the granular layer thickness in unpaved roads and to a 25% reduction in paved roads. There are consistent reports in the technical literature that show that a

geocell mattress, when used at the base of an embankment, is effective in reducing differential settlements and in increasing the bearing capacity of the soft foundation. A geocell mattress at the base of an embankment could also act as a stiff platform and bridge over weak zones in the foundation.

REFERENCES

AASHTO. (1993). *AASHTO Guide for Design of Pavement Structures*. American Association of State Highway and Transportation Officials, Washington, DC.

AASHTO. (2008). *Mechanistic-empirical pavement design guide, a manual of practice*. American Association of State Highway and Transportation Officials, Washington, DC.

AASHTO. (2017). *Standard Specification for Geosynthetic Specification for Highway Applications*. AASHTO M 288-17. American Association of State Highway and Transportation Officials, Washington, DC.

ABAQUS. (2016). *Getting Started with ABAQUS: Interactive Edition*. Version 2016. Dassault Systèmes Simulia Corp., Providence, RI, USA.

Abu-Farsakh, M. Y., & Chen, Q. (2011). Evaluation of geogrid base reinforcement in flexible pavement using cyclic plate load testing. *International Journal of Pavement Engineering*, 12(03), 275-288.

Abu-Farsakh, M. Y., Gu, J., Voyiadjis, G. Z., & Chen, Q. (2014). Mechanistic–empirical analysis of the results of finite element analysis on flexible pavement with geogrid base reinforcement. *International Journal of Pavement Engineering*, *15*(9), 786-798.

Al-Qadi, I. L., Dessouky, S. H., Kwon, J., & Tutumluer, E. (2008). Geogrid in flexible pavements: validated mechanism. *Transportation Research Record*, 2045(1), 102-109.

Al-Qadi, I.L., Brandon, T.L., and Bhutta, A. (1997).Geosynthetic stabilized flexible pavements. In *Proceedings of the Conference Geosynthetics '97*, Long Beach, CA, pp. 647-662.

Aran, S. (2006). Base reinforcement with biaxial geogrid: long-term performance. *Transportation research record*, 1975(1), 114-123.

Ashmawy, A. K. (1995). *Analysis and modeling of the response of geotextile-reinforced soil to monotonic and cyclic loading.* PhD Dissertation, Purdue University, West Lafayette, Indiana, November 1995, 268 p.

Bathurst, R. J., & Jarrett, P. M. (1988). Large-scale model tests of geocomposite mattresses over peat subgrades. *Transportation Research Record*, 1188, 28–36.

Bathurst, R. J., & Karpurapu, R. (1993). Large-scale triaxial compression testing of geocell-reinforced granular soils. *Geotechnical testing journal*, *16*(3), 296-303.

Bergado, D. T., Long, P. V., Lee, C. H., Loke, K. H., & Werner, G. (1994). Performance of reinforced embankment on soft Bangkok clay with high-strength geotextile reinforcement. *Geotextiles and Geomembranes*, *13*(6-7), 403-420.

Bonaparte, R., Holtz, R. D., & Giroud, J. P. (1987). Soil reinforcement design using geotextiles and geogrids. *Geotextile Testing and the Design Engineer*, ASTM STP 952, ed. J. E. Fluet, Jr. American Society for Testing and Materials, Philadelphia, PA, pp. 69-116.

Bortz, B., Hossain, M., Halami, I., & Gisi, A. (2012). Accelerated pavement testing of low-volume paved roads with geocell reinforcement. *Advances in Pavement Design through Full-scale Accelerated Pavement Testing*, 215.

Bourdeau P. L., Harr M. E., and Holtz R. D. (1982). Soil–fabric interaction: an analytical model. In *Proceedings of the 2nd International Conference on Geotextiles*, Las Vegas, Nevada, pp. 387–391.

Bourdeau, P. L. (1989). Modeling of membrane action in a two-layer reinforced soil system. *Computers and Geotechnics*, Vol 7, Nos1 & 2, pp. 19-36.

Bourdeau, P. L., Pardi, L. and Recordon, E. (1990). Observation of soil-reinforcement interaction by X-Ray radiography. *Performance of Reinforced Soil Structures (Edited by A. McGown, K. C. Yeo and K. Z. Andrawes), Proc. International Reinforced Soil Conference, Glasgow*, Institution of Civil Engineers, pp. 347-352.

Bourdeau, P.L. and Ashmawy, A.K. (2012). Chapter 7, Unpaved roads, In *Handbook of Geosynthetic Engineering, 2nd Edition (Edited by S.K. Shukla)*. ICE Publishing & Thomas Telford Ltd, London, pp. 163-177.

Bush, D. I., Jenner, C. G., & Bassett, R. H. (1990). The design and construction of geocell foundation mattresses supporting embankments over soft grounds. *Geotextiles and Geomembranes*, *9*(1), 83-98.

California Department of Transportation. (2020). *Highway Design Manual: Chapter 660: Pavement Foundations.* Sacramento, CA. https://dot.ca.gov/-/media/dot-media/programs/design/documents/chp0660-a11y.pdf

Chen, Q., & Farsakh, M. A. (2012). Structural contribution of geogrid reinforcement in pavement. In *Proceedings of GeoCongress 2012: State of the Art and Practice in Geotechnical Engineering*, Oakland, CA, pp. 1468-1475.

Clyne, T. (2011). *Monitoring Geosynthetics in Local Roadways (LRRB 768) 10-Year Performance Summary*. Minnesota Department of Transportation, Saint Paul, MN, 55155. http://www.lrrb.org/pdf/201120.pdf

Cowland, J. W., & Wong, S. C. K. (1993). Performance of a road embankment on soft clay supported on a geocell mattress foundation. *Geotextiles and Geomembranes*, *12*(8), 687-705.

Duncan, J. M., & Chang, C. Y. (1970). Nonlinear analysis of stress and strain in soils. *Journal of the Soil Mechanics and Foundations Division, ASCE*, *96*(5), 1629-1653.

Emersleben, A., & Meyer, N. (2008). The use of geocells in road constructions over soft soil: vertical stress and falling weight deflectometer measurements. In *Proceedings of 4th European Geosynthetics Conference,* Edinburgh, UK.

Espinoza R. D. (1994). Soil–geotextile interaction: evaluation of membrane support. *Geotextiles and Geomembranes*, Vol. 13, pp. 281–293.

Espinoza R. D. and Bray J. D. (1995). An integrated approach to evaluating single-layer reinforced soils. *Geosynthetics International*, Vol. 2, No. 4, pp. 723–739.

Getchell, A., Garzon Sabogal, L., Bourdeau, P. L., Santagata, M. (2020). Investigation of design alternatives for the subbase of concrete pavements (Joint Transportation Research Program Publication No. FHWA/IN/JTRP-2020/03).West Lafayette, IN: Purdue University. https://doi.org/10.5703/1288284317114

Gross, F., Eccles, K., & Nabors, D. (2011). Low-volume roads and road safety audits: lessons learned. *Transportation research record*, *2213*(1), 37-45.

Haas, R., Walls, J., & Carroll, R. G. (1988). Geogrid reinforcement of granular bases in flexible pavements. *Transportation research record*, *1188*, 19-27.

Han, J., Yang, X. M., Leshchinsky, D., Parsons, R. L., & Rosen, A. (2008). Numerical analysis for mechanisms of a geocell-reinforced base under a vertical load. In *Geosynthetics in Civil and Environmental Engineering*. Springer, Berlin, Heidelberg, pp. 741-746.

Hausmann M. R. (1990). *Engineering Principles of Ground Modification*. McGraw-Hill, New York, NY.

Hegde, A., & Sitharam, T. G. (2015). 3-Dimensional numerical modelling of geocell reinforced sand beds. *Geotextiles and Geomembranes*, *43*(2), 171-181.

Henkel, D. J., & Gilbert, G. D. (1952). The effect of the rubber membrane on the measured triaxial compression strength of clay specimens. *Géotechnique*, *3*(1).

Holtz, R. D., Christopher, B. R., & Berg, R. R. (2008). Geosynthetic design & construction guidelines: reference manual. Report No. FHWA-NHI-07-092, US Department of Transportation, Federal Highway Administration, National Highway Institute, Washington, DC, pp. 612.

Holtz, R.D. (2001). *Geosynthetics for Soil Reinforcement*. The 9th Spencer J. Buchanan Lecture, November 2001, College Station, Texas.

Huang, W.-C., Bourdeau, P.L., & Kim, D. (2010). The problem of wet subgrades (Joint Transportation Research Program Publication No FHWA/IN/JTRP-2007/7). West Lafayette, IN: Purdue University.

Humphrey, D. N., & Holtz, R. D. (1986). Reinforced embankments—a review of case histories. *Geotextiles and geomembranes*, *4*(2), 129-144.

Illinois Department of Transportation. (2005). *Subgrade Stability Manual.* http://idot.illinois.gov/Assets/uploads/files/Doing-Business/Manuals-Guides-&-Handbooks/Highways/Bridges/Geotechnical/Subgrade%20Stability%20Manual.pdf

Illinois Department of Transportation. (2016). *Standard Specifications for Road and Bridge Construction.* http://www.idot.illinois.gov/Assets/uploads/files/Doing-Business/Manuals-Guides-&-Handbooks/Highways/Construction/Standard-Specifications/Standard%20Specifications%20for%20Road%20and%20Bridge%20Construction%202016.pdf

Indiana Department of Transportation. (2020). *Standard Specifications: Division 200: Earthwork*. https://www.in.gov/dot/div/contracts/standards/book/sep19/200-2020.pdf

Jewell R. A. (1996). *Soil Reinforcement with Geotextiles*. Construction Industry Research and Information Association, London, CIRIA. Special publication 123.

Jewell, R. A. (1988). The mechanics of reinforced embankments on soft soils. *Geotextiles and Geomembranes*, 7, 237–273.

Jewell, R.A. (1987). Reinforced soil walls analysis and behaviour. In: Jarret, P.M., McGown, A. (Eds.), *The Application of Polymeric Reinforcement in Soil Retaining Structures*. Kluwer Academic, Norwell, MA, pp. 365–408.

John N. W. M. (1987). *Geotextiles*. Blackie, Glasgow.

Jung, C., & Bobet, A. (2008). Post-construction evaluation of lime-treated soils (Joint Transportation Research Program Publication No. FHWA/IN/JTRP-2007/25). Purdue University. https://doi.org/10.5703/1288284313443

Kentucky Transportation Cabinet. (2019). *Standard Specifications for Road and Bridge Construction.* Frankfort, KY. https://transportation.ky.gov/Construction/StdSpecsWSupplSpecs/2019%20Standard%20Spec%20with%20Supplemental%20Spec%20July%202019.pdf

Kief, O., Schary, Y., & Pokharel, S. K. (2015). High-modulus geocells for sustainable highway infrastructure. *Indian Geotechnical Journal*, *45*(4), 389-400.

Kim, W. H., Edil, T. B., Benson, C. H., & Tanyu, B. F. (2005). Structural contribution of geosynthetic-reinforced working platforms in flexible pavement. *Transportation research record*, 1936(1), 43-50.

Koerner R. M. (1998). *Designing with Geosynthetics, 4th edition*. Prentice Hall, Englewood Cliffs, NJ.

Koerner R. M. (2005). *Designing with geosynthetics, 5th edition*. Prentice Hall, Englewood Cliffs, NJ.

Krishnaswamy, N. R., Rajagopal, K., & Latha, G. M. (2000). Model studies on geocell supported embankments constructed over a soft clay foundation. *Geotechnical Testing Journal*, *23*(1), 45-54.

Ludlow, S. J., Chen, W.-F., Bourdeau, P. L. & Lovell, C. W. (1992). Phase II – Embankment Widening and Grade Rising on Soft Foundation Soils, Report No FHWA/IN/JHRP-92/19, Joint Highway Research Project, Purdue University, 356p.

Luo, R., Gu, F., Luo, X., Lytton, R.L., Hajj, E.Y., Siddharthan, R.V., Elfass, S., Piratheepan, M., & Pournoman, S. (2017). Quantifying the influence of geosynthetics on pavement performance (No. NCHRP Project 01-50). National Academies Press, Washington, DC.

Madhavi Latha, G. (2000). *Investigations on the behaviour of geocell supported embankments*. PhD dissertation, Department of Civil Engineering, Indian Institute of Technology Madras, Chennai, India.

Madhavi Latha, G., & Rajagopal, K. (2007). Parametric finite element analyses of geocell-supported embankments. *Canadian Geotechnical Journal*, *44*(8), 917-927.

Massachusetts Department of Transportation. (2020). *Standard Specification for Highways and Bridges.* https://www.mass.gov/doc/2020-standard-specifications-for-highways-and-bridges/download

Montanelli, F., Zhao, A., & Rimoldi, P. (1997). Geosynthetic-reinforced pavement system: testing and design. In *Proceeding of the Conference Geosynthetics 97'*, Long Beach, CA, pp. 619-632.

New York State Department of Transportation. (2018). *Geotechnical Design Manual: Chapter 18: Geosynthetic Design*. Albany, NY. https://www.dot.ny.gov/divisions/engineering/technical-services/geotechnical-engineering-bureau/geotech-eng-repository/GDM_Ch-18_Geosynthetic_Design.pdf

Ohio Department of Transportation. (2019). *Construction and Material Specifications*. Columbus, OH. http://www.dot.state.oh.us/Divisions/ConstructionMgt/OnlineDocs/Specifications/2019CMS/2019_CMS_10162018%20Final%20to%20Printer.pdf

Pennsylvania Department of Transportation. (2018*). Geotechnical Engineering Manual*. http://www.dot.state.pa.us/public/pubsforms/Publications/Pub%20293.pdf

Perkins, S. W., Berg, R. R. and Christopher, B. R. (2012). Chapter 8, Paved roads. *In Handbook of Geosynthetics Engineering, 2nd Ed. (Edited by S. K. Shukla)*, ICE Publishing & Thomas Telford Ltd, London, UK, pp. 179-192.

Pinto, M.I.M. (2003). Applications of geosynthetics for soil reinforcement. *Ground Improvement*, Vol. 7, No. 2, pp. 61-72.

Pokharel, S. K. (2010*). Experimental study on geocell-reinforced bases under static and dynamic loading*, PhD dissertation, University of Kansas.

Pokharel, S. K., Han, J., Leshchinsky, D., Parsons, R. L., & Halahmi, I. (2010). Investigation of factors influencing behavior of single geocell-reinforced bases under static loading. *Geotextiles and Geomembranes*, *28*(6), 570-578.

Pokharel, S. K., Han, J., Manandhar, C., Yang, X., Leshchinsky, D., Halahmi, I., & Parsons, R. L. (2011). Accelerated pavement testing of geocell-reinforced unpaved roads over weak subgrade. *Transportation research record*, 2204(1), 67-75.

Rajagopal, K., Krishnaswamy, N. R., & Latha, G. M. (1999). Behaviour of sand confined with single and multiple geocells. *Geotextiles and Geomembranes*, *17*(3), 171-184.

Rajagopal, K., Krishnaswamy, N. R., & Madhavi Latha, G. (2001). Finite element analysis of embankments supported on geocell layer using composite model. In *Proceedings of 10th International Conference on Computer Methods and Advances in Geomechanics*, Tucson, Arizona, January 2001, pp. 1251-1254.

Rajagopal, K., Veeragavan, A., & Chandramouli, S. (2012*).* Studies on geocell reinforced road pavement structures. In *Proceedings of the 5th Asian Regional Conference of Geosynthetics*, Bangkok, Thailand.

Rowe, R. K., & Li, A. L. (2005). Geosynthetic-reinforced embankments over soft foundations. *Geosynthetics International*, *12*(1), 50-85.

Rowe, R. K., & Soderman, K. L. (1984). Comparison of predicted and observed behaviour of two test embankments. *Geotextiles and Geomembranes*, *1*(2), 143-160.

Rowe, R.K., Liu, K., Taechakumthorn, C. (2015). Chapter 19 – Use of Geosynthetics to Aid Construction over Soft Soil. *Ground Improvement Case Histories: Compaction, Grouting and Geosynthetics*, pp. 559-582.

Sandoval, E., Ardila Quiroga, A., Bobet, A., & Nantung, T. (2019). Subgrade stabilization alternatives (Joint Transportation Research Program Publication No. FHWA/IN/JTRP-2019/30). West Lafayette, IN: Purdue University. https://doi.org/10.5703/1288284317110

Shukla, S.K. (2004). Discussion: Applications of geosynthetics for soil reinforcement. In *Proceedings of the Institution of Civil Engineers – Ground Improvement*, Vol. 8, No. 4, pp. 179-182.

Sun, X., Han, J., & Corey, R. (2017). Equivalent modulus of geogrid-stabilized granular base back-calculated using permanent deformation. *Journal of Geotechnical and Geoenvironmental Engineering*, 143(9), 06017012.

Sun, X., Han, J., Parsons, R. L., & Thakur, J. (2018). Equivalent California Bearing Ratios of Multiaxial Geogrid-Stabilized Aggregates over Weak Subgrade. *Journal of Materials in Civil Engineering*, 30(11), 04018284.

Tensar (2019). *Tensar's Spectrapave software - always advancing.* The Tensar Coorporation, Atlanta, GA. https://info.tensarcorp.com/hubfs/WH_Files/WH_Tensar%20Software/WH_TensarApp/SpectraPaveOverview.pdf

Terzaghi, K. (1943). *Theoretical soil mechanics*. John Wiley & Sons. New York, 11-15.

Texas Department of Transportation. (2019). *Pavement Manual*. http://onlinemanuals.txdot.gov/txdotmanuals/pdm/manual_notice.htm

Washington State Department of Transportation. (2020). *WSDOT Design Manual: Chapter 630: Geosynthetics.* M-22-01.19. Olympia, WA. https://wsdot.wa.gov/publications/manuals/fulltext/M22-01/630.pdf

Webster, S. L. (1979). Investigation of Beach Sand Trafficability Enhancement Using Sand-grid Confinement and Membrane Reinforcement Concepts: Sand test sections 1 and 2. Report 1. US Army Engineer Waterways Experiment Station. Technical Report GL-79-20. Geotechnical Laboratory, US Army Corps of Engineers Waterways Experimentation Station, Vicksburg, MS.

Webster, S. L. (1981). Investigation of Beach Sand Trafficability Enhancement Using Sand-Grid Confinement and Membrane Reinforcement Concepts. Report 2. Sand Test Sections 3 and 4. Technical Report GL-79-20. Geotechnical Laboratory, US Army Corps of Engineers Waterways Experimentation Station, Vicksburg, MS.

Wisconsin Department of Transportation. (2021). *Standard Specifications for Highway and Structure Construction: Chapter 645: Geosynthetics.* https://wisconsindot.gov/rdwy/stndspec/ss-06-45.pdf

Wu, J. T., Siel, B. D., Chou, N. N., & Helwany, H. B. (1992). The effectiveness of geosynthetic reinforced embankments constructed over weak foundations. *Geotextiles and Geomembranes*, *11*(2), 133-150.

Yang, X., Han, J., Parsons, R. L., & Leshchinsky, D. (2010). Three-dimensional numerical modeling of single geocell-reinforced sand. *Frontiers of Architecture and Civil Engineering in China*, *4*(2), 233-240.

Yang, X., Han, J., Pokharel, S. K., Manandhar, C., Parsons, R. L., Leshchinsky, D., & Halahmi, I. (2012). Accelerated pavement testing of unpaved roads with geocell-reinforced sand bases. *Geotextiles and Geomembranes*, 32, 95-103.

Zhang, L., Zhao, M., Shi, C., & Zhao, H. (2010). Bearing capacity of geocell reinforcement in embankment engineering. *Geotextiles and Geomembranes*, *28*(5), 475-482.